REPORT DOCUMENTATION PAGE

AFRL-SR-BL-TR-00-

0446

1. AGENCY USE ONLY (Leave blank)	2. REPORT DATE	3. REPORT TYPE AND DATES COVERED
	June 28, 2000	Final Report 3/1/95 - 2/28/99

4. TITLE AND SUBTITLE
High-Temperature Micromechanics and Mechanisms of Damage and Failure in Advanced Ceramic-Matrix Composites

5. FUNDING NUMBERS
F49620-95-1-0204

6. AUTHOR(S)
S.S. Wang

7. PERFORMING ORGANIZATION NAME(S) AND ADDRESS(ES)
University of Houston
4800 Calhoun Rd.
Houston, TX 77204-0903

8. PERFORMING ORGANIZATION REPORT NUMBER

9. SPONSORING/MONITORING AGENCY NAME(S) AND ADDRESS(ES)
AirForce Office of Scientific Research / NA
110 Duncan Avenue, Room B115
Bolling AFB, DC 20332-8080

10. SPONSORING/MONITORING AGENCY REPORT NUMBER

11. SUPPLEMENTARY NOTES

12a. DISTRIBUTION/AVAILABILITY STATEMENT
"UNLIMITED"

12b. DISTRIBUTION CODE

13. ABSTRACT (Maximum 200 words)

In this project, research efforts have been made to address some of the most critical and complex issues on high-temperature damage, degradation and failure of advanced composites. For the convenience of program planning and execution, the research as been formulated in the form of several interrelated technical tasks with distinct focuses. In the study of high-temperature ceramic-matrix the following tasks have been conducted: (1). High-temperature fiber/matrix interface properties and failure mechanics; (2). High-temperature micromechanics theories for thermoelastic constitutive equations for whisker-reinforced ceramic composites with large temperature traverse; (3). High-temperature creep deformation and micromechanics modeling of inelastic composite constitutive properties with composite microstructure and damage, and (4). High-temperature toughening mechanisms, and mechanics of crack growth and fracture. For the high-temperature polymer-matrix composite study, the following thermomechanics issues with internal and external damage have been addressed: (1). thermal oxidation reaction and stability at elevated temperatures; (2). chemical and physical aging in extreme thermal environments; (3). mircrostructure changes and property degradation associated with aging at elevated temperatures; and (4). long-term

14. SUBJECT TERMS thermomechanical creep and associated damage modes.

15. NUMBER OF PAGES
22

16. PRICE CODE

17. SECURITY CLASSIFICATION OF REPORT	18. SECURITY CLASSIFICATION	19. SECURITY CLASSIFICATION OF ABSTRACT	20. LIMITATION OF ABSTRACT

NSN 7540-01-280-5500

Standard Form 298 (Rev. 2-89)
Prescribed by ANSI Std. Z39-18

Final Technical Report
for the Project
(under US AFOSR Grant No.: F49620-95-1-0204)

on

HIGH TEMPERATURE MICROMECHANICS AND MECHANISMS OF DAMAGE AND FAILURE IN ADVANCED CERAMIC-MATRIX COMPOSITES

by

S. S. Wang, Principal Investigator
Department of Mechanical Engineering, and
Composites Engineering and Applications Center (CEAC)
University of Houston
4800 Calhoun Road
Houston, TX 77204-0903

Phone No.: (713)-743-5053
Fax: (713)-743-5063

E-Mail Address: SSWang@UH. EDU

Submitted to

U.S. Air Force Office of Scientific Research
110 Duncan Ave., Suite B115
Bolling AFB, Washington, D. C. 20332-0001

Executive Summary

Recent advances in high-temperature materials and processing science have led to significant interests in high-temperature ceramic- and polymer-matrix composite (CMC & PMC) systems. High-temperature CMC and PMC materials are considered critical in the current development of many advanced engineering systems, such as high-performance jet engines, high-speed aircraft structures, and advanced microelectronics. Advanced composite materials used in these systems must be capable of withstanding extreme temperature environments and still maintain their long-term thermomechanical properties and load-bearing structural integrity.

In this project, research efforts have been made to address some of the most critical and complex issues on high-temperature damage, degradation and failure of advanced ceramic- and polymer-matrix composites. The objectives of the project are to: (1) Investigate fundamental *microscopic* mechanisms and associated micromechanics of high-temperature composite damage and degradation under thermomechanical loading; (2). Evaluate and predict elevated-temperature *macroscopic* effective properties and failure strength of the composites in long-term high-temperature service conditions, and (3). Determine individual roles of, and their *interplay* among, the matrix, reinforcing fibers, composite microstructure and the fiber/matrix interface on property degradation and failure modes in high-temperature environments.

For the convenience of program planning and execution, the research has been formulated in the form of several interrelated technical tasks with distinct focuses. In the study of high-temperature CMC materials the following tasks have been conducted:

(1). High-temperature ceramic-matrix composite processing and microstructure study;
(2). High-temperature fiber/matrix interface properties and failure mechanics;
(3). High-temperature micromechanics theories for thermoelastic constitutive equations for whisker-reinforced ceramic composites with large temperature traverse;
(4). High-temperature creep deformation and micromechanics modeling of inelastic composite constitutive properties with composite microstructure and damage, and
(5). High-temperature toughening mechanisms, and mechanics of crack growth and fracture in CMC's.

For the high-temperature polymer-matrix composite study, the following thermomechanics issues with internal and external damage have been addressed: (1). thermal oxidation reaction and stability at elevated temperatures; (2). chemical and physical aging in extreme thermal environments; (3). microstructure changes and property degradation associated with aging at elevated temperatures; and (4). long-term thermomechanical creep and associated damage modes.

Both short- and long-term high-temperature experiments have been conducted on selected CMC and PMC materials. Fundamental theories and associated computational methods, based on high-temperature mechanics, damage and failure modes and thermodynamics for multi-component systems, have been developed . The analytical solutions are compared well with experimental results for the composite systems studied under various thermal and mechanical loading.

5. INTRODUCTION

The introduction of advanced composite materials has rapidly revolutionized the infrastructures of a wide range of industry, ranging from aerospace, propulsion, machinery to marine and automotive systems. With rapid advances in high stiffness and strength fibers, advanced structural ceramics, and processing and manufacturing sciences, developments of new ceramic-matrix composites (CMC) for load-bearing components in high-temperature environments have recently attract significant attention. High-temperature ceramic-matrix composites are considered critical in the current development of high-performance fuel-efficient aeropropulsion systems for supersonic and hypersonic aircraft.

While significant advantages of high-temperature applications of advanced ceramic composite materials have been recognized, many fundamental scientific issues on their thermomechanical properties and performance in a high-temperature environment remain unresolved. In the pursuit of solutions for these problems, various complexities are encountered, including heterogeneous composite microstructures, the unknown nature of the fiber-matrix interface at elevated temperatures, unusual temperature-dependent inelastic properties of constituent phases and the composite, multiple microscopic damage and failure modes, and the deleterious effect of high-temperature reaction and degradation. Obviously, the full potential of advanced ceramic-matrix composites will not be realized until these critical issues are resolved.

This research project, entitled "High-Temperature Micromechanics and Mechanisms of Damage and Failure in Ceramic-Matrix Composite Materials" and funded by AFOSR under the Grant F49620-95-1-0204, has attempted to address some of the most critical and complex high-temperature micromechanics issues on damage, degradation and failure of advanced ceramic-matrix composites in elevated-temperature environments. During the course of the study, several meetings were held with Dr. N. J. Pagano of the Air Force

Materials Research Laboratories (AFML) in Wright-Patterson AFB, Dayton, OH. Discussions and exchanges of ideas were made on the proposed project and the AFML's ongoing activities. Based on these discussions, this research has been planned and carried out with direct interactions with several research staff of AFML and some of the tasks in the program were conducted complimentary to the AFML's efforts.

In the context of composite micromechanics and mechanisms, the research has been conducted both at microscopic and macroscopic scales, which involve processing studies, high-temperature thermomechanical experiments, heterogeneous-media micromechanics modeling, and computational analysis and simulation. For the convenience of project planning and program execution, the research has been formulated into the following interrelated technical tasks with different focuses in the individual tasks:

(1). High-temperature ceramic-matrix composite processing and microstructure studies.

(2). High-temperature fiber-matrix interface microstructures, properties and failure mechanics.

(3). High-temperature micromechanics theories for thermoelastic constitutive equations for whisker-reinforced ceramic matrix composites under large temperature change..

(4). High-temperature creep behavior and micromechanics modeling of inelastic constitutive properties with composite microstructure and damage.

(5). High-temperature toughening mechanisms, and mechanics of crack growth and fracture in CMC's.

After several discussions with the Program Managers, Dr. Walter F. Jones and Dr. Ozden Ochoa, additional efforts have also been made in this project to address similar and equally important micromechanics and micromechansim issues on high-temperature oxidation, chemical and physical aging and failure of advanced thermoset polymer-matrix composite systems.

2. OBJECTIVES OF THE RESEARCH PROJECT

The research project has been carried out to realize the following technical objectives:

(1). Understanding fundamental *microscopic* mechanisms and associated micromechanics of high-temperature creep deformation, interface properties and degradation, matrix and interface damage, and their evolution in advanced ceramic-matrix composites;

(2). Evaluation and prediction of high-temperature *macroscopic* effective properties and failure strength of heterogeneous ceramic-matrix composites with complex reinforce microstructures and damage under coupled thermal and mechanical loading;

(c). Determination of individual roles of, and the *interplay* among, the matrix, reinforcing fibers, composite microstructure (i.e., fibers vs. whiskers), the fiber-matrix interface, and different damage modes in the elevated temperature performance and degradation of the composite.

Throughout the research, an important emphasis is focused on the influence of *high-temperature* environments on the various aforementioned micromechanics and micromechanism issues addressed in the proposal.

As mentioned earlier, in discussions with the Program Managers, Dr. W. F. Jones and Dr. Ozden Ochoa, a part of the effort in this project has also been devoted to look into similar micromechanics and micromechanisms issues on thermal oxidation, aging, damage, degradation and failure of high-temperature thermoset polymeric-matrix composites.

3. SUMMARY OF THE RESEARCH WORK

The project was started in March 1995 and continued 36 months with a no-cost extension for completion. Two initial research meetings were conducted in 1995 with AFML researchers who were working in the same research areas. The first meeting was with Dr. N.J. Pagano on May 3-4, 1995 in Houston, and the second, with Dr. Pagano again and his AFML high-temperature composites researchers at Wright Patterson AFB on July 26-27, 1995 to review our AFOSR project and AFML's ceramic composites program. A strategy of technical approach and a collaborative research plan were developed to address the critical micromechanics and micromechanism issues of common interests in high-temperature ceramic-matrix composites. It was agreed that Dr. Pagano and his colleagues at AFML would concentrate on micromechanics modeling of damage and failure of ceramic composites at *room temperature* and attempt to perform only few selected tests at elevated temperatures. The research project conducted at University of Houston was set to completely focus on *high-temperature* mechanics and mechanisms issues of damage and failure in CMC's. All experiments conducted at the University of Houston would be at elevated temperatures. Both groups would attempt to use the same ceramic composite material systems in their the experimental work and in analytical/computational modeling so that experimental data and observations at room and elevated temperatures could be related and analytical/numerical results would be meaningfully discussed and compared.

During the reporting period of the research project, technical efforts were initiated and conducted on all the following inter-related tasks simultaneously. A summary for each of these individual tasks is briefly described below. Detailed research results obtained from these tasks in the project were given in the research reports previously submitted with individual annual progress reports and in the attachments with this report.

3.1 High-Temperature Ceramic-Matrix Composite Processing and Microstructure Studies

This task was conducted in conjunction with Dr. R. Dutton of AFML for fabrication of the ceramic-matrix composites needed for various planned experiments. In the experiments, attempts were made to use the CMC material systems consistent with the AFML's test program, as defined in the project. The experiments included fiber/matrix interface oxidation and degradation studies, high-temperature creep deformation, and damage and failure studies. In the processing and microstructure study, a novel processing method was introduced to develop continuous SCS-6 fiber reinforced glass (Corning 7040) matrix composites. Effects of processing variables on the CMC microstructure and composite interface morphology have been investigated. Optimal processing conditions and associated variables have been obtained for the CMC with desired microstructure and interfacial bonding. A part of the work was conducted in the AFML laboratories because of the availability of the needed processing and microstructure characterization facilities there.

Results derived from the study were presented in a paper, entitled "A Processing and Microstructure Study of SiC Fiber Reinforced Glass-Matrix Composites," by M. S. Wong and S. S. Wang, (Paper No. C-0065-97F), in *the 21st Annual Cocoa Beach Conference on Composites, Advanced Ceramics, Materials and Structures*, The America Ceramic Society, Cocoa Beach, Florida. The method developed in the study was used for fabrication of SiC fiber reinforced glass composites for the subsequent micromechanics and damage mechanism studies in the project.

3.2 High-Temperature Fiber-Matrix Interface Structure and Properties, and Mechanics of Interface Failure

It has been well recognized that the microstructure and properties of a fiber-matrix interface in a ceramic-matrix composite have a profound influence on its high-temperature

performance and failure behavior. However, very little, if any, information is available on the *in-situ* high-temperature interface properties and failure strength of advanced CMC materials. (Even though many studies have been reported on CMC interfacial properties at room temperature, controversial issues on this subject remain.) Both microscopic in-situ interface deformation and strength experiments as well as a micromechanics fiber/matrix interface analysis have been conducted in this Task.

In the microscopic interface experiment, a major effort has been made to design and construct an elevated-temperature in-situ fiber-matrix interface test system. The experimental facility was designed to conduct elevated temperature fiber-matrix interface tests on a microscopic scale in bulk ceramic-matrix composite specimens. The test system consisted of the following components: a high-resolution optical microscope, a load-application actuator with a micro-indenter, transducers and a high-precision load cell, a three-axis micro-stage controller for microscopic specimen positioning and motion, a heating device with a temperature controller, a high-resolution camera and a video monitor, and a data acquisition system. All of the system components were designed in-house, manufactured (or acquired) individually, and assembled by participating students and research associates in our laboratory. An accompanying effort has also been made on development of analytical micromechanics methods to model the high-temperature composite interface problem with temperature-dependent interfacial conditions, including slip-stick contact and partial debonding along a fiber-matrix interface. The associated computational mechanics method introduced in this Task included a local interface asymptotic solution obtained for full-field finite-dimensional modeling of push-in and push-through debonding experiments conducted.

Experimental and analytical results derived from this effort have been reported in a paper, entitled "High-Temperature Fiber-Matrix Interface Degradation in Silicon-Carbide Fiber Reinforced Ceramic-Matrix Composite: Experiments and Micromechanics Analysis," by S. S. Wang, M. Karayaka, T.P. Yu, H. Suzuki and M.S. Wong (Paper Number: C-0110-97F), in *the 21st Annual Cocoa Beach Conference on Composites, Advanced Ceramics, Materials and Structures*, The America Ceramic Society, Cocoa Beach, Florida.

3.3 High-Temperature Micromechanics Theories for Thermoelastic Constitutive Equations for Whisker-Reinforced Ceramic Composites under Large Temperature Change

Before investigating high-temperature inelastic creep deformation and damage evolution in a ceramic-matrix composite, proper thermoelastic constitutive theory for the CMC's under a large temperature traverse needed to be established first. In this task, detailed micromechanics formulation for effective thermoelastic constitutive properties of a ceramic matrix composite has been developed, based on a nonlinear thermoelasticity treatment of heterogeneous media. The effective thermoelastic behavior of a 3-D randomly oriented whisker reinforced ceramic composite under a large temperature change has been determined by a combined micromechanics inclusion theory and a proper averaging scheme to account for the microstructure characteristics of the composite. Results obtained from a self-consistent scheme and a differential analysis both show that effective thermoelastic properties of a ceramic composites under a large temperature change are independent of thermal expansion mismatch between the constituent phrases. Consequently the basic effective thermoelastic constitutive equations for a whisker reinforced ceramic composite under a large temperature change are decoupled, and could be treated by a superposition of a pure nonisothermal process on an isothermal mechanical problem. An alternative approach for this problem has also been formulated by modifying the Levin-Hashin's solution. Systematic numerical studies of the effects of material and microstructural parameters, such as reinforcement volume fraction, whisker (fiber) aspect ratio and temperature-dependent constituent thermal and mechanical properties on the effective thermoelastic properties of SiC-whisker reinforced alumina matrix composites under a large temperature change have been conducted. Details are given in the attached reports, entitled: (1). "Estimation of Temperature Dependent Transversely Isotropic Elastic Properties of Single-Crystal SiC Whiskers," by Y. Yuan and S. S. Wang; and (2). High-Temperature Thermoelastic Constitutive Theories for Random Whisker Reinforced Ceramic Composites under a Large Temperature Change," by Y. Yuan and S. S. Wang.

3.4 High-Temperature Creep Behavior and Micromechanics Modeling of Inelastic Constitutive Equations for CMC's with Microstructure and Damage

High-temperature creep deformation and creep damage experiments have been systematically conducted on the SCS6 fiber-reinforced glass-matrix composites. The emphasis of this investigation was placed on the matrix-dominated transverse creep deformation and damage. To understand the contributions of individual constituent phases in the CMC, elevated creep experiments have also been performed on the monolithic glass matrix. Effective composite long-term creep deformation of the CMC was determined in the experiment and compared with analytical predictions at different temperatures. Creep deformation and damage mechanisms at the selected temperatures were studied and introduced into the micromechanics model development effort. In the theoretical and numerical parts of the Task, the recently developed nonlinear, inelastic homogenization theory has been modified to include high-temperature creeping constitutive equations of both amorphous and crystalline matrices for long-term composite creep deformation and degradation predictions. Nonlinear computational micromechanics schemes, involving coupled incremental and iterative numerical algorithms, have been formulated and constructed. Numerical results for high-temperature creep deformation and degradation in the CMC's, such as SCS6/7040 glass and Nicalon/LAS, have been obtained for comparison with the experimental data.

Both the experimental results and the nonlinear inelastic homogenization solutions for CMC creep deformation and damage problems have been reported in a paper, entitled " High-temperature Creep Deformation of Silicon-Carbide Fiber (SCS6) Reinforced Glass-Matrix Composites, by A. Miyase, T.P. Yu and S. S. Wang, in the *21st Annual Cocoa Beach Conference on Composites, Advanced Ceramics, Materials and Structures*, The America Ceramic Society, Cocoa Beach, Florida.

3.5 High-Temperature Toughening Mechanisms, and Mechanics of Crack Growth and Fracture

In this task, a detailed investigation of elevated-temperature crack growth behavior and associated toughening mechanisms has been conducted on both monolithic and fiber-reinforced ceramic composites by a combined experimental and analytical modeling approach. In the experimental phase of the project, notched SiC-fiber (Nicalon) reinforced glass-matrix composite and notched monolithic glass (Corning 7740 glass) specimens were used to study crack initiation and growth behavior at elevated temperatures, ranging from room temperature to 550°C. A complete high-temperature crack growth test system was constructed for this purpose. The system contained a servohydraulic loading frame, a high-temperature furnace, a high-temperature extensometer, a temperature control system, a data acquisition and analysis system, and gripping fixtures. At elevated temperatures, crack-tip branching with mixed-mode crack growth was always observed in the CMC material system studied. The mixed mode crack branching and growth behavior was modeled by a micromechanism-based crack analysis with the aid of high-temperature creeping constitutive equations of the matrix and fibers and the composite constitutive equations derived from the inelastic homogenization theory discussed in the previous task. The high-temperature crack-growth resistance curves for the SiC/7040 glass-matrix composite have been constructed in the study. Correlations have been made among the high-temperature experimental observations, measurements and the crack growth analysis to establish a micromechanisms-based relationship among the material toughening resistance, damage modes, and applied external loading.

Results obtained in this Task have been presented in the paper, entitle "Elevated Temperature Crack Growth and Fracture Resistance in SiC Fiber Reinforced Glass-Matrix Composites," by M. Karayaka, T. P. Yu and S. S. Wang in the *21st Annual Cocoa Beach Conference on Composites, Advanced Ceramics, Materials and Structures*, The America Ceramic Society, Cocoa Beach, Florida.

3.6 High-Temperature Oxidation, Aging, Viscoelastic Creep and Fracture of Carbon-Fiber Reinforced Polyimide Composites

A parallel effort to the ceramic-matrix composite study has also been made on studying advanced polymer-matrix composites at elevated temperatures. The focus of the study was on the complex and interactive issues of thermal oxidation, long-term aging, viscoelastic creep deformation and fracture of carbon-fiber reinforced polyimide-matrix composites in aggressive high-temperature environments. In the experimental phase of the study, two composite material systems were used: IM6/AVMID N and G30-500/PMR-15 composites. Elevated-temperature thermal oxidation was studied first. The reaction-induced thermal transport was found to be strongly anisotropic in nature, and subsequently modeled by a reaction-controlled degradation process, involving the matrix, fibers, and the interface. The fiber/matrix interface reaction during thermal oxidation was identified as the dominant mechanism for the composite degradation due to its high thermodynamic driving force. Long-term elevated-temperature aging of the composites was investigated in the context of physical and chemical aging. Aging experiments were conducted to determine the kinetics parameters of the aging processes and associated relationships among the dimension (free volume) change, glass transition temperature increase, aging duration and the elevated temperature environment. Theoretical models for both physical and chemical aging processes have been developed to predict the long-term aging behavior of the thermoset-matrix composites at high-temperatures. The aging-induced property changes and the associated aging parameters were incorporated into a homogenization model to evaluate and predict long-term, high-temperature deformation of the composites under thermomechanical loading. The experiments and theoretical models were reported in a report, entitled, "Isothermal High-Temperature Oxidation, Aging, and Creep of Carbon-Fiber/Polyimide Composites," and in a number of papers presented in different national and international conferences, as reported in the previous Annual Reports.

To address the effect of an elevated-temperature environment on crack growth and fracture of a high-temperature carbon-fiber reinforced composite system, a fundamental study on the aging effect on high-temperature fracture behavior of a polyimide resin matrix has been

conducted first. High-Temperature thermomechanical and notched fracture experiments were conducted on the neat PMR-15 resin and the G30-500/PMR-15 composite. In conjunction with the experiments a thermoelastic crack analysis has been introduced to determine the crack initiation and fracture behavior of the materials at various temperatures and aging times. The fracture toughness of the high-temperature polyimide polymer matrix is found to increase initially in the thermal aging process, but dramatically decrease with the long-term aging time. Increasing the aging temperature during the thermal exposure of the material reduces the material fracture resistance regardless of the aging conditions applied. Quantitative correlations between high-temperature aging parameters and the material fracture resistance of the polyimide polymer have been established. Research results derived from this study have been reported in the attached report entitled, "Effects of Aging on High-Temperature Fracture of Polyimide Polymers."

4. ACCOMPLISHMENTS AND NEW FINDINGS

1. In conjunction with Dr. R. Dutton and his colleagues at AFML, a novel processing method has been developed for fabrication of high-quality, continuous SiC-fiber reinforced glass-matrix composites. Optimal processing parameters have been determined for construction of CMC panels with desired microstructures. The short processing time required and its operational simplicity may render the processing method for high-speed production of large quantity of CMC's with different geometry.

4 The high-temperature microscopic fiber/matrix interface property test system constructed in this project is among the first of its kind with a testing temperature capability ranging from room temperature up to 2,200°F. This apparatus enables us to conduct various *in-situ elevated-temperature* fiber/matrix interface strength, stiffness and other related microscopic expeiriments for evaluation of composite interface degradation with almost unlimited capabilities on different CMC's in selected thermal environments.

3. The current study which combines the high-temperature microscopic experiment and micromechanics analysis of fiber/matrix interface properties in a CMC composite is the first to provide high-temperature interface strength and their degradation data as well as other related information. The long-standing controversial issue on high-temperature fiber/matrix interface degradation and damage, and their effects on CMC toughening mechanics may now be rationally examined rigorously with the device constructed and the method of analysis developed here.

5 The experimental system assembled in the project for elevated-temperature creep damage and fracture experiments provides a unique facility with a significant capability to assist the comprehensive high-temperature mechanics study on micromechanics of inelastic deformation and damage mechanisms in a CMC under long-term, coupled thermal and mechanical loading.

5. The development of a homogenization theory for high-temperature inelastic creep deformation in CMC composites has been completed. The theory and associated computational-mechanics algorithm are able to take account of the creeping matrix and fiber phases with distributed damage and various fiber/matrix interface conditions in the CMCs. The theoretical/computational development has been validated by conducting the high-temperature creep experiments on selected CMC's. The results obtained from the experiments are compared well with the high-temperature micromechanics homogenization solution for the problem.

6. The high-temperature crack growth experiments on the Nicalon/7740 glass CMC provide an important insight into the micromechanisms responsible for subcritical crack initiation and multiple crack growth at elevated temperatures. Also, the associated high-temperature crack mechanics modeling and analysis give the first information of elevated-temperature resistance curves for multiple crack-tip damage growth in the silicon carbide fiber reinforced glass-matrix composite.

7. The study in the current project on high-temperature mechanics and degradation of carbon-fiber reinforced polyimide-matrix composites is believed to be the first one in the world to address the combined effect of high-temperature oxidation, coupled chemical and physical aging, and viscoelastic damage and creep deformation in advanced PMC's.

8. Thermal oxidation in the G30-500/PMR-15 composite was found to be strongly anisotropic and governed by a reaction-controlled (in contrast to a diffusion-controlled) mechanism. The high-temperature oxidation reaction rate at the fiber-matrix interface is further found to be at least eight times higher than that in the polyimide matrix. Micromechanics models, involving oxidation reactions both in the matrix and along the fiber matrix interface, have been constructed for accurate evaluation of the high-temperature oxidation in the composites.

9. A theory, based on the well-known polymer free-volume concept and the kinetic theory of crosslinking reactions in an amorphous thermoset polymer, has been formulated for predicting the combined physical and chemical aging in the polyimide-matrix composites under long-term, high-temperature exposure. Elevated temperature experiments conducted on both G30-500/PMR-15 and IM7/Avimid N composites up to 750°F have shown various unique features of long-term aging of the composites in high-temperature environments.

10. The high-temperature oxidation and aging induced changes in the microstructure and physical and chemical properties of the polymer composite also affect its long-term deformation and damage resistance. In conjunction with the experiments, a new viscoelastic theory has been developed for the polymer composite system to include the coupled effect of thermal oxidation and physical and chemical aging on its high-temperature creep deformation and stress relaxation under long-term thermomechanical loading. Experimental results obtained have been compared well with the theoretical solution derived from the high-temperature composite viscoelastic theory.

5. PERSONNEL SUPPORTED

The following graduate students and post-doctoral research associates with advanced training and background in solid mechanics, ceramics, and materials science were actively participating in the project during the course of the study:

S. S. Wang,	Professor,	Mechanical Engineering
Akira Miyase,	Research Asso. Professor,	Mechanical Engineering
Metin. Karayaka#,	Research Associate,	Mechanical Engineering;
Arne Skontorp*,	Graduate Research Assistant,	Materials Engineering;
S. A. Swan§,	Graduate Research Assistant,	Mechanical Engineering;
Hiroshi Suzuki**,	Visiting Research Associate,	Mechanical Engineering;
M.S. Wong,	Research Scientist,	Mechanical Engineering
Y. S. Yuan+,	Graduate Research Assistant,	Mechanical Engineering
T. P. Yu,	Research Associate,	Mechanical Engineering

Now with Aker Engineering, Houston, TX

* Now with Swedish Aeronautical Research laboratory, Stockholm, Sweden

§ Now with NASA Johnson Space Center, Houston, TX

** Now returned to Tohoku University, Sendai, Japan

+ Now with Baker Hughes Oil Tools Company, Houston, TX

6. PUBLICATIONS

A. Skontorp, Y. Shibuya and S. S. Wang, "High-Temperature Viscoelastic Creep Constitutive Equations for Polymer Composites: Homogenization Theory and Experiments," in *Proceedings of the 9th American Society for Composites Annual Conference*, Newark, DE, September 1994, pp. 433-441.

A. Skontorp and S. S. Wang, "High-Temperature Creep with Physical and Chemical Aging, and Associated Viscoelastic Constitutive Equations of Polyimide Matrix Composites," in *Recent Advances in Composite Materials*, S. R. White, H.T. Hahn and W. F. Jones, Eds, ASME MD Vol.56, American Society of Mechanical Engineers, New York, June 1995, pp. 57-70.

H.K. Kung, A. Skontorp and S. S. Wang, "High-Temperature Physical and Chemical Aging in Carbon Fiber Reinforced Polyimide Composites: Experiments and Theory," *in Recent Advances in Composite Materials*, S. R. White, H.T. Hahn and W. F. Jones, ASME MD Vol. 56, American Society of Mechanical Engineers, New York, June 1995, pp. 193-202.

A. Skontorp, M.S. Wong and S. S. Wang, "High-Temperature Anisotropic Oxidation of Carbon Fiber Reinforced Composites," *Proceedings of the Tenth International Conference on Composite Materials (ICCM-X),* A. Poursartip and K. Street, Eds., Woodhead Publishing Ltd., Cambridge, U.K., Vol. 6, 1995, pp. 375-384.

M. S. Wong and S. S. Wang, "A Processing and Microstructure Study of SiC Fiber Reinforced Glass Matrix Composites," *21st Annual Cocoa Beach Conference and Exposition, (Paper No.: C-0065-97F),* The American Ceramic Society, January 1997.

S. S. Wang, M. Karayaka and H. Suzuki, "High-Temperature Fiber-Matrix Interface Degradation in Silicon Carbide Fiber Reinforced Ceramic Matrix Composites: Experiments

and Micromechanics Analysis," *21st Annual Cocoa Beach Conference and Exposition, (Paper No.: C-0110-97F),* The American Ceramic Society, January 1997.

Akira Miyase, T. P. Yu, and S. S. Wang, "High-Temperature Creep Deformation in Silicon Carbide Fiber (SCS6) Reinforced Glass-Matrix Composite," *21st Annual Cocoa Beach Conference and Exposition, (Paper No.: C-0081-97F),* The American Ceramic Society, January 1997.

M. Karayaka, T.P. Yu and S. S. Wang, "Elevated Temperature Crack Growth and Fracture in Silicon Carbide Fiber Reinforced Glass-Matrix Composite," *21st Annual Cocoa Beach Conference and Exposition, (Paper No.: C-0082-97F),* The American Ceramic Society, January 1997.

S. A. Swan, "Effect of Aging on High-Temperature Fracture of Polyimide Polymers," M.S. Thesis, Department of Mechanical Engineering, University of Houston, Houston, TX, December 1997.

Y. Yuan and S. S. Wang, "High-Temperature Thermoelastic Constitutive Theories for Random Whisker-Reinforced Ceramic Composites Under Large Temperature Change," Technical Report, Department of Mechanical Engineering, University of Houston, TX, 1998.

Y. Yuan and S. S. Wang, "Estimation of Temperature Transversely Isotropic Thermoelastic Properties of Single Crystal SiC Whiskers," *in International Conference on Engineering and Technological Sciences 2000 – International Symposium on Advanced Materials (ICET 2000-ISAM),* Bejing, China, October 2000.

7. INTERACTIONS AND TRANSITIONS

(i). Participation/presentations at meetings, conference and seminars.

"High-Temperature Durability of Carbon-Fiber/Polyimide Matrix Composites: Theories and Experiments," Seminar given at U.S. Air Force Materials Laboratories, Wright-Patterson AFB, OH, July 26-27, 1995.

"High-Temperature Thermal Oxidation, Aging, Creep Damage and Their Interactions in Carbon-Fiber Reinforced Composites," invited General Lecture in the 8th International Conference on Durability Analysis of Composites Systems, Brussels, Belgium, July 18-21, 1995.

"High-Temperature Creep with Physical and Chemical Aging, and Associated Viscoelastic Constitutive Equations of Polyimide Matrix Composites," Presentation in Symposium on Recent Advances in Composite Materials, 1995 Joint ASME Applied Mechanics and Materials Summer Meeting, UCLA, Los Angeles, CA, June 28-30, 1995.

"High-Temperature Anisotropic Thermal Oxidation in Carbon Fiber Composites," Invited Lecture in the Tenth International Conference on Composite Materials (ICCM-X), Whistler, Vancouver, British Columbia, Canada, August 14-18, 1995.

"High-Temperature Fiber Composites: Chemical, Physical and Mechanical Effects on Long-Term Durability," Special Seminar to Materials Division and Engineering Mechanics Division, NASA Langley Research Center, Hampton, VA, October 25-26, 1995.

"High-Temperature Mechanics and Thermomechanical Behavior of Fiber Composite Materials," Mechanical Engineering Department Colloquia, Washington State University, Pullman, WA, February 24-25, 1996.

NSF Institute of Mechanics (UC San Diego) Meeting on *Development of Experimental Mechanics*, University of Houston, March 1996.

"A Processing and Microstructure Study of SiC Fiber Reinforced Glass Matrix Composites," Paper presentation in the *21st Annual Cocoa Beach Conference and Exposition, (Paper No.: C-0065-97F),* The American Ceramic Society, January 1997.

"High-Temperature Fiber-Matrix Interface Degradation in Silicon Carbide Fiber Reinforced Ceramic Matrix Composites: Experiments and Micromechanics Analysis," Paper presentation in the *21st Annual Cocoa Beach Conference and Exposition, (Paper No.: C-0110-97F),* The American Ceramic Society, January 1997.

"High-Temperature Creep Deformation in Silicon Carbide Fiber (SCS6) Reinforced Glass-Matrix Composite," Paper presentation in the *21st Annual Cocoa Beach Conference and Exposition, (Paper No.: C-0081-97F),* The American Ceramic Society, January 1997.

"Elevated-Temperature Crack Growth and Fracture in Silicon Carbide Fiber Reinforced Glass-Matrix Composite," Paper presentation in the *21st Annual Cocoa Beach Conference and Exposition, (Paper No.: C-0082-97F),* The American Ceramic Society, January 1997.

"High-Temperature Micromechanics and Mechanisms of Damage and Failure in Ceramic Matrix Composites," Presentation in AFOSR Mechanics and Materials Program Annual Review, Dallas, TX, November 19-20, 1997.

(ii) Consultative and Advisory Functions

Consultant to Materials Division, NASA Langley Research Center, Hampton, VA, for High-Temperature Composite Materials Development, 1996-98.

Consultant to Amoco and Conoco, Houston, TX, for High-Temperature Composites Applications for Hydrocarbon Production Offshore, 1997-98.

Program Development Committee, for Advanced Materials and Chemicals, U.S. Department of Commerce - Advanced Technology Program, 1998-99.

(iii). Transitions

None.

8. NEW DISCOVERIES, INNOVATIONS & PATENT DISCLOSURES

None.

9. HONORS AND AWARDS

General Lecturer, The 8th International Conference on Durability Analysis of Composite Systems, Brussels, Belgium, July 18, 1995.

Exxon Foundation Award on Composite Engineering Education, Exxon Education Foundation, Houston, TX, June 15, 1995

1995 -96 Du Pont Award on Education, Du Pont Foundation, Wilmington, DE, May 31, 1995.

CMOO-2 Award for Outstanding Leadership and Technical Achievement, Houston, TX, October 28-31, 1997.

Shell Foundation Award, Houston, TX, 1997 and 1998.

Keynote Lecturer, The 3rd International Conference on Materials Engineering for Resources (ICMR-3), Akita, Japan, October 26-28, 1998.

Distinguished Lecturer, The 22nd National Theoretical and Applied Mechanics Conference, December 118-20, 1998

Distinguished Alumni Award, National Cheng-Kung University Alumni Foundation, Washington, D.C., Aprii 21, 1999

Appendices

1. Estimation of Temperature-Dependent Transversely Isotropic Thermoelastic Properties of Single-Crystal SiC Whiskers*

2. High-Temperature Thermoelastic Constitutive Theories for Random Whisker-Reinforced Ceramic Composites Under Large Temperature Change

3. Effects of Aging on High-Temperature Fracture of Polyimide Polymers

Estimation of Temperature-Dependent Transversely Isotropic Thermoelastic Properties of Single-Crystal SiC Whiskers*

Y. S. Yuan and S. S. Wang
Department of Mechanical Engineering, University of Houston, Houston, Texas 77204-4792, U. S. A.

Silicon carbide (SiC) whiskers are recently utilized as a common reinforcement material for advanced high-temperature metal- and ceramic-matrix composites owing to their outstanding mechanical properties and thermal stability at elevated temperatures. Clear understanding of thermomechanical properties of the whiskers at elevated temperatures is obviously essential. Single-crystal SiC whiskers are generally very small in size with anisotropic elastic properties. Experimental determination of the temperature-dependent, anisotropic thermoelastic properties of the whiskers has not been reported, to the authors' knowledge. In this paper, thermoelastic properties of a cubic-single-crystal SiC whisker are studied with consideration of their transverse isotropy in the plane perpendicular to the symmetric major axis of the whisker. Theoretical evaluation of the transversely isotropic thermoelastic properties of the whiskers is conducted, based on the temperature-dependent elastic properties of a cubic SiC single crystal. A complete set of transversely isotropic elastic properties (five elastic constants) of the cubic-single-crystal SiC whisker is reported in the paper for the temperature range from room temperature to 1,500 °C.
Keywords: Silicon Carbide Whisker; Silicon Carbide Cubic Crystal; Thermoelastic Properties; Transversely Isotropic Elastic Properties.

1. Introduction

Silicon carbide (SiC) fibers and whiskers are recently utilized as common reinforcement materials for advanced high-temperature metal- and ceramic-matrix composites owing to their outstanding mechanical properties and thermal stability at elevated temperatures [1-4]. Clear understanding of the thermomechanical properties of these reinforcements at elevated temperatures is essential for the future development of advanced metal-matrix and ceramic-matrix composites. Continuous SiC fibers, for example, the Nicalon fiber, possess polycrystalline microstructures which lead to isotropic thermoelastic properties. The isotropic thermoelastic properties of a Nicalon fiber have been determined experimentally by several researchers [5,4]. The SiC whiskers, however, are generally very small single-crystal filaments, typically 0.1 to several μm in diameter and 20 to 1000 in aspect ratio, with anisotropic thermoelastic properties. Experimental determination of the anisotropic thermoelastic properties for such whiskers is not an easy task. Searching through the open literature we can find only measured room-temperature tensile moduli in a range of 360 to 800 GPa by Op Het Veld, et al. [3] and Petrovic, et al.[4]. A complete set of anisotropic elastic properties of the SiC whiskers has not been reported, to the authors' knowledge, not to mention their temperature-dependence at elevated temperatures. In this paper, thermoelastic properties of a cubic single-crystal SiC whisker are studied with consideration of their transverse isotropy in the plane perpendicular to the symmetric major axis of the whisker. Theoretical evaluation of the transversely isotropic thermoelastic properties of the whiskers is conducted, based on the temperature-dependent elastic properties of a cubic SiC single crystal. A complete set of transversely isotropic elastic properties (five elastic constants) of the cubic-single-crystal SiC whiskers is reported in the paper for the temperature range from room temperature to 1,500 °C.

2. Basic and Formulation

SiC whiskers are commonly in a single-crystal filament form [3]. A single-crystal SiC exists in several crystalline forms, known as polytypes. Among these SiC polytypes, the cubic crystal (β-SiC) and the hexagonal crystal (α-SiC) are the most common ones [6, 7]. The β-SiC crystal is considered to be an unstable phase that can exist at all temperatures below the melting point, and may transform slowly to the α-SiC phase above 1650 °C [7]. The cubic (β) SiC crystal can be prepared at much lower temperatures (1200 to 2000 °C) than a hexagonal (α) crystal (2200 to 2500 °C)[8]. For this reason, most single-crystal SiC whiskers available for reinforcement are cubic (β) SiC [9-14], although some α-SiC whiskers are reported also [15,16].

The cubic SiC whiskers can be synthesized by numerous methods. Among those methods, the carbothermal reduction of SiO_2, or the vapor-liquid-solid (VLS) process [9-14], is the most popular one, which has been considered to be a continuous process for commercial production [11, 14]. The crystalline phase of a single-crystal SiC whisker produced has been examined by X-ray diffraction, and identified to be purely or predominantly

* The work reported here was supported in part by U.S. Air Force Office of Scientific Research (Grant No.: F49620-95-10204).

cubic (β) phase [9-14]. It has been also identified by XRD and TEM that the whisker axial direction, i.e., the whisker growth direction, coincides with the [111] direction of the cubic SiC crystals in the whisker [4,12,13], as illustrated in Fig. 1. In the Fig. 1, the coordinate system (x'_1, x'_2, x'_3) denotes the cubic lattice system, and the $(\tilde{x}_1, \tilde{x}_2, \tilde{x}_3)$ denotes the whisker principal material system with $\tilde{x}_1$ being the major symmetric axis of the whisker.

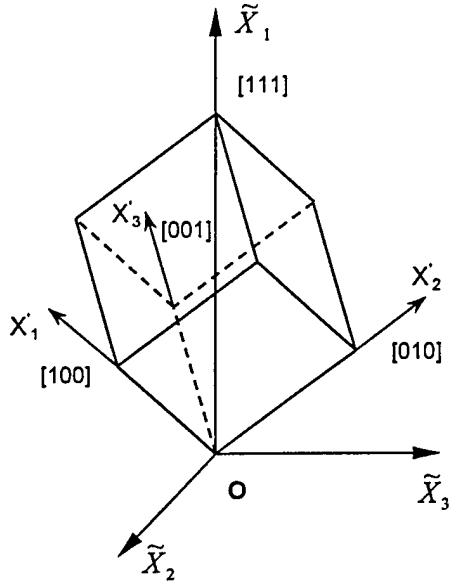

Fig. 1 Lattice structure of cubic SiC crystal and its orientation in a SiC whisker, where $\tilde{X}_1$ denotes the whisker major axial direction.

The anisotropic elastic properties of a cubic crystal, referred to (x'_1, x'_2, x'_3) coordinates, can be described by three independent stiffness constants, C'_{11}, C'_{12} and C'_{44}, or three compliance constants, S'_{11}, S'_{12} and S'_{44}. The relationships between C'_{ij} and S'_{ij} are [17]

$$S'_{11} = (C'_{11}+C'_{12})/(C'_{11}-C'_{12})(C'_{11}+2C'_{12}), \quad (1a)$$

$$S'_{12} = -C'_{12}/(C'_{11}-C'_{12})(C'_{11}+2C'_{12}), \quad (1b)$$

$$S'_{44} = 1/C'_{44}. \quad (1c)$$

According to Turley[18], the anisotropic Young's modulus, shear modulus and Poisson's ratio referred to an arbitrary coordinate system (x_1, x_2, x_3) in the cubic crystal with its lattice system (x'_1, x'_2, x'_3), as shown in Fig. 2 (similar to the Fig. 1 of Turley's), can be determined from the compliance constants of the cubic crystal, S'_{11}, S'_{12} and S'_{44}, as follows:

$$E_{11} = 1/(S'_{12}+\frac{1}{2}S'_{44}+\alpha\Omega_{11}), \quad (2a)$$

$$\mu_{12} = 1/(S'_{44}+4\alpha\Omega_{12}), \quad (2b)$$

$$\mu_{23} = 1/(S'_{44}+4\alpha\Omega_{23}), \quad (2c)$$

$$\nu_{12} = -(S'_{12}+\alpha\Omega_{12})/(S'_{12}+\frac{1}{2}S'_{44}+\alpha\Omega_{11}), \quad (2d)$$

where $\alpha = S'_{11} - S'_{12} - (1/2)\,S'_{44}$, and Ω_{ij} are orientation parameters of the system (x_1, x_2, x_3) related to the system (x'_1, x'_2, x'_3), as functions of the Eulerian angles (α, β, θ), which are defined in Turley's paper [18]. If the [111] direction of the cubic crystal is taken as the x_1 direction [*hkl*] of the arbitrary coordinate system (x_1, x_2, x_3), then the Eulerian angles, α and β, will be defined or fixed, and the system (x_1, x_2, x_3) can only rotate around the x_1 axis with a varied angle θ, referred to Fig. 2. It is found in this case that the orientation parameters, Ω_{ij}, in equations (2a) to (2d) become constants, i.e., $\Omega_{11}=1/3$, $\Omega_{22}=1/2$, $\Omega_{12}=1/3$, and $\Omega_{23}=1/6$, which are independent of the Eulerian angle θ. Consequently, the anisotropic elastic properties of the cubic crystal, E_{11}, μ_{12}, μ_{23} and ν_{12} with respect to the specified coordinate system (x_1, x_2, x_3) are also independent of θ, according to Equations (2a) to (2d). This results in a conclusion that if the [111] direction of a cubic crystal is taken as the principal material axis, the crystal will then reveal a transverse isotropy with the major symmetric axis coinciding the [111] direction of the crystal.

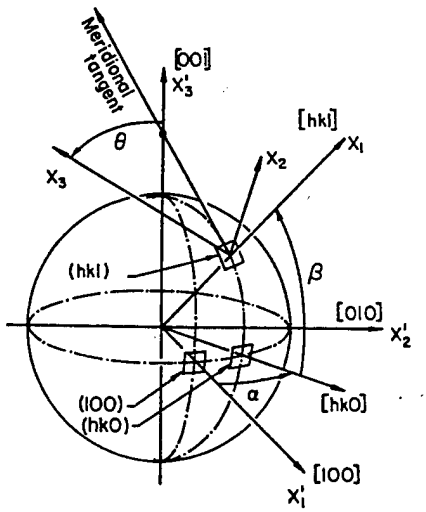

Fig. 2 An arbitrary coordinate system (x_1, x_2, x_3) with Eulerian angles (α, β, θ) referred to a cubic lattice system $(x'_1 x'_2, x'_3)$.

For a SiC whisker constructed by SiC cubic crystals aligned with their [111] directions in the whisker axial direction, it is reasonable to treat the elastic properties of the whisker as transversely isotropic with the isotropic plane perpendicular to the major symmetric axis $\tilde{x}_1$ of the whisker, where the coordinate system $(\tilde{x}_1, \tilde{x}_2, \tilde{x}_3)$, in Fig. 1, is the principal material axes of the whisker. In whisker material coordinate, we treat the cubic-SiC whisker different from a SiC cubic crystal since they possess different material symmetries. Elastic properties between a

transversely isotropic, cubic-SiC whisker and a SiC cubic crystal are related. In this paper, a complete set of the transversely isotropic elastic constants of the SiC whisker is estimated based on the elastic properties of the SiC cubic crystal.

It is known that the transversely isotropic elastic properties of a SiC whisker can be defined by five independent stiffness constants, $\tilde{C}_{11}, \tilde{C}_{12}, \tilde{C}_{22}, \tilde{C}_{23}$ and $\tilde{C}_{66}$. The relationships between the stiffness constants and engineering constants of a transversely isotropic body can be expressed as [19]:

$$\tilde{C}_{11} = \tilde{E}_{11} + 4\,\tilde{\nu}_{12}^{2}\,\tilde{\kappa}_{23}, \tag{3a}$$

$$\tilde{C}_{12} = 2\,\tilde{\kappa}_{23}\,\tilde{\nu}_{12}, \tag{3b}$$

$$\tilde{C}_{22} = \tilde{\mu}_{23} + \tilde{\kappa}_{23}, \tag{3c}$$

$$\tilde{C}_{23} = -\,\tilde{\mu}_{23} + \tilde{\kappa}_{23}, \tag{3d}$$

$$\tilde{C}_{66} = \tilde{\mu}_{12}. \tag{3e}$$

The engineering constants of the SiC whisker, $\tilde{E}_{11}$, $\tilde{\mu}_{12}$, $\tilde{\mu}_{23}$ and $\tilde{\nu}_{12}$, except $\tilde{\kappa}_{23}$, the plane-strain bulk modulus of the whisker in plane $\tilde{x}_2\,\tilde{x}_3$, can be determined from equations (2a) to (2d):

$$\tilde{E}_{11} = 3 / (S'_{11} + 2S'_{12} + S'_{44}), \tag{4}$$

$$\tilde{\mu}_{12} = 3 / (4S'_{11} - 4S'_{12} + S'_{44}), \tag{5}$$

$$\tilde{\mu}_{23} = 3 / 2(S'_{11} - S'_{12} + S'_{44}), \tag{6}$$

$$\tilde{\nu}_{12} = -(2S'_{11} + 4S'_{12} - S'_{44}) / 2(S'_{11} + 2S'_{12} + S'_{44}), \tag{7}$$

where, Ω_{11}=1/3, Ω_{12}=1/3, and Ω_{23}=1/6 have been substituted.

Stress-strain relationships of a transversely isotropic body with the major symmetric axis $\tilde{x}_1$ can be generally expressed with the following equations[19]:

$$\sigma_{11} = \tilde{C}_{11}\,\varepsilon_{11} + \tilde{C}_{12}\,\varepsilon_{22} + \tilde{C}_{12}\,\varepsilon_{33}, \tag{8a}$$

$$\sigma_{22} = \tilde{C}_{12}\,\varepsilon_{11} + \tilde{C}_{22}\,\varepsilon_{22} + \tilde{C}_{23}\,\varepsilon_{33}, \tag{8b}$$

$$\sigma_{33} = \tilde{C}_{12}\,\varepsilon_{11} + \tilde{C}_{23}\,\varepsilon_{22} + \tilde{C}_{22}\,\varepsilon_{33}, \tag{8c}$$

$$\sigma_{12} = 2\,\tilde{C}_{66}\,\varepsilon_{12}, \tag{8d}$$

$$\sigma_{23} = (\tilde{C}_{22} - \tilde{C}_{23})\,\varepsilon_{23}, \tag{8e}$$

$$\sigma_{31} = 2\,\tilde{C}_{66}\,\varepsilon_{31}. \tag{8f}$$

To determine $\tilde{\kappa}_{23}$, applying a hydrostatic pressure, σ_{11}= σ_{22}= σ_{33}= σ and σ_{12}= σ_{23}= σ_{31}= 0, to the equations (8a) to (8f) results

$$\tilde{C}_{11}\,\varepsilon_{11} + \tilde{C}_{12}\,\varepsilon_{22} + \tilde{C}_{12}\,\varepsilon_{33} = \sigma, \tag{9a}$$

$$\tilde{C}_{12}\,\varepsilon_{11} + \tilde{C}_{22}\,\varepsilon_{22} + \tilde{C}_{23}\,\varepsilon_{33} = \sigma, \tag{9b}$$

$$\tilde{C}_{12}\,\varepsilon_{11} + \tilde{C}_{23}\,\varepsilon_{22} + \tilde{C}_{22}\,\varepsilon_{33} = \sigma. \tag{9c}$$

Solving equations (9a) to (9c) for ε_{11}, ε_{22} and ε_{33}, the volumetric strain then can be evaluated as

$$e = \varepsilon_{11} + \varepsilon_{22} + \varepsilon_{33} = \frac{2\tilde{C}_{11} + \tilde{C}_{22} + \tilde{C}_{23} - 4\tilde{C}_{12}}{\tilde{C}_{11}(\tilde{C}_{22} + \tilde{C}_{23}) - 2\tilde{C}_{12}^{2}}\sigma \tag{10}$$

Then the bulk modulus of the cubic SiC whisker can be determined as

$$\kappa = \frac{\sigma}{e} = \frac{\tilde{C}_{11}(\tilde{C}_{22} + \tilde{C}_{23}) - 2\tilde{C}_{12}^{2}}{2\tilde{C}_{11} + \tilde{C}_{22} + \tilde{C}_{23} - 4\tilde{C}_{12}}, \tag{11}$$

which is an invariant.

Eliminating $\tilde{\kappa}_{23}$ and solving Equations (3a) to (3e) for $\tilde{E}_{11}$, $\tilde{\nu}_{23}$, $\tilde{\mu}_{12}$ and $\tilde{\mu}_{23}$ we have

$$\tilde{E}_{11} = \tilde{C}_{11} - \frac{2\tilde{C}_{12}^{2}}{\tilde{C}_{22} + \tilde{C}_{23}}, \tag{12a}$$

$$\tilde{\nu}_{12} = \frac{\tilde{C}_{12}}{\tilde{C}_{22} + \tilde{C}_{23}}, \tag{12b}$$

$$\tilde{\mu}_{12} = \tilde{C}_{66}, \tag{12c}$$

$$\tilde{\mu}_{23} = \frac{1}{2}(\tilde{C}_{22} - \tilde{C}_{23}). \tag{12d}$$

Solving Equations (12a) to (12d) with (11) for $\tilde{C}_{11}$, $\tilde{C}_{12}$, $\tilde{C}_{22}$, $\tilde{C}_{23}$, $\tilde{C}_{66}$, and comparing the resulting equations with equations (3a) to (3d), $\tilde{\kappa}_{23}$ can be determined in terms of $\tilde{E}_{11}$, $\tilde{\nu}_{12}$ and κ:

$$\tilde{\kappa}_{23} = -\frac{\kappa \tilde{E}_{11}}{(\kappa - \tilde{E}_{11} - 4\kappa \tilde{\nu}_{12}) + 4\kappa \tilde{\nu}_{12}^2}, \qquad (13)$$

where, the bulk modulus, κ, is an isotropic quantity and identical for both the SiC whisker and the SiC cubic crystal. It can be calculated from the compliance constants of the SiC cubic crystal [17]:

$$\kappa = \frac{1}{3(S'_{11} + 2S'_{12})}. \qquad (14)$$

Following Equations (4) to (7) and (13) with (14), the five independent elastic constants for the transversely isotropic SiC whisker, $\tilde{E}_{11}$, $\tilde{\nu}_{12}$, $\tilde{\mu}_{12}$, $\tilde{\mu}_{23}$ and $\tilde{\kappa}_{23}$, can be evaluated based on the compliance constants, S'_{11}, S'_{12} and S'_{44}, of the SiC cubic crystal.

3. Results and Discussion

As mentioned in Sec. 1, for transversely isotropic elastic properties of the SiC whiskers, only a room temperature, longitudinal tensile modulus, $\tilde{E}_{11}$, has been reported in the literature [3,4]. Based on the thermoelastic constitutive formulation developed in Sec. 2, we now focus on searching the temperature-dependent stiffness constants of the cubic (β) SiC single crystal, C'_{11}, C'_{12} and C'_{44}. Unfortunately, there are no measured data for the SiC cubic crystal available in the open literature, to the authors' knowledge. The major reason resulting in this situation may be the small size (<1mm^3) of the highly pure SiC cubic crystal currently available [20,8]. Tolpygo [21] gives his calculated results of the stiffness constants at room temperature for a cubic (β) SiC single crystal, C'_{11} = 352.3*GPa*, C'_{12} = 140.4 *GPa* and C'_{44} = 232.9 *GPa*, based on a comparison between acoustic vibration equations of the microscopic theory and equations of the macroscopic theory of elasticity. These data have been cited extensively by materials researchers, and good agreements have been obtained in their indirect experimental verification [20,22]. However, the temperature dependence of the stiffness constants at elevated temperatures has not been available for a long time. Recently, Li and Bradt [23] have presented their temperature-dependent stiffness constants, C'_{11}, C'_{12} and C'_{44}, for a SiC cubic crystal from room temperature to 1000 °C, based on Tolpygo's calculated values at room temperature, experimental measurements of temperature-dependent elastic moduli of several cubic SiC polycrystalline aggregates, a linear temperature-dependence assumption of elastic properties in a temperature range above room temperature for both the cubic SiC polycrystalline aggregates and the single crystal, and an averaging approach for estimation of the overall elastic properties of the polycrystalline aggregates. Li and Bradt's temperature-dependent stiffness constant data of the SiC cubic crystal are listed in Table 1. For illustration, in the early research on high-temperature constitutive thermoelastic properties of hot-pressed, SiC whisker-reinforced ceramic composites [24,25], Li and Bradt's data have been extrapolated to 1,700 °C. It is noted that Li and Bradt apply the linear temperature dependence to the stiffness constants of the SiC cubic crystal only up to 1,000 °C, based on certain experimental results of polycrystalline cubic SiC. Above 1,000 °C, this linear assumption may not be valid. To investigate this further, more studies have been conducted. Shaffer and Jun [25] have pointed out that for a high modulus, dense silicon carbides (polycrystalline solids), the presence of even a trace amount of soft phases in the sample material would reduce the observed elastic moduli drastically. A material with impurity may exhibit an entirely different behavior from that of a pure single-phase material, especially at elevated temperatures. Many early experimental data, such as in [26], would be suspected because of the lack of proper data analysis and sample characterization. In Shaffer and Jun's study [25], two SiC sample materials, a highly pure, highly dense, single phase polycrystalline SiC, the Sublimed SiC, and a less pure, dense polycrystalline SiC, the KT-SiC, have been tested. The measured results indicate that Young's modulus of the Sublimed SiC is about 50 GPa higher than that of the KT-SiC at room temperature, and decreases slightly and linearly with temperature up to 1,440 °C. However, the measured Young's modulus of the KT-SiC decreases slightly and linearly with temperature up to about 900 °C, and then shows a change in slope of the modulus-temperature curve at this temperature, indicating a higher modulus-reduction rate above 900 °C. Based on these experimental results for the polycrystalline silicon carbides, we may apply a similar linear temperature-dependence assumption to the stiffness constants of a pure, SiC cubic crystal up to 1,500 °C without losing validity. Based on above study, Li and Bradt's data have been linearly extrapolated to 1,500 °C here. The extrapolated data have been added in Table 1 for the need of high-temperature applications of the single-crystal SiC whiskers.

Table 1 Temperature-Dependent Elastic Properties of Cubic (β) SiC Crystal

T (°C)	C'_{11} (GPa)	C'_{12} (GPa)	C'_{44} (GPa)
25	352.30	140.40	232.90
100	350.33	139.71	232.34
300	345.15	137.40	230.90
500	340.05	134.85	229.50
700	334.95	132.55	228.10
900	329.90	130.30	226.70
1100	324.90	128.10	225.30
1300	319.90	125.90	223.90
1500	314.90	123.70	222.50

Following Equations (4) to (7) and (13) with substitutions of Equations (14), (1a) to (1c), and the data listed in Table 1, the complete temperature-dependent

elastic properties, $\tilde{E}_{11}$, $\tilde{\nu}_{12}$, $\tilde{\mu}_{12}$, $\tilde{\mu}_{23}$ and $\tilde{\kappa}_{23}$, of the SiC whiskers from 25 °C to 1,500 °C can be estimated, which are listed in Table 2, and illustrated in Fig. 3. It is interesting to find from the Fig. 3 that all the elastic constants of the single-crystal SiC whisker, including the Poisson's ratio $\tilde{\nu}_{12}$ in plane $\tilde{x}_1\tilde{x}_2$, decrease with temperature. This behavior is quit different from that in a common isotropic material where, in general, the elastic moduli decrease with the temperature whereas the Poisson's ratio increases with the temperature. This unusual behavior is attributed to the strong elastic anisotropy of the SiC cubic crystal and the increase in elastic anisotropy with the temperature increase, as indicated by Li and Bradt [23]. It is important to know that the elastic properties of a cubic-single-crystal SiC whisker are essentially different from those of a SiC cubic crystal since they have different overall material symmetries. If, in your analysis, a cubic-SiC whisker (five independent stiffness constants) is simply treated as a SiC cubic crystal (three independent stiffness constants) or as an isotropic solid (two independent elastic constants), a large amount of discrepancy may occur.

Table 2 Temperature-Dependent Transversely Isotropic Elastic Properties of SiC Whisker

T (°C)	$\tilde{E}_{11}$ (GPa)	$\tilde{\mu}_{12}$ (GPa)	$\tilde{\mu}_{23}$ (GPa)	$\tilde{\nu}_{12}$	$\tilde{\kappa}_{23}$ (GPa)
25	510.8	129.5	166.4	.09659	288.7
100	509.2	128.8	165.7	.09574	287.4
300	504.7	127.2	164.0	.09294	283.6
500	500.2	125.8	162.5	.08981	279.8
700	495.8	124.2	160.9	.08685	276.1
900	491.4	122.7	159.2	.08388	272.4
1100	487.1	121.1	157.6	.08092	268.8
1300	482.7	119.6	155.9	.07787	265.2
1500	478.3	118.0	154.3	.07473	261.6

To ensure the validity of the current approach, it is necessary to compare the current estimation with existing experimental results. The only measured elastic property of the cubic-single-crystal SiC whiskers currently available is the longitudinal Young's modulus at room temperature, measured by a micro-tensile test technique. The results have been reported to be 530 and 630 *GPa* for two cubic SiC whiskers, respectively, by OP Het Veld and Veldkamp [3], and 578 *GPa* (average value) for 26 cubic SiC whiskers by Petrovic, et al.[4]. The current estimated longitudinal Young's modulus at room temperature is found to be 511*GPa*, according to the calculated transversely isotropic elastic properties of the cubic-SiC whisker, presented in Table 2. Comparing with the above results, we find that the current estimated longitudinal Young's modulus is about 12 % less than the experimental results. Since the data involved in the comparison are at room temperature only and the current calculated longitudinal Young's modulus for the whiskers is based on Tolpygo's data [21] for the stiffness constants of a SiC cubic crystal and Turley's formulation [18] based on a fourth-rank compliance tensor transformation of a cubic single crystal, the discrepancy in the comparison may be resulted from a low estimation of the stiffness constants of the SiC cubic crystal in Tolpygo's work. The same comments have also been given in [4,22]. As mentioned early in this section that Arlt and Schodder [20] have evaluated Tolpygo's data indirectly by a resonance and a double-pulse method for a 6H α-SiC single crystal, and they have given a positive conclusion. This may also imply that some discrepancy may exist between the mechanical test and acoustic test methods. Although a 12 % discrepancy has been found between the current estimation and the measured longitudinal Young's modulus of the cubic-SiC whiskers, the authors consider that the complete, temperature-dependent, transversely isotropic elastic properties of the cubic-SiC whisker presented in this study are still a valuable source for thermomechanical analysis of SiC-whisker-reinforced, high-temperature composite materials due to the lack of measured materials data currently available [24,25]. More importantly, this study gives a general concept with an advanced analytical method to evaluate the transversely isotropic elastic properties of cubic SiC whiskers. If better stiffness constant data, experimental or theoretical, of the SiC cubic crystal are available in the future, the current approach will give an accurate estimation of the elastic properties of the cubic-SiC whiskers.

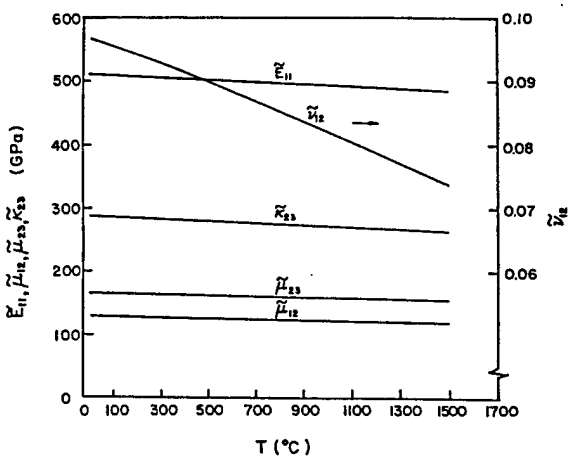

Fig. 3 Temperature-dependent transversely isotropic elastic properties of the cubic-single-crystal SiC whiskers.

4. Summary

Based on information available in the literature on the crystal structure and the stiffness constants of a SiC cubic crystal and its whiskers, and the thermoelastic constitutive formulation for the SiC cubic crystal and the cubic-SiC whisker, elastic properties of the SiC whisker are considered to be transversely isotropic with the isotropic plane perpendicular to the major symmetric axis of the whisker. A complete set of temperature-dependent, transversely isotropic elastic properties of the cubic-SiC

whisker has been estimated from room temperature to 1,500 °C.. Compared with the measured room-temperature longitudinal Young's modulus of the whisker, the authors consider that this estimation is a valuable source of the SiC- whisker elastic properties for thermomechanical analysis of SiC-whisker-reinforced, high-temperature composite materials. This study also gives a general concept with an advanced analytical method to evaluate the transversely isotropic elastic properties of cubic SiC whiskers.

ACKNOWLEDGMENT

The authors are indebted to Professor Z. Hashin of Tel Aviv University and Professor J. Homeny of University of Illinois at Urbana-Champaign for their comments and discussion during the course of this study.

REFERENCES

1 M. Taya and R. J. Arsenault: *Metal Matrix Composites*, Chap. 1, Pergamon Press, Oxford, 1989.
2 G. G. Wei and P. F. Becher: *Amer. Ceram. Soc. Bull.*, 1985, **64**(2), 298.
3 A. J. G. OP Het Veld and J. D. B. Veldkamp:*Fiber Sci. Technol.* , 1970, **2**, 269.
4 J. J. Petrovic, J. V. Milewski, D. L. Rohr and F. D. Gac:*J. Mater. Sci.*, 1985, **20**, 1167.
5 G. Simon and A. R. Bunsell:*J. Mater. Sci.*, 1984, **19**, 3649.
6 P. T. B. Shaffer:*Acta Cryst. (B)*, 1969, **B25**, 477.
7 J. F. Lynch, C. G. Ruderer and W. H. Duckworth:*Engineering Properties of Selected Ceramic Materials*,The Amer. Ceram. Soc., Columbus, OH, 1966, Chap. 5.2.0.
8 S. N. Gorin and L. M. Ivanova: *phys. stat. sol. (b)*, 1997**202**, 221
9 R. S. Wagner and W. C. Ellis: Appl. Phys. Lett., 1964**4** (5), 89.
10 G. A. Bootsma, W. F. Knippenberg and G. Verspui: *J. Cryst. Growth*, 1971, 11, 297.
11 J. V. Milewski, F. D. Gac, J. J. Petrovic and S. R. Skaggs: *J. Mater. Sci.*, 1985, **20**,1160.
12 L. Wang and H. Wada:*J. Mater. Res.*, 1992,**7**(1), 148.
13 G. Urretavizcaya and J. M. Porto Lopez:*J. Mater. Res.*, 1994, **9** (11), 2981.
14 H. J. Choi and J. G. Lee:*J. Mater. Sci.*, 1995, **30**, 1982.
15 W. F. Knippenberg and G. Verspui: in*Silocon Carbide-1992*, edited by R. C. Marshall, J. W. Faust Jr. and C. E. Ryan, University of South Carolina Press, 1973, 108.
16 J. Homeny, W. L. Vaughn and M. K. Ferber:*Amer. Ceram. Soc. Bull.*, 1987, **66**(2), 333.
17 G. Grimvall: *Thermophysical Properties of Materials*, Chap. 3, North Holland, Amsterdam, 1986.
18 J. Turley and G. Sines:*J. Phys. D: Appl. Phys.*, 1971,**4**, 264.
19 R. M. Christensen: *Mechanics of Composite Materials*, Chap. 4, Wiley-Interscience, New York, 1979.
20 G. Arlt and G. R. Schodder: *J.Acoust. Soc. Amer.*, 1965, **37**, 384.
21 K. B. Tolpygo: *Soviet Physics-Solid State*, 1960, **2**, 2367.
22 B. P. Pandey and B. Dayal:*Phys. Stat. Sol. (b)*, 1973, **58**, K53.
23 Z. Li. and R. C. Bradt:*J. Mater. Sci.*, 1987, **22**, 2557.
24 Y. S. Yuan and S. S. Wang: unpublished research report , 1989.
25 Y. S. Yuan and S. S. Wang: unpublished research report, 1989.
26 P. T. B. Shaffer and C. K. Jun:*Mater. Res. Bull.*, 1972,**7**, 63.
27 J. B. Wachtman, Jr. and D. G. Lam, Jr.:*J. Amer. Ceram. Soc.*, 1959, **42**, 254.

Contract Technical Report
CEAC-CR-98-0104

HIGH-TEMPERATURE THERMOELASTIC CONSTITUTIVE THEORIES FOR RANDOM WHISKER-REINFORCED CERAMIC COMPOSITES UNDER LARGE TEMPERATURE CHANGE

by

Y. S. Yuan* and S. S. Wang**
Department of Mechanical Engineering, and
Composites Engineering and Applications Center
University of Houston
Houston, TX 77024-0903

Technical Report for Aerospace Sciences Directorate,
U.S. Air Force Office of Scientific Research,
Bolling AFB, Washington, D. C.

Contract No.: F49620-1-00204

---

* Graduate Research Assistant,
** Professor of Mechanical Engineering and Director CEAC

ABSTRACT

A high-temperature effective thermoelastic constitutive theory has been developed for a randomly oriented, whisker-reinforced ceramic composite system under a large temperature change. Starting from a nonlinear thermoelasticity consideration, basic thermoelastic constitutive equations for a monolithic ceramic solid under a large temperature change are obtained and extended to statistically homogeneous, anisotropic ceramic composites. Effective thermoelastic properties of a 3-D random whisker ceramic composite under a large temperature change are determined by using several micromechanics approaches. Results obtained from the self-consistent scheme and the differential analysis show that effective elastic properties of the ceramic composite under a large temperature change are independent of thermal expansion mismatch between the constituents. Consequently, the basic effective thermoelastic constitutive equations for a ceramic composite under a large temperature change are uncoupled, and may be treated by superposition of a pure nonisothermal (uniform temperature change) process and an isothermal mechanical process. An alternative approach for determining effective thermal expansion coefficients of a ceramic composite under a large temperature change is conducted by proper modifications of Levin-Hashin's solution. Systematic numerical studies of effects of material and microstructural parameters, e.g., volume fraction, aspect ratio of the whiskers, and temperature-dependent constituent properties, on effective thermoelastic properties of a SiC-whisker/Al_2O_3-matrix composite system under a large temperature change are conducted, and detailed results are given in the paper.

1. INTRODUCTION

It is well known that classical linear thermoelasticity (LTE) for a homogeneous, monolithic solid restricts itself to the cases of small strains and temperature changes, and assumes material thermoelastic properties (TEP) under a small temperature change to be constant at a reference temperature. Recently developed linear effective thermoelastic constitutive theories for heterogeneous composites, based on various averaging schemes, for example, the direct approach (DA), the self-consistent scheme (SCS) and the differential scheme (DS), can only predict effective TEP of a statistically homogeneous (SH) system at or near the reference temperature. These theories may not be adequate to describe the temperature-dependent nature of the effective TEP of the composite subjected to a large temperature change (LTC) (Yuan and Wang, 1998 a). The concept prevalent in linear effective thermoelastic constitutive theories that the composite effective elastic properties are independent of thermal expansion mismatch between constituent materials due to a small temperature change appears to be valid since linear effective thermoelastic constitutive theories predict effective elastic properties of the composite on the basis of an isothermal mechanical process at the reference temperature. Complications may be developed when the heterogeneous composite is in a high-temperature environment with large temperature changes.

Recent advances in high-temperature ceramic-matrix composites (CMC) require stringent analysis and design considerations of various CMC systems operating at extremely high temperatures and undergoing large temperature traverses. For example, a hot-pressed SiC-whisker reinforced CMC is generally fabricated at about 1800 °C (Wei and Becher, 1985) and commonly experiences in service a wide range of temperature changes from room temperature to 1500 °C, or even more severe environments. Theoretical predictions and experimental measurements of effective TEP of the composite at elevated temperatures and their associated temperature dependence are critically important in future developments and applications of advanced CMC systems.

It is obvious that, in the evaluation of effective composite TEP undergoing a LTC, the TEP of the material system may no longer be assumed to be constant. Thus, the linear thermoelastic constitutive equations previously discussed (Yuan and Wang, 1998 a) may not be valid, and the effective elastic properties of a composite at certain operating temperatures may no longer be determined by taking an isothermal process at the initial reference temperature. More importantly, it is not clear if effective elastic properties of the composite can be evaluated on the basis of an isothermal process at the operating temperature. The concern of severe internal microscopic thermal stresses in the heterogeneous composite caused by the LTC may introduce additional complexities. Furthermore, the well known fact that effective elastic properties are coupled with the effective thermal expansion coefficients which are highly dependent on thermal expansion mismatch between constituent materials may lead to further complications of the LTC problem.

To establish a rigorous theory for determining effective thermoelastic constitutive properties for a CMC material under a LTC, basic thermoelastic constitutive equation for a heterogeneous composite must be reconstructed. The temperature-dependent nature of constituent TEP and the effect of thermal expansion mismatch between constituent

materials must be taken into consideration in determining effective TEP of the composite under a LTC, especially for composites with various phase materials, interface states and microstructures.

A brief literature review on linear effective thermoelastic constitutive theories for heterogeneous composites is given in an accompanying paper (Yuan and Wang, 1998 a). However, to the authors' knowledge, a systematic study of effective thermoelastic constitutive theory for advanced high-temperature CMC composites subjected to a LTC is not available. Recently, Hashin (1984) has conducted a study on effective thermoelastic constitutive equations for determining thermal expansion of polycrystalline aggregates with temperature-dependent constituent properties. A linear, uncoupled effective stress-strain relationship is assumed. The influence of microstructural parameters and microscopic internal state variables on effective composite thermoelastic properties is not discussed in the brief formulation. Limitations and validity of the formulation to actual ceramic material systems subjected to large temperature traverse are not addressed.

The objectives of this research are to: (1) construct thermoelastic constitutive equations for a general homogeneous ceramic material under a LTC, and extend this theory to a SH anisotropic ceramic composite; (2) determine effective TEP of a CMC with random whisker distribution under a LTC using various micromechanics averaging schemes; (3) illustrate fundamental characteristics of the CMC by examining effective TEP of a hot-pressed, SiC-whisker/Al_2O_3-matrix composite under a LTC; (4) study the effect of thermal expansion mismatch between constituent materials on effective properties of the composite under LTC; and (5) analyze effects of constituent-modulus ratio, volume fraction, temperature change and whisker geometry on effective TEP of the composite under LTC.

In this study, a general theory is developed for a ceramic composite with randomly oriented, transversely isotropic whiskers and an isotropic ceramic matrix subjected to a LTC. In the next section, thermoelastic constitutive equations for a general homogeneous ceramic material under a LTC are constructed and extended to SH anisotropic ceramic composites. Effective TEP of a ceramic composite with 3-D randomly oriented whiskers are formulated and determined by the DA, SCS and DS in Sec. 3. Important additional remarks to effective thermoelastic constitutive theory with a LTC are presented of the composite under a LTC is proposed in Sec. 5. Systematic studies of the effects of material and microstructural parameters on effective TEP for a hot-pressed. SiC-whisker/Al2O3-matrix composite system under a LTC are conducted, while the numerical results and discussion are presented in Sec. 6. Finally, important conclusions are presented in Sec. 7.

2. BASIC GOVERNING EQUATIONS FOR THERMOELASTICITY WITH LTC

To establish an effective thermoelastic constitutive theory for a composite undergone a LTC, basic governing equations, the thermoelastic constitutive equations for a homogeneous monolithic solid under a LTC, must be constructed first. Then extension to a SH composite can be made by introducing the effective TEP concept for the composite and the volume average scheme for state variable.

2.1 Thermoelastic Constitutive Equations for Homogeneous Solids under LTC

To construct thermoelastic stress-strain relations of a homogeneous solid under a LTC, the following stress-strain relations of a homogeneous solid under a LTC, the following stress-strain laws of nonlinear thermoelasticity discussed by D. E. Carlson (1984) are used:

$$\mathbf{S} = \mathbf{F}\,\tilde{S}(\mathbf{D},T) \tag{2.1}$$

with

$$\mathbf{F} = \mathbf{1} + \nabla\mathbf{u}, \qquad \mathbf{D} = \frac{1}{2}\,(\mathbf{F}^T\mathbf{F} - \mathbf{1}) \tag{2.2a, b}$$

where $\mathbf{S}$ is a stress tensor, $\mathbf{F}$, a deformation gradient, $\mathbf{D}$, a finite strain tensor, $\mathbf{u}$, a displacement vector; T, the absolute operating temperature, and ∇, a gradient operator.

In present thermoelasticity, the following basic assumptions are introduced:

(1) $|\nabla\mathbf{u}|, |\nabla\dot{\mathbf{u}}|, |\dot{T}| \le \delta$, where δ is small, and the dot denotes a rate change.

(2) The temperature change, $|T-T_0|$, from a reference temperature (T_0) is uniform within the body, but not small (may be large) in the present problem.

(3) The initial state of the solid in a uniform temperature field (T_0) is taken as a reference state and is stress-free.

Based on equations (2.1), (2.2a, b) and the assumptions (1) and (3), and with the aid of Taylor's expansion of $\tilde{\mathbf{S}}(\mathbf{D},T)$ at $\mathbf{D} = \mathbf{0}$ and T (an arbitrary operating temperature), a thermoelastic constitutive equation for a homogeneous solid under a LTC can be written as:

$$\mathbf{S} = \mathbf{C}(T)\,\mathbf{E} + \mathbf{m}(T) + \mathbf{m}(T)\,O(\delta) + o(\delta). \tag{2.3}$$

where $\mathbf{C}(T)$ is the elasticity tensor of the material at T, $\mathbf{m}(T)$ is the thermal stress tensor only due to the temperature change, $T-T_0$. Let

$$\mathbf{m}(T) = \int_{T_o}^{T} \beta(T)\,dT, \tag{2.4}$$

where $\beta(T)$ is the thermal stress coefficient tensor, as a function of T. Detailed derivation for Eq. (2.3) can be found in Appendix I.

In Eq. (2.3), the first term on the right side denotes mechanical stresses at T; the second term, thermal stresses due to $T-T_0$, and the third is a coupling term in which the $O(\delta)$ represents the small $\nabla\mathbf{u}$. The coupling term makes the situation quite complex.

For some engineering materials, especially ceramic materials, Eq. (2.3) can be simplified further. First, the order of magnitude of $\mathbf{m}(T)$ can be estimated with the help of linear thermoelasticity:

$$\mathbf{m}(T) = - \mathbf{C}\, \mathbf{e}(T), \tag{2.5}$$

where $\mathbf{C}$ is the elasticity tensor of the material, and $\mathbf{e}(T) = \alpha\ (T-T_0)$, the thermal expansion. Obviously, $\mathbf{m}(T)$ relates to the TEP of the materials. For ceramic materials, the following considerations are noted: (1) the temperature change is assumed to be large and $|T-T_0| < T_0$, (2) thermal expansion coefficients, α, are infinitesimal quantities with an order of 10^{-6}. Then thermal expansions, $\mathbf{e}(T)$, have the order of 10^{-2} to 10^{-3} when $|T-T_0| >$ 1000 °C. Actually, from Table 1 and 2 in Part I of this study (Yuan and Wang, 1998 a) it is noted that thermal contractions from 1700 °C to 25 °C are 0.01439 and 0.00794 for an Al_2O_3 polycrystalline solid and SiC whiskers, respectively. Thus, it is reasonable to regard $\mathbf{e}(T)$ as a $O(\delta)$ term. Consequently, from (2.5) and (2.3) $\mathbf{m}(T)$ and $\mathbf{C}(T)\mathbf{E}$ have almost the same order, and the coupling term, $\mathbf{m}(T)O(\delta)$, is a second-order small term. Therefore, we can eliminate the term of $\mathbf{m}(T)O(\delta)$ and $o(\delta)$ in (2.3) and write it in the following simple form:

$$\mathbf{S} = \mathbf{C}(T)\, \mathbf{E} + \mathbf{m}(T), \tag{2.6}$$

or,

$$\mathbf{E} = \mathbf{M}(T)\, \mathbf{S} + \mathbf{e}(T) \tag{2.7}$$

with

$$\mathbf{M}(T) = [\, \mathbf{C}(T)]\text{-}\mathbf{1}, \qquad \mathbf{m}(T) = -\mathbf{C}(T)\, \mathbf{e}(T), \tag{2.8a, b}$$

where $\mathbf{M}(T)$ is the compliance tensor at T; $\mathbf{e}(T)$ is the thermal expansion (strain) tensor due to a LTC of $T-T_0$. Let

$$\mathbf{e}(T) = \int_{T_0}^{T} \alpha(T)\, dT, \qquad \text{or} \qquad \alpha(T) = \frac{de(T)}{d\,T}, \tag{2.9a, b}$$

where $\alpha(T)$ is the thermal expansion coefficient tensor, as a function of T.

Equations (2.6) and (2.7), together with (2.8a,b) and (2.4), (2.9), are the basic thermoelastic constitutive equations for high-temperature homogeneous ceramic solids (with $\alpha(T)$ of order of 10-6/°C or lesser) under a LTC. Comparing these with the expressions in linear thermoelasticity, it is clear that the present constitutive equations have considered the TEP temperature dependence of the materials, and the stress (strain) no longer linearly depends on the temperature change.

2.2 Extension to Statistically Homogeneous Ceramic Composites

By introducing volume averages of states variables and effective TEP of the composite, the basic thermoelastic constitutive equations for a homogeneous solid undergone a LTC may be extended to the case of SH ceramic composites. For

convenience, effective thermoelastic constitutive equations for a SH anisotropic ceramic composite under a LTC can be written as follows with the index notation of tensors:

$$\langle \sigma_{ij} \rangle = C^*_{ijkl}(T)\langle \varepsilon_{kl} \rangle + m^*_{ij}(T) \tag{2.10}$$

$$\langle \varepsilon_{ij} \rangle = M^*_{ijkl}(T)\langle \sigma_{kl} \rangle + e^*_{ij}(T) \tag{2.11}$$

with

$$m^*_{ij}(T) = -C^*_{ijkl}(T)e^*_{kl}(T), \tag{2.12}$$

$$m^*_{ij}(T) = \int_{T_0}^{T} \beta^*_{ij}(T)dT, \tag{2.13}$$

$$e^*_{ij}(T) = \int_{T_0}^{T} \alpha^*_{ij}(T)dT, \tag{2.14}$$

where $\langle \phi \rangle$ represents the volume average of ϕ, and $(^*)$ refers to composite effective properties.

It is important to note that the effective TEP, $C_{*ijkl}(T)$, $M^*_{ijkl}(T)$, $\beta^*_{ij}(T)$ and $\alpha^*_{ij}(T)$, must be considered, at current stage, to be dependent on both T and T0, although they are only written as functions of T. At this moment, it is not clear if the composite effective elastic properties are independent of thermal expansion mismatch between constituent materials and the associated microscopic residual stresses in the heterogeneous solids. Both effects of the temperature-dependent constituent TEP and the thermal expansion mismatch on effective TEP of the composite under a LTC must be considered. Thus, the determination of C^*_{ijkl}, M^*_{ijkl}, β^*_{ij}, and α^*_{ij} for a whisker ceramic composite under a LTC may involve temperature history, complex microscopic stresses, and various constitutive material properties and microstructural parameters in the composite.

3. EFFECTIVE TEP OF COMPOSITES UNDER LTC

Based on the thermoelastic constitutive equations with LTC given in Sec. 2, the direct approach, self-consistent scheme and differential scheme are used to predict the effective TEP of a whisker-reinforced ceramic composite under a LTC. Same assumptions about the materials as those in Sec. 3 of Part I of this study (Yuan ans Wang, 1998 a) are made for further developments.

3.1 Direct Approach

The direct approach (DA) is a approximate for predicting effective properties of the composite with a dilute reinforcement concentration, based on the well-known equivalent inclusion method (Eshelby, 1957) and the concept of volume averaging (Christensen, 1979).

3.1.1 Equivalent Inclusion Method with LTC

Assume a single ellipsoidal inclusion with $C_{ijkl}^{(I)}$ and $\alpha_{ij}^{(I)}$ is embedded in an infinite matrix with $C_{ijkl}^{(m)}$ and $\alpha_{ij}^{(m)}$, subjected to a uniform strain ε^0_{ij} and a uniform LTC of $T\text{-}T_0$ at infinity. Then the strains within the inclusion are uniform and can be evaluated by (Eshelby, 1957)

$$\varepsilon_{ij}^{(I)} = \varepsilon_{ij}^0 + \varepsilon_{ij}^c \text{ with } \quad \varepsilon_{ij}^c = S_{ijkl}\varepsilon_{ij}^T, \tag{3.1a,b}$$

where ε_{kl}^T are eigenstrains in the equivalent inclusion due to both elastic and thermal inhomogeneities; ε_{ij}^c are constrained strains in the equivalent inclusion and S_{ijkl} is Eshelby's tensor whose components on principal axes of the inclusion in an isotropic medium can be found from Appendix I in the report by Yuan and Wang (1998 b).

Following the thermoelastic constitutive equations with LTC and the concept of equivalent inclusion, stresses within the inhomogeneity are

$$\sigma_{ij}^{(I)} = C_{ijkl}^{(I)}(T)(\varepsilon_{kl}^0 + \varepsilon_{kl}^c) - C_{ijkl}^{(I)}(T)e_{kl}^{(I)}(T), \tag{3.2}$$

and stresses within the equivalent inclusion are

$$\sigma_{ij}^{(I)} = C_{ijkl}^{(m)}(T)(\varepsilon_{kl}^0 + \varepsilon_{kl}^c - \varepsilon_{kl}^T) - C_{ijkl}^{(m)}(T)e_{kl}^{(m)}(T), \tag{3.3}$$

where $e_{kl}^{(I)}(T)$ are eigenstrains in the inhomogeneity due to $T\text{-}T_0$, and $e_{kl}^{(m)}(T)$ are eigenstrains in the matrix due to $T\text{-}T_0$. Then the equivalent condition gives

$$\varepsilon_{mn}^T = \varepsilon_{mn}^{T1} + \varepsilon_{mn}^{T2}, \tag{3.4}$$

$$\varepsilon_{mn}^{T1} = B_{mnij}[C_{ijpq}^{(I)}(T) - C_{ijpq}^{(m)}(T)]\varepsilon_{pq}^0, \tag{3.5}$$

$$\varepsilon_{mn}^{T2} = B_{mnij}[C_{ijpq}^{(I)}(T)e_{pq}^{(I)} - C_{ijpq}^{(m)}(T)e_{pq}^{(m)}(T)], \tag{3.6}$$

with

$$B_{mnij} = -\{[C_{ijkl}^{(I)}(T) - C_{ijkl}^{(m)}(T)]S_{klmn} + C_{ijmn}^{(m)}(T)\}^{-1}, \tag{3.7}$$

where ε_{mn}^{T1} and ε_{mn}^{T2} are eigenstrains within the equivalent inclusion and related to ε^0_{ij} and $T\text{-}T_0$, respectively.

3.1.2 Volume and Orientation Averaging

Considering the contributions from both ε^0_{ij} and $(T\text{-}T_0)$ to a representative volume element (RVE) of the composite with randomly oriented whiskers in a dilute concentration, we can write the average stresses within the RVE as:

$$\langle\sigma_{ij}\rangle = C_{ijkl}^{(m)}(T)\langle\varepsilon_{kl}\rangle - C_{ijkl}^{(m)}(T)e_{kl}^{(m)}(T) + c_I[\overline{\sigma_{ij}^{(I)}} - C_{ijkl}^{(m)}(T)\overline{\varepsilon_{kl}^{(I)}} + C_{ijkl}^{(m)}(T)e_{kl}^{(m)}(T)], \tag{3.8}$$

where c_I is the volume fraction of the whiskers, and the overbars denote orientation averages for random orientation of the whiskers within the RVE as defined by (3.10) in Part I of this report. Following (3.1) and (3.2), it comes that

$$\overline{\varepsilon_{kl}^{(I)}} = \overline{\varepsilon_{kl}^{0}} + \overline{\varepsilon_{kl}^{c}} = \varepsilon_{kl}^{0} + \overline{S_{klmn}\varepsilon_{mn}^{T}}, \tag{3.9}$$

$$\overline{\sigma_{ij}^{(I)}} = \overline{C_{ijkl}^{(I)}(T)\varepsilon_{kl}^{(I)}} - \overline{C_{ijkl}^{(I)}(T)e_{kl}^{(I)}(T)}. \tag{3.10}$$

Rewrite (3.8), we have the expression,

$$C_{ijkl}^{*}(T)\varepsilon_{kl}^{0} - C_{ijkl}^{*}(T)e_{kl}^{*}(T) = C_{ijkl}^{(m)}(T)\varepsilon_{kl}^{0} - C_{ijkl}^{(m)}(T)e_{kl}^{(m)}(T)$$
$$c_I[\overline{\sigma_{ij}^{(I)}} - C_{ijkl}^{(m)}(T)\overline{\varepsilon_{kl}^{(I)}} + C_{ijkl}^{(m)}(T)e_{kl}^{(m)}(T)] \tag{3.11}$$

for later use in determining the effective TEP of the composite, $C^{*}_{ijlk}(T)$ and $e^{*}_{kl}(T)$.

3.1.3 Effective TEP with LTC

(1) To determine t he effective thermal expansion, $e^{*}(T)$, take a free thermal expansion process:

$$\langle \sigma_{kl} \rangle = \sigma_{ij}^{0} = 0 \tag{3.12}$$

and

$$\langle \varepsilon_{kl} \rangle = \varepsilon_{kl}^{0} = e_{kl}^{*}(T) = e^{*}(T)\delta_{kl}. \tag{3.13}$$

Since $\varepsilon_{kl}^{(I)}$ and $\sigma_{ij}^{(I)}$ only have normal components in the present case, their orientation averages would be isotropic tensors:

$$\overline{\varepsilon_{kl}^{(I)1}} = \frac{1}{3}\overline{\varepsilon_{rr}^{(I)1}}\delta_{kl} = \frac{1}{3}e_{rr}^{(I)1}\delta_{kl}, \tag{3.14}$$

$$\overline{\sigma_{kl}^{(I)1}} = \frac{1}{3}\overline{\sigma_{rr}^{(I)1}}\delta_{kl} = \frac{1}{3}\sigma_{rr}^{(I)1}\delta_{ij}, \tag{3.15}$$

where the superscript 1 denotes the superscribed quantities are in a free thermal expansion process, and $\varepsilon_{rr}^{(I)1}$ and $\sigma_{rr}^{(I)1}$ both are invariants of second rank tensors.

The effective thermal expansion of the composite with randomly oriented whiskers under a LTC then can be determined by substituting Eqs. (3.12) to (3.15) into (3.11):

$$e^{*}(T) = e_m(T) - \frac{c_I}{9\kappa_m(T)}\{\sigma_{rr}^{(I)1} - 3\kappa_m(T)[\varepsilon_{rr}^{(I)1} - 3e_m(T)]\}. \tag{3.16}$$

To find $\varepsilon_{rr}^{(I)1}$ and $\sigma_{rr}^{(I)1}$, consider a single inclusion problem, and take

$$\varepsilon_{kl}^{0} = e_{kl}^{*}(T) \approx e_{kl}^{(m)}(T) = e_m(T)\delta_{kl} \,. \tag{3.17}$$

Using Eq. (3.17) in (3.1a) and (3.5) and substituting (3.4) to (3.6) into (3.1a) with the aid of (3.1b) result in

$$\varepsilon_{kl}^{(I)1} = \varepsilon_{kl}^{0} + \varepsilon_{kl}^{c} = e_{kl}^{(m)}(T) - S_{klmn}B_{mnij}C_{ijpq}^{(I)}(T)[e_{pq}^{(I)}(T) - e_{pq}^{(m)}(T)] \,, \tag{3.18}$$

further,

$$\varepsilon_{rr}^{(I)1} = 3e_m(T) - S_{klmn}B_{mnij}C_{ijpq}^{(I)}(T)[e_I(T) - e_m(T)] \,,$$

$$\sigma_{rr}^{(I)1} = -[C_{rrpp}^{(I)}(T) + C_{rref}^{(I)}(T)S_{efmn}B_{mnij}C_{ijpq}^{(I)}(T)[e_I(T) - e_m(T)] \,, \tag{3.20}$$

where equation (3.2) has been used.

The thermal expansion coefficient, $\alpha^*(T)$, then can be calculated from

$$\alpha^{*}(T) = \frac{de^{*}(T)}{dT}. \tag{3.21}$$

For a composite with isotropic whiskers, $C_{ijkl}^{(I)}$ is an isotropic tensor, the solution (3.16) can be degenerated into

$$e^{*}(T) = e_m(T) + c_I \frac{\kappa_I(T)}{\kappa_m(T)} \frac{T_{rrss}}{3}[e_I(T) - e_m(T)], \tag{3.22}$$

where

$$T_{klpq} = I_{klpq} + S_{klmn}B_{mnij}(C_{ijpq}^{(I)} - C_{ijpq}^{(m)}) \tag{3.23}$$

with

$$I_{klpq} = \frac{1}{2}(\delta_{kp}\delta_{lq} + \delta_{kq}\delta_{lp}) \,, \tag{3.24}$$

and components of T_{klpq} for a composite with an isotropic matrix and isotropic inclusion can be found in Appendix III of the report by Yuan and Wang (1998 b). Obviously, Eq. (3.22) is completely the same as the solution (5.6) in the report by Yuan and Wang (1998 b).

(2) To determine the effective bulk modulus, $\kappa^*(T)$, a uniform temperature change with a condition of $\varepsilon_{kl}^{0} = 0$ should be imposed. Using a similar procedure as that for determining $e^*(T)$, the effective bulk modulus of the composite with randomly oriented whiskers under a LTC then can be evaluated by

$$\kappa^{*}(T)e^{*}(T) = \kappa_m(T)e_m(T) - \frac{c_I}{9}\{\sigma_{rr}^{(I)2} - 3\kappa_m(T)[\varepsilon_{rr}^{(I)2} - 3e_m(T)]\} \,, \tag{3.25}$$

with

$$\varepsilon_{rr}^{(I)2} = -S_{rrmn}B_{mnij}[C_{ijpp}^{(I)}e_I(T) - C_{ijpp}^{(m)}(T)e_m(T)] \tag{3.26}$$

and

$$\varepsilon_{rr}^{(I)2} = -C_{rrkl}^{(I)}(T)S_{klmn}B_{mnij}[C_{ijpp}^{(I)}e_I(T) - C_{ijpp}^{(m)}(T)e_m(T)] - C_{rrkk}^{(I)}(T)e_I(T), \qquad (3.27)$$

if $e^*(T)$ is known, where the superscript 2 denotes the superscribed quantities are in a uniform temperature change process with $\varepsilon^0_{kl} = 0$, and $\varepsilon_{rr}^{(I)2}$ and $\sigma_{rr}^{(I)2}$ both are the invariants of the second rank tensors.

For a composite with isotropic whiskers, $C_{ijkl}^{(I)}(T)$ is an isotropic tensor, the solution (3.25) can be degenerated to be

$$\kappa^*(T)e^*(T) = \kappa_m(T)e_m(T) + c_I\frac{T_{rrpp}}{3}[\kappa_I(T)e_I(T) - \kappa_m(T)e_m(T)] \qquad (3.28)$$

with (3.23) and (3.24). Obviously, equation (3.28) is completely the same as the solution (5.9) in the report by Yuan and Wang (1998 b).

(3) Effective shear moduli of the composite under a LTC are the same as isothermal, effective shear moduli at the operating temperature (T) because the average shear stresses and strains are independent of the thermal expansions for a composite with orthotropic matrix, randomly oriented and orthotropic inclusions, and orthotropic thermal expansion of both matrix and inclusions.

The effective shear modulus of the composite with randomly oriented whiskers in an isothermal process has been determined by the DA with two kinds of orientation averaging methods in Part I of this study. Only the solution containing the tensor invariants describing the orientation averages are written here for current use:

$$\mu^*(T) = \mu_m(T) + \frac{c_I}{30}[(3H_{rprp} - H_{rrpp}) - 2\mu_m(T)(3T_{rprp} - T_{rrpp})] \qquad (3.29)$$

with T_{klpq} defined by (3.23), and

$$H_{ijpq} = C_{ijkl}^{(I)}(T)T_{klpq}\ . \qquad (3.30)$$

Solutions (3.16), (3.25) and (3.29), called as the DA solutions with LTC, can directly give the effective TEP of the whisker-reinforced ceramic composite at an arbitrary temperature level, but can only be used in the case of dilute concentration.

Comparing the present DA solution of κ^*, Eq. (3.25), with the isothermal solution (3.14) in Part I of this study, we see from the present solution that the effective bulk modulus seems to depend on the thermal expansion mismatch. However, to conclude this issue, further studies should be conducted by more exact approaches owing to the stronger limitations of the direct approach.

3.2 Self-Consistent Scheme

Based on the DA solutions with LTC, the self-consistent scheme (SCS) can be applied to predict effective TEP of the composite under a LTC with the considerations of taking the interactions among the inclusions into account. Using SCS to (3.16), (3.25) and (3.29) results a system of nonlinear algebraical equations for $e^*(T)$, $\kappa^*(T)$ and $\mu^*(T)$:

$$e^*(T) = e_m(T) - \frac{c_I}{9\kappa_m(T)}\{\sigma_{rr}^{(I)1*} - 3\kappa_m(T)[\varepsilon_{rr}^{(I)1*} - 3e_m(T)]\}, \tag{3.31}$$

$$\kappa^*(T)e^*(T) = \kappa_m(T)e_m(T) - \frac{c_I}{9}\{\sigma_{rr}^{(I)2*} - 3\kappa_m(T)[\varepsilon_{rr}^{(I)2*} - 3e_m(T)]\}, \tag{3.32}$$

$$\mu^*(T) = \mu_m(T) + \frac{c_I}{30}[(3H^*_{rprp} - H^*_{rrpp}) - 2\mu_m(T)(3T^*_{rprp} - T^*_{rrpp})], \tag{3.33}$$

with

$$\varepsilon_{rr}^{(I)1*} = 3e^*(T) - S^*_{rrmn}B^*_{mnij}C^{(I)}_{ijpp}(T)[e_I(T) - e^*(T)], \tag{3.34}$$

$$\sigma_{rr}^{(I)1*} = -[C^{(I)}_{rrpp}(T) + C^{(I)}_{rref}(T)S^*_{efmn}B^*_{mnij}C^{(I)}_{ijpp}(T)[e_I(T) - e^*(T)], \tag{3.35}$$

$$\varepsilon_{rr}^{(I)2*} = -S^*_{rrmn}B^*_{mnij}[C^{(I)}_{ijpp}(T)e_I(T) - C^*_{ijpp}(T)e^*(T)], \tag{3.36}$$

$$\sigma_{rr}^{(I)2*} = -C^{(I)}_{rrkl}S^*_{klmn}B^*_{mnij}[C^{(I)}_{ijpp}(T)e_I(T) - C^*_{ijpp}(T)e^*(T)] - C^{(I)}_{rrkk}(T)e_I(T), \tag{3.37}$$

where tensors H_{ijpq} and T_{klpq} are defined by (3.30) and (3.23); the symbol "*" superscribing a tensor component implies that the matrix properties are replaced by the effective properties of the composite in the corresponding component.

Solving (3.31), (3.32) and (3.33) simultaneously results the effective TEP, $e^*(T)$, $\kappa^*(T)$ and $\mu^*(T)$, of the whisker-reinforced ceramic composite at an arbitrary temperature level.

3.3 Differential Scheme

Based on the DA solutions with LTC, the differential scheme (DS) can be applied to predict effective TEP of the composite under a LTC more precisely. The DS regards the effective TEP of the instantaneous composite as the functions of c_I, and the instantaneous volume fraction of a differential increment of inclusions in the newly formed instantaneous composite is $c^*_I = \delta c_I/(1-c_I)$. Using the concepts of DS to (3.16), (3.25) and (3.29) and comparing with Taylor's expansions of $e^*(c_I + dc_I)$, $\kappa^*(c_I + dc_I)$ and $\mu^*(c_I + dc_I)$ result a system of nonlinear ordinary differential equations:

$$\frac{de^*(c_I)}{dc_I} = -\frac{1}{9\kappa^*(c_I)(1-c_I)}\{\sigma_{rr}^{(I)1*} - 3\kappa^*(c_I)[\varepsilon_{rr}^{(I)1*} - 3e^*(c_I)]\}, \tag{3.38}$$

$$\kappa^*(c_I)\frac{de^*(c_I)}{dc_I} + e^*(c_I)\frac{d\kappa^*(c_I)}{dc_I} = -\frac{1}{9(1-c_I)}\{\sigma_{rr}^{(I)2*} - 3\kappa^*(c_I)[\varepsilon_{rr}^{(I)2*} - 3e^*(c_I)]\}, \tag{3.39}$$

$$\frac{d\mu^*(c_I)}{dc_I} = \frac{1}{30(1-c_I)}[(3H^*_{rprp} - H^*_{rrpp}) - 2\mu^*(c_I)(3T^*_{rprp} - T^*_{rrpp})] \tag{3.41}$$

with the initial conditions at $c_I = 0$:

$$e^*(c_I) = e_m\,, \quad \kappa^*(c_I) = \kappa_m \quad \text{and} \quad \mu^*(c_I) = \mu_m\,, \tag{3.41}$$

where $\varepsilon_{rr}^{(I)1*}$, $\sigma_{rr}^{(I)1*}$, $\varepsilon_{rr}^{(I)2*}$ and $\sigma_{rr}^{(I)2*}$ are defined by (3.34) to (3.37); tensors H_{ijpq} and T_{klpq} are defined by (3.30) and (3.23); the symbol "*" superscribing a tensor component implies that the matrix properties are replaced by the effective properties of the instantaneous composite in the corresponding component.

Solving the differential equations (3.38), (3.39) and (3.40) with the initial conditions (3.41), simultaneously, results the effective TEP, $e^*(c_I)$, $\kappa^*(c_I)$ and $\mu^*(c_I)$, of the whisker-reinforced ceramic composite at an arbitrary temperature level.

4. ADDITIONAL REMARKS

4.1 Effect of Microscopic Thermal Mismatch on Effective Elastic Properties

In this section, the issue of the effect of thermal expansion mismatch between constituents on effective elastic properties of the whisker composite with random orientations under a LTC is addressed.

4.1.1 Self-Consistent Approximation

The development starts from the SCS equations (3.31), (3.32) and (3.33). Multiplying (3.31) by κ_m and subtracting the resulted equation from (3.32) yield:

$$(\kappa^* - \kappa_m)e^* = \frac{c_I}{9}[(\sigma_{rr}^{(I)1*} - \sigma_{rr}^{(I)2*}) - 3\kappa_m(\varepsilon_{rr}^{(I)1*} - \varepsilon_{rr}^{(I)2*})], \tag{4.1}$$

where

$$\sigma_{rr}^{(I)1*} - \sigma_{rr}^{(I)2*} = C_{rrpp}^{(I)}e^* + C_{rref}^{(I)}S_{efmn}^*B_{mnij}^*(C_{ijpp}^{(I)} - C_{ijpp}^*)e^*, \tag{4.2}$$

$$\varepsilon_{rr}^{(I)1*} - \varepsilon_{rr}^{(I)2*} = 3e^* + S_{rrmn}^*B_{mnij}^*(C_{ijpp}^{(I)} - C_{ijpp}^*)e^*. \tag{4.3}$$

Substituting Eqs. (4.2) and (4.3) into (4.1) leads to

$$\kappa^* = \kappa_m + \frac{c_I}{9}(C_{iief}^{(I)}T_{efpp}^* - 3\kappa_m T_{rrpp}^*) \tag{4.4}$$

with

$$T_{efpq}^* = I_{efpq} + S_{efmn}^*B_{mnij}^*(C_{ijpq}^{(I)} - C_{ijpq}^*)\quad, \tag{4.5}$$

With $H_{iipp}^* = C_{iief}^{(I)}T_{efpp}^*$, it is clear that Eq. (4.4) with (4.5) are identical to the SCS equations (3.23) with (3.25) in Part I of this report, derived for an isothermal mechanical

process, where thermal expansion terms disappear. Obviously, the SCS Eqs. (3.31), (3.32) and (3.33) for the case of LTC for T0 to T are identical with the SCS Equations. (3.23) and (3.24) in Part I of this report for an isothermal process at T in determination of $\kappa^*(T)$ and $\mu^*(T)$ with LTC.

4.1.2 Differential Approximation

The proof starts from the DS differential equations (3.38), (3.39) and (3.40) with the initial conditions (3.41). Multiplying (3.38) by $\kappa^*(c_1)$ and subtracting the resulted equation from (3.39) yield:

$$e^*(c_1)\frac{d\kappa^*(c_1)}{dc_1}=\frac{1}{9(1-c_1)}[(\sigma_{rr}^{(I)1*}-\sigma_{rr}^{(I)2*})-3\kappa^*(c_1)(\varepsilon_{rr}^{(I)1*}-\varepsilon_{rr}^{(I)2*})], \tag{4.6}$$

where

$$\sigma_{rr}^{(I)1*}-\sigma_{rr}^{(I)2*}=C_{rrpp}^{(I)}e^*(c_1)+C_{rref}^{(I)}S_{efmn}^*B_{mnij}^*(C_{ijpp}^{(I)}-C_{ijpp}^*)e^*(c_1), \tag{4.7}$$

$$\varepsilon_{rr}^{(I)1*}-\varepsilon_{rr}^{(I)2*}=3e^*(c_1)+S_{rrmn}^*B_{mnij}^*(C_{ijpp}^{(I)}-C_{ijpp}^*)e^*(c_1). \tag{4.8}$$

Substituting Eqs. (4.7) and (4.8) into (4.6) results:

$$\frac{d\kappa^*(c_1)}{dc_1}=\frac{1}{9(1-c_1)}[C_{iief}^{(I)}T_{efpp}^*-3\kappa^*(c_1)T_{rrpp}^*] \tag{4.9}$$

with the T_{efpq}^* are defined by (4.5) also.

With $H_{iipp}^*=C_{iief}^{(I)}T_{efpp}^*$, it is easy to see that the differential equation (4.9) with the initial conditions (3.41) are identical to the differential equation (3.28) with the initial conditions (3.30) in Part I of this report, derived for an isothermal mechanical process, where thermal expansions terms disappear also. Obviously, the DS differential equations (3.38), (3.39) and (3.40) with the initial conditions (3.41) for the case of LTC for T0 to T are identical with the DS differential equations (3.28) and (3.29) with the initial conditions (3.30) in Part I of this report for an isothermal process at T in determination of $\kappa^*(c_1)$ and $\mu^*(c_1)$ with LTC.

The above analyses imply that, in the SCS and DS approximations, effective elastic properties of the whisker ceramic composite under a LTC are independent of thermal expansion mismatch between the constituents even though the effect of the thermal expansion mismatch have been considered in determination of effective TEP of the composite in the beginning.

However, it is important to point out here that (1) this conclusion is based on the simplified basic thermoelastic constitutive equations with LTC in which the coupling term in Eq. (2.3) was eliminated. If thermal expansion coefficients of the materials are not very small, the problem may become quite complex. Further studies are needed to clarify these issues; (2) obviously, effective thermal expansion coefficients are highly dependent on thermal expansion mismatch between constituent materials.

4.2 Uncoupled Effective Thermoelastic Constitutive Equations

Since the composite effective elastic properties are independent of the thermal expansion mismatch, the effective elastic moduli, $\kappa^*(T)$ *and* $\mu^*(T)$, under a LTC only depend on T, not on T_0, and they can be determined in an isothermal mechanical process at T which is regarded as a reference temperature. Thus, in effective thermoelastic constitutive equations with LTC, (2.10) and (2.11), the contributions $\langle\sigma_{ij}\rangle$ (or $\langle\varepsilon_{ij}\rangle$) from $T\text{-}T_0$ and ε^0_{ij} (or σ^0_{ij}) are independent each other. Consequently, equations (2.10) or (2.11) can be regarded as a superposition of a uniform temperature change process from T_0 to T with $\varepsilon^0_{ij} = 0$ (or $\sigma^0_{ij} = 0$) and an isothermal process with an applied uniform field ε^0_{ij} (or σ^0_{ij}) at T. Up to now, it is clear that the effective thermoelastic constitutive equations with LTC, (2.10) and (2.11), can be regarded as uncoupled.

5. AN ALTERNATIVE SOLUTION FOR EFFECTIVE THERMAL EXPANSION UNDER LTC

Based on linear effective thermoelastic constitutive theory, Levin (1967), further Rosen and Hashin (1970), provide the exact relationships between effective thermal expansion coefficients and effective elastic properties for general two-phase thermoelastic composites. This solution can only predict the α^* at or near the reference temperature, can not describe the temperature dependence of $\alpha^*(T)$ for the composite under a LTC.

For a ceramic-matrix composite under a LTC, since (1) the effective elastic moduli are independent of thermal expansion mismatch, which can be determined in an isothermal process at T, (2) the simplified effective thermoelastic constitutive equation with LTC, (2.11), can be regarded as a superposition of a uniform temperature rise from T0 to T with $\sigma°ij = 0$ (free thermal expansion) and an isothermal process at T with an applied uniform stress $\sigma°ij$, an exact relationship between the effective thermal expansion and the effective elastic properties for a generally anisotropic composite under a LTC can be obtained by a similar derivation procedure to Levin's and Hashin's as follows:

$$e^*_{ij}(T) = e^{(m)}_{ij}(T) + [e^{(I)}_{kl}(T) - e^{(m)}_{kl}(T)]P_{klmn}[M^*_{mnij}(T) - M^{(m)}_{mnij}(T)] \tag{5.1}$$

with

$$P_{klmn}[M^{(I)}_{mnrs}(T) - M^{(I)}_{mnrs}(T)] = I_{klrs}, \tag{5.2}$$

where $M^{(m)}_{mnrs}(T)$, $M^{(I)}_{mnrs}(T)$ and $M^*_{mnij}(T)$ are the compliance tensors of the matrix, inclusion and composite, respectively, and P_{klmn} is a fourth rank tensor defined by (5.2). A detailed derivation for Eq. (5.1) is given in Appendix II.

For the case of small temperature change (STC), TEP of the constituents and composite are taken as constants at T_0, thermal expansions can be defined by the products of thermal expansion coefficients and small temperature changes. Immediately, Eq. (5.1)

can be degenerated to Levin-Hashin's solution, Eq. (3.31) in Part I of this report, for effective thermal expansion coefficients of the composite under a STC.

Equations (5.1) and (5.2), named as the modified Levin-Hashin's solution for effective thermal expansions of the composite under a LTC, can predict the effective thermal expansions, $e^*_{ij}(T)$, of the composite due to an arbitrary temperature change from T0 to T if the effective elastic properties are known. The effective thermal expansion coefficients at T, $\alpha^*_{ij}(T)$, then can be obtained from the derivatives of $e^*_{ij}(T)$.

For the present composite, $e^{(m)}_{ij}(T)$, $e^{(I)}_{ij}(T)$ and $e^*_{ij}(T)$ are isotropic, second-rank tensors, and $M^*_{mnij}(T)$ and $M^{(m)}_{mnij}(T)$ are isotropic, fourth-rank tensors. Then Eq. (5.1) can be reduced to:

$$e^*(T) = e_m(T) + \frac{e_I(T) - e_m(T)}{9} P_{kkrr}\left[\frac{1}{\kappa^*(T)} - \frac{1}{\kappa_m(T)}\right] \tag{5.3}$$

with P_{klmn} are defined by (5.2).

Up to now, we have two methods to predict effective thermal expansions of the present composite under a LTC: (1) directly solve the present SCS equations (3.31), (3.32) and (3.33), or solve the present DS differential equations (3.38), (3.39) and (3.40) with the initial conditions (3.41), simultaneously; (2) evaluate isothermal $\kappa^*(T)$ and $\mu^*(T)$ first by solving isothermal SCS or DS equations provided by Yuan and Wang (1998 a), the $e^*(T)$ with the corresponding approximations then can be obtained by substituting the resulting $\kappa^*(T)$ into the modified Levin-Hashin's solution (5.3). Although we can not prove theoretically that the present SCS or DS equations are identical with the modified Levin-Hashin's solution for evaluation of $e^*(T)$, the exactly identical numerical results by the two methods give clear conclusion in the next section.

6. NUMERICAL RESULTS AND DISCUSSION

6.1 Thermoelastic Properties of Constituent Materials

For illustrative purposes, a hot-pressed SiC-whisker/Al_2O_3-matrix composite is considered in numerical calculation. The hot-pressing temperature (1700 °C) is taken to be a reference temperature.

Since the Al_2O_3 matrix is polycrystalline, TEP of the matrix are assumed to be isotropic. Detailed properties of the Al_2O_3 matrix and their temperature dependence (from 25 °C to 1700 °C) are given in Table 1 in Part I of this study.

The SiC whiskers considered here contain mainly cubic SiC single crystals. Since the [111] direction of the cubic crystal system coincides with the whisker growth direction, the SiC whiskers are considered to be transversely isotropic in elastic properties with the isotropic plane perpendicular to the whisker axis (Yuan and Wang, 1998e). Thermal expansion of the SiC whiskers is, however, isotropic owing to the isotropy of thermal expansion of the SiC cubic crystal. To determine the complete temperature-

dependent TEP of the SiC whiskers is not easy. Some basic theoretical and computational studies are made on the SiC whiskers by Yuan and Wang (1998e) based on an analysis of elastic properties of cubic SiC crystals. The complete temperature-dependent (from 25 °C to 1700 °C) transversely isotropic elastic properties and the thermal expansions of the SiC whiskers from T_0 = 1700 °C are given in Table 2 of Part I in this study.

6.2 Solution Procedure

To evaluate numerically effective TEP of the composite under LTC, the three approximate methods mentioned in Section 3 are used.

By using the direct approach (DA), results of $e^*(T)$, $\kappa^*(T)$ and $\mu^*(T)$ are directly determined from Eqs. (3.16), (3.25) and (3.29). Since $\kappa^*(T)$ *and* $\mu^*(T)$ are independent of thermal expansion mismatch between the constituents, the isothermal solutions, i.e., Eqs. (3.14) in Part I of this report can be applied to evaluate the $\kappa^*(T)$ and $\mu^*(T)$ first. Values of $e^*(T)$ from T_0 to T then can be calculated from the modified Levin-Hashin solution, Eq. (5.3).

By using above mentioned SCS and DS, two methods are taken to evaluate $e^*(T)$, $\kappa^*(T)$ and $\mu^*(T)$. The first method requires solving simultaneously the present SCS equations (3.31), (3.32) and (3.33), or the DS differential equations (3.38), (3.39) and (3.40) with the initial conditions (3.41). An alternative is to evaluate the isothermal $\kappa^*(T)$ and $\mu^*(T)$ at T by the SCS or DS first; then $e^*(T)$ from T_0 to T can be evaluated by substituting the resulting $\kappa^*(T)$ into the modified Levin-Hashin solution (5.3). The purpose is to compare the results of $e^*(T)$ by the present solution (5.3). The purpose is to compare the results of $e^*(T)$ by the present solutions with those by the modified Levin-Hashin solution. For the $\kappa^*(T)$ and $\mu^*(T)$, the two methods give the identical results. Actually these results are obtained in Part I of this report already, which can be directly taken as the current results.

Owing to the complexities of present mathematical formulation, explicit analytical solutions are not obtainable from the SCS and DS equations. Numerical methods for solving the above equations are necessary. The numerical methods are the same as those discussed in Part I of this report, thus not repeated here.

To study the temperature dependence of effective TEP of the ceramic composite, the range of operating temperature considered, from 1700 °C to 25 °C, is divided into ten steps, i.e., 1700 °C, 1500 °C,1300 °C, ...300 °C, 100 °C and 25 °C. To study effects of volume fraction and aspect ratio of the whiskers on effective composite TEP, volume fractions, from 0.0 to 0.6 with each increment of 0.05, are considered; and a broad range of aspect ratio of the whiskers, from 1.005 to 1000 with seven regions, i.e., 1.005, 10, 20, 50, 500 and 1000, is studied.

General computer programs are written for the DA, SCS and DS formulations to calculate the effective TEP of a ceramic composite with randomly oriented whiskers under a LTC. Numerical results are obtained for the effective thermal expansion e^*, bulk modulus κ^*, shear modulus μ^*, Young's modulus E^* and Poisson's ratio ν^* for the

SiC_w/Al_2O_3 composite at different volume fractions, operating temperatures and aspect ratios.

6.3 Results and Discussion

Since effective elastic properties of the composite under a LTC are independent of thermal expansion mismatch between the matrix and the whiskers, values of $\kappa^*(T)$ and $\mu^*(T)$ under a LTC from T_0 to T are identical with that of isothermal κ^* and μ^* at T. Thus, results of $\kappa^*(T)$, $\mu^*(T)$, $E^*(T)$ and $\nu^*(T)$ shown in Figs. 2, 3, 4, 7, 8, and 10 in Part I of this report may be used also for the present cases except the results at 1700 °C, since the effective thermoelastic constitutive theory with a LTC can not be used without temperature change. The various reference temperature levels (T_0) in the above figures should be replaced by the operating temperatures (T) of the composites for the current cases.

Since effective thermal expansion coefficients of a composite under a LTC depend on a reference temperature, results for $\alpha^*(T)$ of the present composite under a temperature change from 1700 °C to T are different from those at a reference temperature T. The present effective thermoelastic constitutive theory with a LTC predict the value of $e^*(T)$ under a temperature change from 1700 °C to T first; then $\alpha^*(T)$ can be evaluated from Eq. (3.21) by numerical differentiation.

6.3.1 Effects of Constituent-Modulus Ratio and Volume Fraction

It is well-known that properties of constituent materials and volume fraction, cI, of the reinforcing material severely affect effective properties of the composite. Variations of κ^*, μ^*, E^* and ν^* with cI at 1100 °C and 25 °C are shown in Figs. 2, 3 and 4 in Part I of this report. Variations of e^* and α^* with cI at 1100 °C and 25 °C are shown in Figs. 1 and 2 of this paper. It is clear that E^* and μ^* decrease very slightly with cI at 25 °C, but increase with cI at 1100 °C. However, κ^*, ν^* and α^* decrease with cI at all temperatures. Reasons for this are given in Section 5.3 of Part I of this report. Thus changes in effective TEP of a composite with c_I may differ at different temperatures owing to different temperature dependent TEP of constituent materials. The DS and SCS approaches have almost the same accuracy in predicting effective TEP. Also, results obtained by the DA are quite closed to those by the DS and SCS since the orientation average of elastic properties of the SiC whiskers are quite closed to elastic properties of Al_2O_3 matrix (for detail, see Section 5.1 in Part I of this report). All of the solid lines in the figures denote both results given by DS and SCS and the chain lines denote the results by the DA.

It is noted that if the constituent-modulus ratios are large (for example, $E_I/E_m > 8$ to 10), accuracy of the different schemes in predicting the effective TEP are different, as discussed in an accompanying report (Yuan and Wang, 1998 d).

6.3.2 Comparison with a Composite with Isotropic Whiskers

In an accompanying report (Yuan and Wang, 1998 b, c, d), the upper bound of transversely isotropic elastic properties of SiC whiskers is assumed as elastic properties of the isotropic whiskers randomly embedded in the Al_2O_3 matrix. For comparison, corresponding numerical results of effective TEP of the composite with the isotropic whiskers under a LTC are also shown in Figs. 2, 3 and 4 in Part I of this report and Figs. 1 and 2 in this paper. Values of E^*, μ^* and ν^* of the composite with the isotropic whiskers are obviously stiffer than those of the present composite with transversely isotropic whiskers when $c_I>0.3$. For κ^* and α^*, however, no obvious differences are observed between the two kinds of composite. The reasons are presented in Section 5.2 of Part I of this report. Thus transverse isotropy of the SiC whiskers is an important factor governing the effective composite TEP.

6.3.3 Effect of Whisker Geometry

The whisker geometry may be described by the aspect ratio, γ of a prolate ellipsoidal inclusion. Figures 7 and 8 in Part I of this report and Figs. 3 and 4 in this paper show variations of κ^*, μ^*, E^*, e^* and α^* with γ for the composite with $c_I=0.35$, at 1100 °C and 25 °C, respectively. From the figures it is clear that all of the effective TEP are not affected by γ, since orientation average of elastic properties of the SiC whiskers is quite closed to elastic properties of the SiC whiskers is quite closed to elastic properties of the Al_2O_3 matrix. Thus the effect of the whisker geometry may not need to be considered for determining effective TEP of a whisker reinforced ceramic composite (with $E_I/E_m < 2$) under a LTC.

If the constituent-modulus ratio is large (for example, $E_I/E_m > 8$ to 10), the reinforcement aspect ratio will have significant effects on effective TEP of the composite when $\gamma < 50$, as discussed in the report by Yuan and Wang (1998 d).

6.3.4 Temperature Dependence of Effective Thermoelastic Properties

The effective TEP of the present composite depend on temperature change from a reference temperature owing to the temperature-dependent nature of constituent materials and thermal expansion mismatch between the matrix and the whiskers. The present effective thermoelastic constitutive theory with LTC shows that effective elastic properties of the composite are independent of the thermal expansion mismatch, depend only on the temperature-dependent elastic properties of the constituent materials. However, the effective thermal expansion, consequently, the thermal expansion coefficient, depend on both of the temperature-dependent elastic properties and the thermal expansion mismatch of the constituent materials.

Based on the above theory, Fig. 10 in Part I of this report may be directly used to describe the temperature dependence of $E^*(T)$, $\kappa^*(T)$ and $\mu^*(T)$ of the composite under a LTC by replacing T_0 with T. However, for the temperature dependence of $e^*(T)$ and $\alpha^*(T)$, Fig. 11 in Part I of this report can not be used. The present effective thermoelastic constitutive theory with LTC gives results for the present composite shown in Fig. 5 of this paper.

Comparing the results of $\alpha^*(T)$ shown in Fig. 5 with the results shown in Fig. 11 in Part I of this report, it is noted that there is no obvious difference between the two results and discrepancies are less than 0.01. This is because that the variation pattern of the temperature-dependent thermal expansion coefficients of the ceramic materials makes Eq. (3.33) in Part I of this report a good approximation for Eq. (5.3), although Eq. (3.33) in part I of this report is not valid in general for composites under a LTC comparing with Eq. (5.3).

6.4 Some Remarks

The effective thermal expansion, e^*, of the composite under a LTC can be evaluated by two methods presented in Section 6.2. The numerical results show that the results of e^* by present SCS and DS solutions are exactly equal to those by the modified Levin-Hashin solution with the corresponding isothermal κ^* at any numerical steps and in any cases. These results numerically prove the identity between above-mentioned two methods for predicting $e^*(T)$ of the composite with SCS and DS approximations. The reasons for this are: (1) both of the solutions are based on the simplified thermoelastic constitutive equations with LTC; (2) both of the solutions are consistent with the conclusion of independence of the effective elastic properties of the thermal expansion mismatch between constituents; (3) although the modified Levin-Hashin's solution itself is an exact relationship, the precision of e^* depends on the precision of the corresponding κ^*. In this case, the results of e^* by two methods possess same approximation (SCS or DS). Obviously, this identity can not be held for DA approximation.

7. CONCLUSIONS

Based on the high-temperature, LTC micromechanics modeling and analysis of general whisker-reinforced ceramic composite and the numerical results obtained for a hot-pressed SiC-whisker/Al_2O_3-matrix ceramic composite system with various material and microstructural parameters under a LTC, the following conclusion may be reached:

(1) Starting from a nonlinear thermoelasticity consideration outlined in Sec. 2, basic thermoelastic constitutive equations for monolithic ceramic materials at elevated temperature under a LTC have been established and extended to SH anisotropic ceramic composite.

(2) Three micromechanics methods, i.e., the DA, SCS and DS, have been introduced in conjunction with the presently developed basic thermoelastic constitutive equations to evaluated high-temperature effective TEP of whisker-reinforced ceramic composite system under a LTC.

(3) The detailed mechanics analysis, based on the SCS and DS approximations, shows that effective elastic properties of the ceramic composite under a LTC are independent of thermal expansion mismatch between constituent materials.

(4) The effective thermoelastic constitutive equations for ceramic composites under a LTC have been shown to be uncoupled and can be evaluated by superposition of a

pure nonisothermal (uniform temperature change) process and an isothermal mechanical process. Consequently, effective elastic moduli of a ceramic composite under a LTC can be determined by an isothermal mechanical process at the operating temperature. However, effective thermal expansion coefficients should be determined in a uniform LTC process.

(5) For the case of large temperature change, modifications of Levin-Hashin's approach have been made. The solution can be used as an alternative for determining effective thermal expansion coefficients of a whisker composite. The results of e^* obtained from the alternative approach using a corresponding isothermal κ^* are identical to the present micromechanical SCS or DS solution.

(6) The transversely isotropic elastic properties of single-crystal SiC whiskers have a significant effect on effective TEP of the whisker composite with random orientations under a LTC. The anisotropy of the whisker elastic properties should be taken into account in accurate evaluation of whisker-composite properties.

(7) The SCS and DS have almost the same accuracy in determining effective TEP of the present ceramic composite under LTC. This is apparently caused by the fact that orientation average of elastic properties of SiC whiskers are quite close to elastic properties of the Al_2O_3 polycrystalline matrix.

(8) The whisker aspect ratio has almost no effect on the high-temperature effective TEP of the whisker composite under LTC. In design and evaluation of effective TEP of an actual whisker-reinforced ceramic composite, the effect of whisker length may be negligible.

(9) The temperature dependence of effective elastic properties of the ceramic composite depends solely on temperature-dependent elastic properties of constituent materials. In general, effective elastic moduli of whisker ceramic composites decrease almost linearly with T; however, the effective Poisson's ratio does the opposite.

(10) The temperature dependence of the effective thermal expansion coefficients of the ceramic composite depends on both temperature-dependent TEP of the constituent materials and the thermal expansion mismatch. The effective thermal expansion coefficients of the present ceramic composite increase nonlinearly with T and become constant when T exceeds a certain temperature.

REFERENCES

Carlson, D. E., "Linear Thermoelasticity," in Mechanics of Solids, Vol. II, C. Truesdell (Ed.), Spring-Verlag, 1984.

Cristensen, R. M., Mechanics of Composite Materials, Chapter 2, Wiley-Interscience, New York, 1979.

Eshelby, J. D., "The Determination of the Elastic Field of an Ellipsoidal Inclusion, and Related Problems," Proceedings of Royal Society of London, Vol. A241, 1957, pp. 376-396.

Hashin, Z., "Theory of Fiber Reinforced Materials, " NASA Contract Report No. CR-1974, 1972, NASA Langley Research Center, Hampton, VA.

Hashin, Z., "Thermal Expansion of Polycrystalline Aggregates: 1. Exact Analysis,"
International Journal of Mechanics and physics of Solids, Vol. 32, 1984, pp. 149-157.

Levin, V. M., "On the Coefficients of Thermal Expansion of Heterogeneous Materials," Mekh. Tverd. Tela, (in Russian), Vol. 1, 1967, pp.88-94.

Rosen, B. W. and Hashin, Z., "Effective Thermal Expansion Coefficients and Specific Heats of Composite Materials." International Journal of Engineering Science, Vol. 8, 1970, pp. 157-173.

Wei, G. C. and Becher, P. F., "Development of SiC-Whisker-Reinforced Ceramics," American Ceramic Society Bulletin, Vol. 64, No. 2, 1985, pp. 298-304.

Yuan, Yusheng and Wang, S. S., "High-Temperature Thermoelastic Constituve Theories for Random Whisker-reinforced Ceramic composites, Part I: Under Small Temperature Change," CEAC Technical Report, University of Houston, Houston, TX, 1998.

Yuan, Yusheng and Wang, S. S., "Analysis of Thermoelastic Constitutive Properties of Particulate and Random Short-Fiber Reinforcement Ceramic Composites Subjected to Large Temperature Chang, Part I: Basic Formulation and Direct Approach," Unpublished Internal Technical Report, CEAC, University of Houston, Houston, TX, 1998.

Yuan, Yusheng and Wang, S. S., "Analysis of Thermoelastic Constitutive Properties of Particulate and Random Short-Fiber Reinforcement Ceramic Composites Subjected to Large Temperature Chang, Part II: Self-Consistent Approximation," Unpublished Internal Technical Report, CEAC, University of Houston, Houston, TX, 1998.

Yuan, Yusheng and Wang, S. S., "Analysis of Thermoelastic Constitutive Properties of Particulate and Random Short-Fiber Reinforcement Ceramic Composites Subjected to Large Temperature Chang, Part III: Differential Approximation," Unpublished Internal Technical Report, CEAC, University of Houston, Houston, TX, 1998.

Yuan, Yusheng and Wang, S. S., "An Estimation of Temperature-Dependent Transversely Isotropic Elastic Properties of Single-Crystal SiC Whiskers," Unpublished Internal Technical Report, CEAC, University of Houston, Houston, TX, 1998.

Appendix I: Derivation for Thermoelastic Constitutive Equations with LTC

The infinitesimal strain tensor is defined by

$$\mathbf{E} = \frac{1}{2}(\nabla \mathbf{u} + \nabla \mathbf{u}^T) \tag{I-1}$$

Using assumption (1) in (I-1) results

$$\mathbf{E} = O(\delta) \text{ and } \dot{\mathbf{E}} = O(\delta). \tag{I-2}$$

Following (2.2a, b), (I-1), (I-2) and using assumption (1) in section 2.1 also results

$$\mathbf{D} = \mathbf{E} + \frac{1}{2}\nabla \mathbf{u}^T \nabla \mathbf{u} = \mathbf{E} + O(\delta^2) = O(\delta) \tag{I-3}$$

and

$$\dot{\mathbf{D}} = \dot{\mathbf{E}} + \frac{1}{2}(\nabla \mathbf{u}^T \nabla \dot{\mathbf{u}} + \nabla \dot{\mathbf{u}} + \nabla \dot{\mathbf{u}}^T \nabla \mathbf{u}) = \dot{\mathbf{E}} + O(\delta^2) = O(\delta). \tag{I-4}$$

Using assumption (1) in section 2.1 in (2.2a) follows

$$\mathbf{F} = \mathbf{1} + O(\delta).$$

In the initial reference state, $\mathbf{F}=\mathbf{1}$ and $T=T_o$ follow

$$\mathbf{D} = \mathbf{0} \text{ and } \mathbf{S} = \tilde{\mathbf{S}}(\mathbf{0}, T_o),$$

where $\tilde{\mathbf{S}}(\mathbf{0}, T_o)$ represents the residual stress at the reference state, and the assumption (3) in section 2.1 gives

$$\tilde{\mathbf{S}}(\mathbf{0}, T_o) = \mathbf{0}. \tag{I-6}$$

Taylor's expansion of $\tilde{\mathbf{S}}(\mathbf{D}, T)$ at $\mathbf{D}=\mathbf{0}$ and T (an arbitrary final temperature) gives

$$\tilde{\mathbf{S}}(\mathbf{D}, T) = \tilde{\mathbf{S}}(\mathbf{0}, T) + \partial_{\mathbf{D}} \tilde{\mathbf{S}}(\mathbf{D}, T)\big|_{\mathbf{D}=\mathbf{0}} (\mathbf{D} - \mathbf{0}) + o(\delta), \text{ or}$$

$$\tilde{\mathbf{S}}(\mathbf{D}, T) = \tilde{\mathbf{S}}(\mathbf{0}, T) + \mathbf{C}(T)\mathbf{E} + o(\delta), \tag{I-7}$$

where $\mathbf{C}(T) = \partial_{\mathbf{D}} \tilde{\mathbf{S}}(\mathbf{D}, T)\big|_{\mathbf{D}=\mathbf{0}}$ is the elasticity tensor of the materials at T, a fourth rank tensor, $\mathbf{E}$ is the infinitesimal strain tensor.

Following assumption (I-6), it can be written that

$$\tilde{\mathbf{S}}(\mathbf{0}, T) = \tilde{\mathbf{S}}(\mathbf{0}, T_0) + \mathbf{m}(T) = \mathbf{m}(T), \tag{I-8}$$

where $\mathbf{m}(T)$ is the thermal stress tensor only due to the temperature change $T-T_0$.

Substituting (I-7), (I-8) and (I-5) into (2.1), with the aid of (I-2) and assumption (1), results

$$\begin{aligned}\mathbf{S} &= [\mathbf{I} + \mathrm{O}(\delta)][\mathbf{m}(\mathrm{T}) + \mathbf{C}(\mathrm{T})\mathbf{E} + \mathrm{o}(\delta)] \\ &= \mathbf{C}(\mathrm{T})\mathbf{E} + \mathbf{m}(\mathrm{T}) + \mathbf{m}(\mathrm{T})\mathrm{O}(\delta) + \mathrm{o}(\delta).\end{aligned} \tag{I-9}$$

APPENDIX II: Effective Thermal Expansions of Two-Phase Composites Under LTC

According to the uncoupling nature of the effective thermoelastic constitutive equations for a ceramic composite under a LTC, a general thermoelastic process of a representative volume element of the composite (with the boundary surface S and the volume V) under a LTC can be regarded as a superposition of following two independent problems: a uniform temperature rising from T_0 to T with traction-free and an isothermal problem at T with homogeneous boundary conditions.

For the first problem, the boundary conditions are

$$T_i = \sigma^0_{ij} n_j = 0, \tag{II-1}$$

$$\theta = T - T_0 = \theta_0. \tag{II-2}$$

Then, the volume averages are

$$\left\langle \sigma_{ij} \right\rangle = \sigma^0_{ij} = 0, \tag{II-3}$$

$$\langle \theta \rangle = \theta_0, \tag{II-4}$$

$$\left\langle \varepsilon_{ij} \right\rangle = e^*_{ij}(T) = \int_{T_0}^{T} \alpha^*_{ij}(T) dT. \tag{II-5}$$

For the second problem, the boundary conditions are

$$T_i = \sigma^0_{ij} n_j, \tag{II-6}$$

$$\theta = T - T = 0. \tag{II-7}$$

Then, the volume averages are

$$\left\langle \sigma'_{ij} \right\rangle = \sigma^0_{ij}, \tag{II-8}$$

$$\langle \theta \rangle = 0, \tag{II-9}$$

$$\left\langle \varepsilon_{ij}^{'} \right\rangle = M_{ijkl}^{*}(T)\sigma_{kl}^{0} \ , \tag{II-10}$$

where the prime is introduced to distinguish the second problem from the first problem, and the effective composite compliances at T, $M^{*}_{ijkl}(T)$, are independent of thermal expansion mismatch and considered to be known.

Consider a product of $\sigma^{'}_{ij}$ from the second problem and ε_{ij} from the first problem, and write

$$\int_V \sigma_{ij}^{'} \varepsilon_{ij} dv = \int_V (\sigma_{ij}^{'} u_i)_{,j} \, dv \tag{II-11}$$

where $s^{'}_{ij,j} = 0$ has been used. Consequently, the divergence theorem results in

$$\int_V \sigma_{ij}^{'} \varepsilon_{ij} dv = \int_S \sigma_{ij}^{'} u_i n_j ds = \sigma_{ij}^{0} \left\langle \varepsilon_{ij} \right\rangle V \tag{II-12}$$

where nj denotes the unit vector normal to S, and $\sigma^{'}_{ij} = \sigma^{0}_{ij}$ on S has been used in the last equality. Using (II-5) in (II-12) leads to

$$\int_V \sigma_{ij}^{'} \varepsilon_{ij} dv = \sigma_{ij}^{0} e_{ij}^{*}(T) V \tag{II-13}$$

By definition,

$$\left\langle \sigma_{ij}^{'} \right\rangle = \sum_{n=1}^{N} c_n \left\langle \sigma_{ij}^{'(n)} \right\rangle \tag{II-14}$$

where the case of V phases with c_n being phase volume fractions is temporarily considered. Next, a linear transformation between $\left\langle \sigma_{ij}^{'(n)} \right\rangle$ and σ^{0}_{kl} can be written as:

$$\left\langle \sigma_{ij}^{'(n)} \right\rangle = B_{ijkl}^{(n)} \sigma_{kl}^{0} \tag{II-15}$$

where $B_{ijkl}^{(n)}$ can be determined from the isothermal problem. Combining Eqs. (II-14) and (II-15) gives

$$\left\langle \sigma_{ij}^{'} \right\rangle = \sum_{n=1}^{N} c_n B_{ijkl}^{(n)} \sigma_{kl}^{0} \tag{II-16}$$

then

$$\sum_{n=1}^{N} c_n B_{ijkl}^{(n)} = I_{ijkl} \tag{II-17}$$

where $\left\langle \sigma_{ij}^{'} \right\rangle = \sigma_{kl}^{0}$ has been used.

Rewrite Eq. (II-13) in term of the phase contributions as

$$\sum_{n=1}^{N} B_{ijkl}^{(n)} \sigma_{kl}^{0} e_{ij}^{(n)}(T) V^{(n)} = \sigma_{ij}^{0} e_{ij}^{*}(T) V \tag{II-18}$$

where Eqs. (II-15) and (II-5) have been used. Solving for $e^{*}_{ij}(T)$ yields:

$$e_{ij}^{*}(T) = \sum_{n=1}^{N} c_n e_{kl}^{(n)}(T) B_{klij}^{(n)} \tag{II-19}$$

where $c_n = V_n/V$.

According to definition,

$$\left\langle \varepsilon_{ij}^{'} \right\rangle = \sum_{n=1}^{N} c_n \left\langle \varepsilon_{ij}^{'(n)} \right\rangle \tag{II-20}$$

then

$$M_{ijkl}^{*}(T) \sigma_{kl}^{0} = \sum c_n M_{ijkl}^{(n)}(T) \left\langle \sigma_{kl}^{'(n)} \right\rangle \tag{II-21}$$

Substituting Eq. (II-15) into Eq. (II-21) leads to

$$M_{ijkl}^{*}(T) = \sum_{n=1}^{N} c_n M_{ijmn}^{(n)}(T) B_{mnkl}^{(n)} \tag{II-22}$$

For a two-phase composite with unknowns $e^{*}(T)$, $B_{ijkl}^{(1)}$, $B_{ijkl}^{(2)}$, Eqs. (II-19), (II-22) and (II-17) can give the solutions. Equation (II-17) can be rewritten as

$$c_2 B_{ijkl}^{(2)} = I_{ijkl} - c_1 B_{ijkl}^{(1)} \qquad 7 \tag{II-23}$$

Substituting Eq. (II-23) into Eq. (II-22) gives

$$M_{ijkl}^{*}(T) - M_{ijkl}^{(2)}(T) = c_1 [M_{ijmn}^{(1)}(T) - M_{ijmn}^{(2)}(T)] B_{mnkl}^{(1)} . \tag{II-24}$$

Let

$$P_{klmn} [M_{mnrs}^{(1)}(T) - M_{mnrs}^{(2)}(T)] = I_{klrs} , \tag{II-25}$$

then Eq. (II-24) becomes

$$c_1 B_{klij}^{(1)} = P_{klmn} [M_{mnij}^{*}(T) - M_{mnij}^{(2)}(T)] \tag{II-26}$$

Combining Eqs. (II-19) and (II-23) results:

$$e_{ij}^{*}(T) = c_1 [e_{kl}^{(1)}(T) - e_{kl}^{(2)}(T)] B_{klij}^{(1)} + e_{ij}^{(2)}(T) \tag{II-27}$$

Substituting $c_I B_{klij}^{(1)}$ from (II-26) into (II-27) leads to the effective thermal expansions of two-phase composites under LTC:

$$e_{ij}^{*}(T) = [e_{kl}^{(1)}(T) - e_{kl}^{(2)}(T)] P_{klmn} [M_{mnij}^{*}(T) - M_{mnij}^{(2)}(T)] + e_{ij}^{(2)}(T) \qquad \text{(II-28)}$$

where phase 1 represents a reinforcement, and phase 2, a matrix.

LIST OF FIGURES

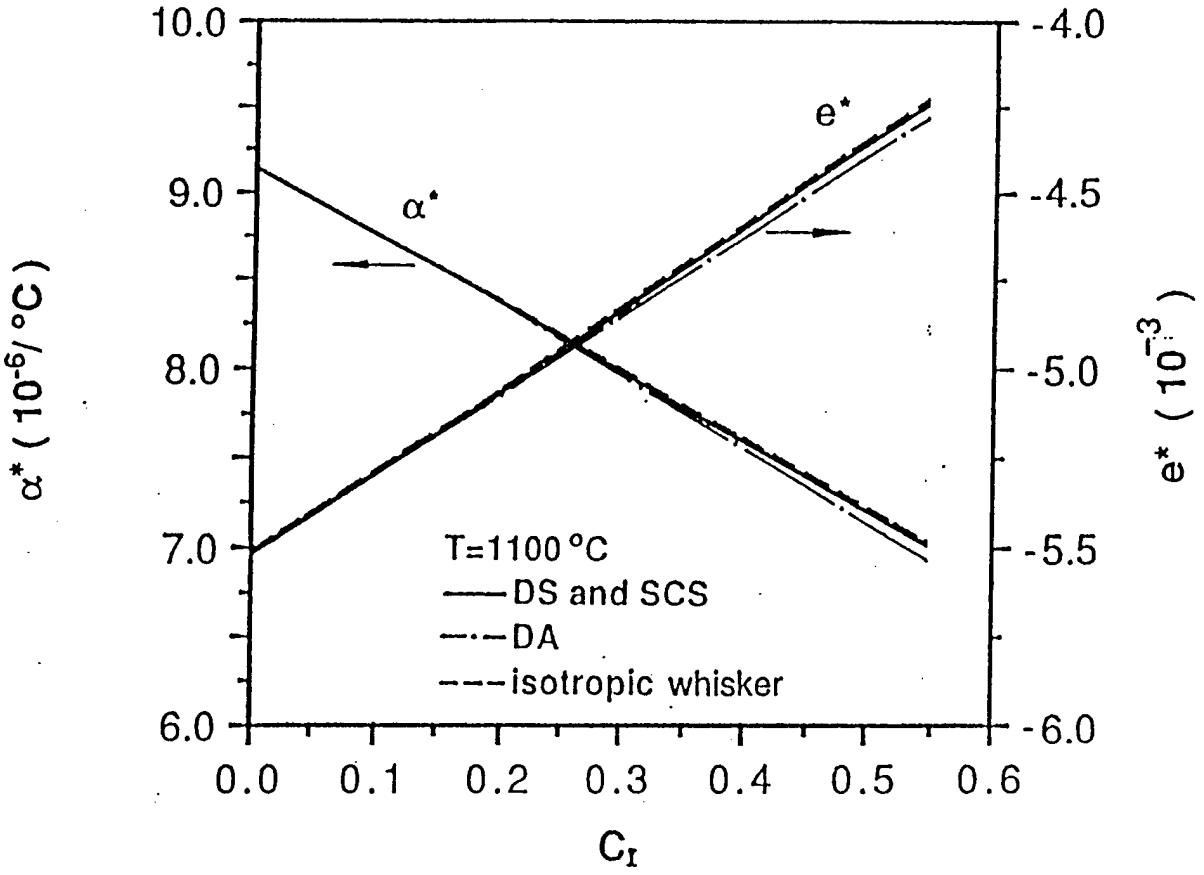

Fig. 1 Variations of e* and α* with c_I at T = 1100°C by different approaches.

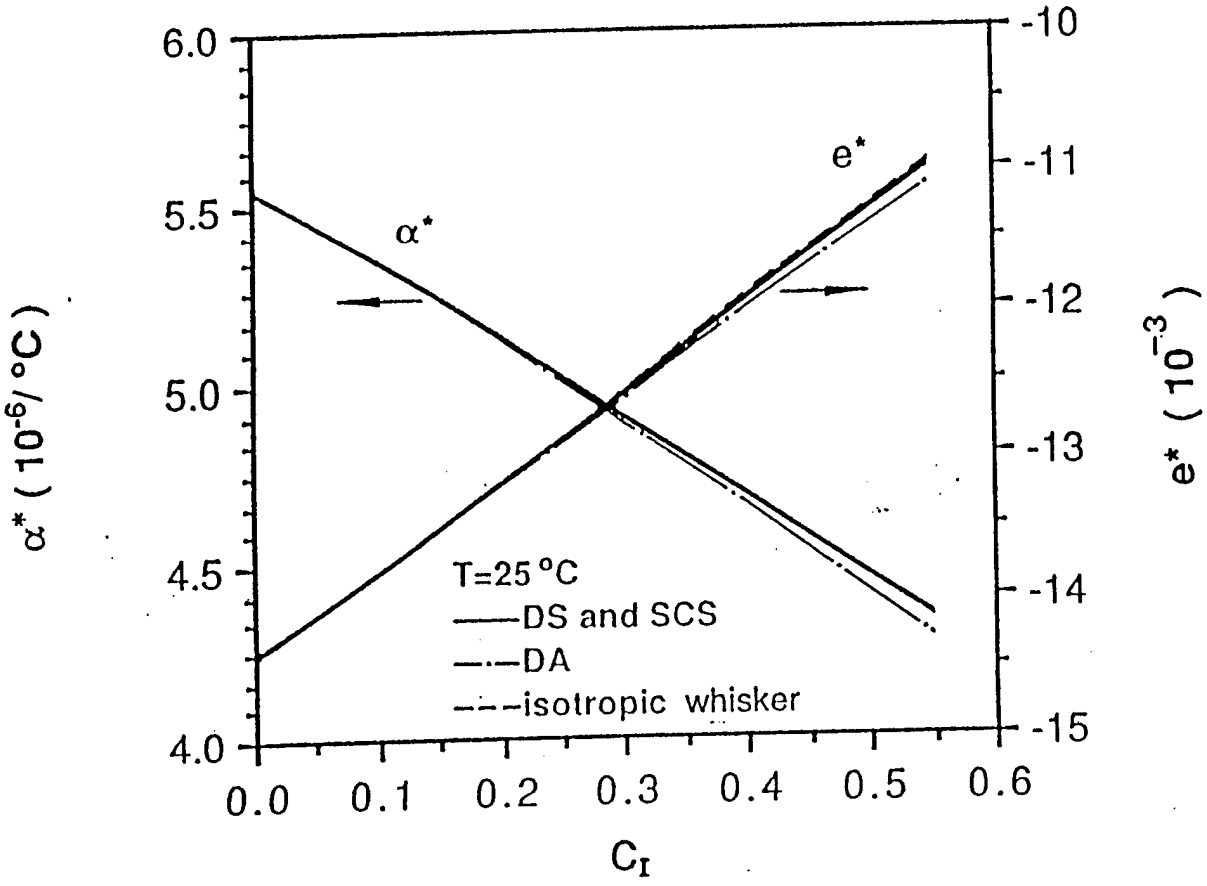

Fig. 2 Variations of e* and α* with c_I at T = 25°C by different approaches.

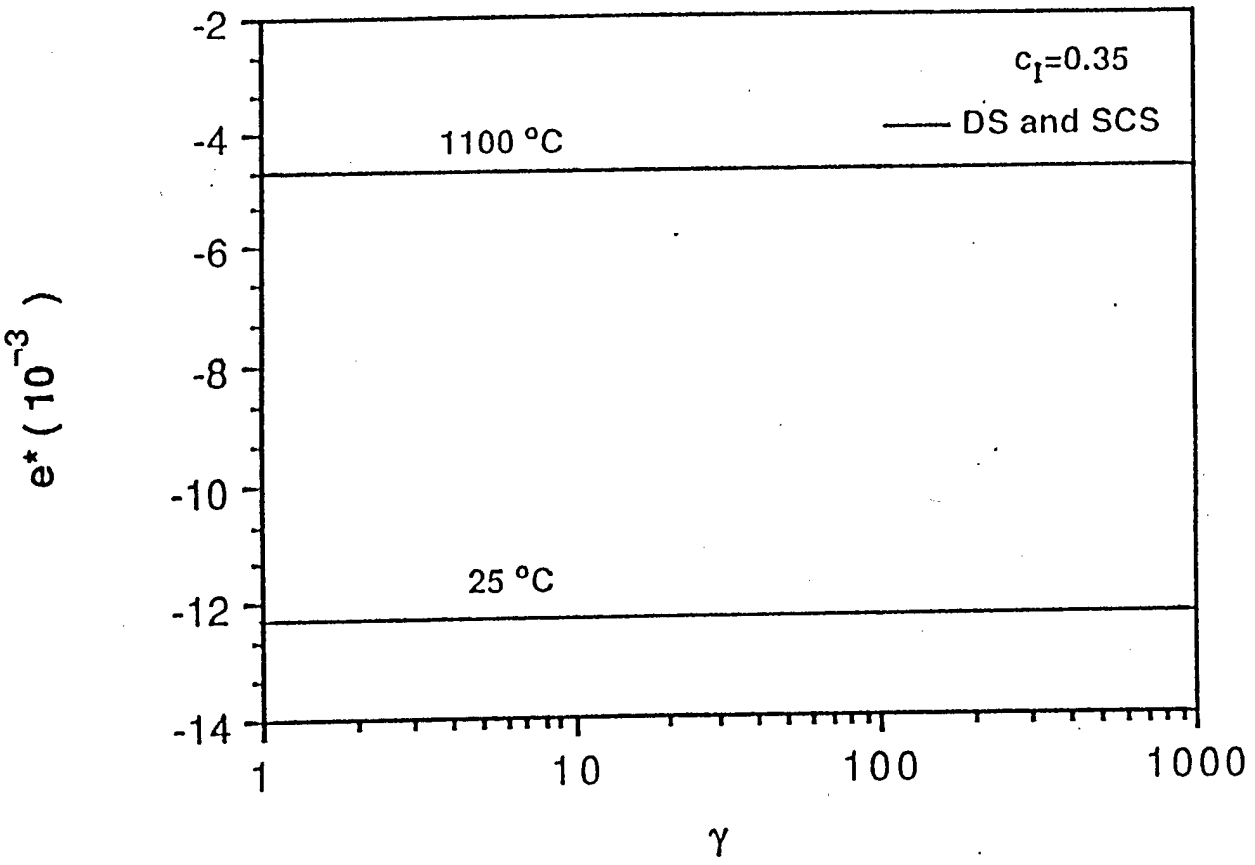

Fig. 3 Effects of aspect ratio on e* at different temperatures.

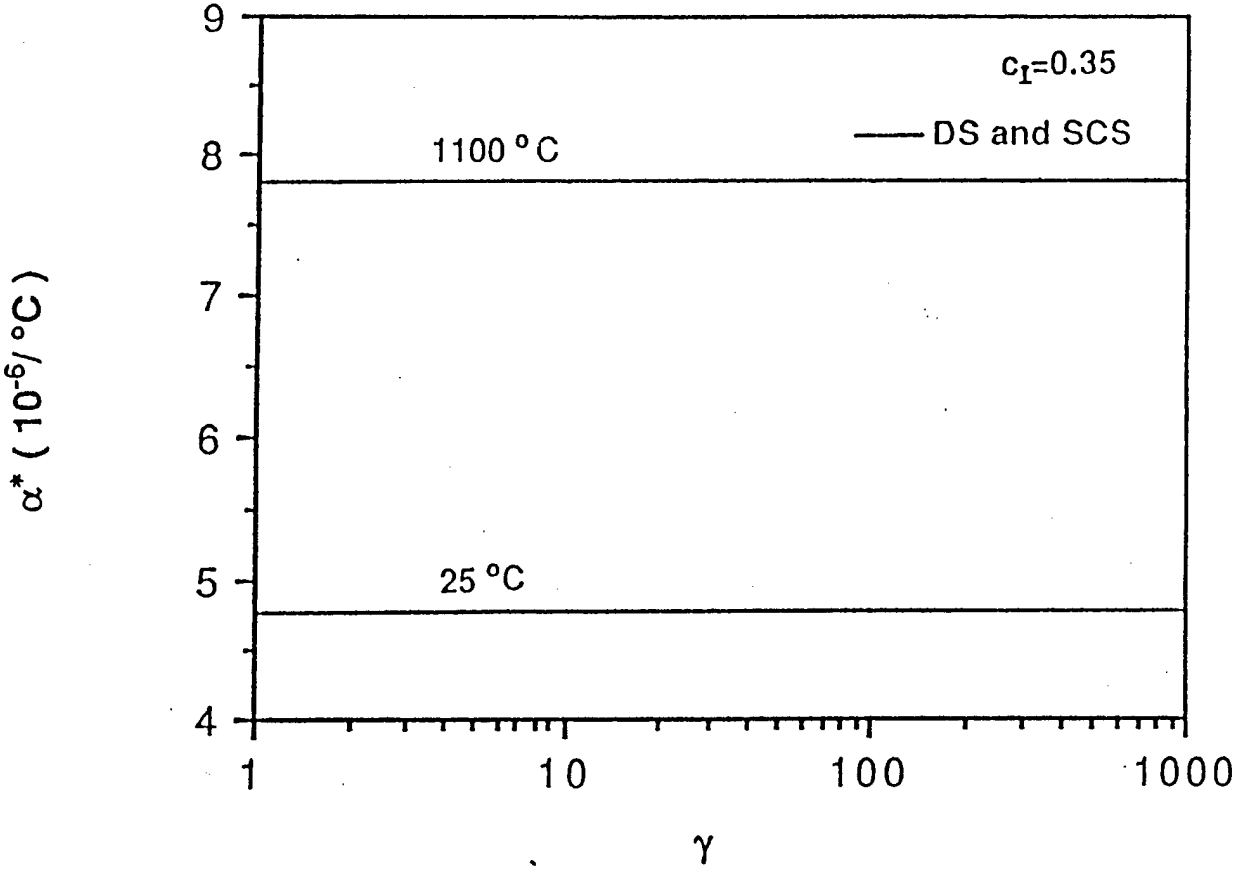

Fig. 4 Effects of aspect ratio on α* at different temperatures.

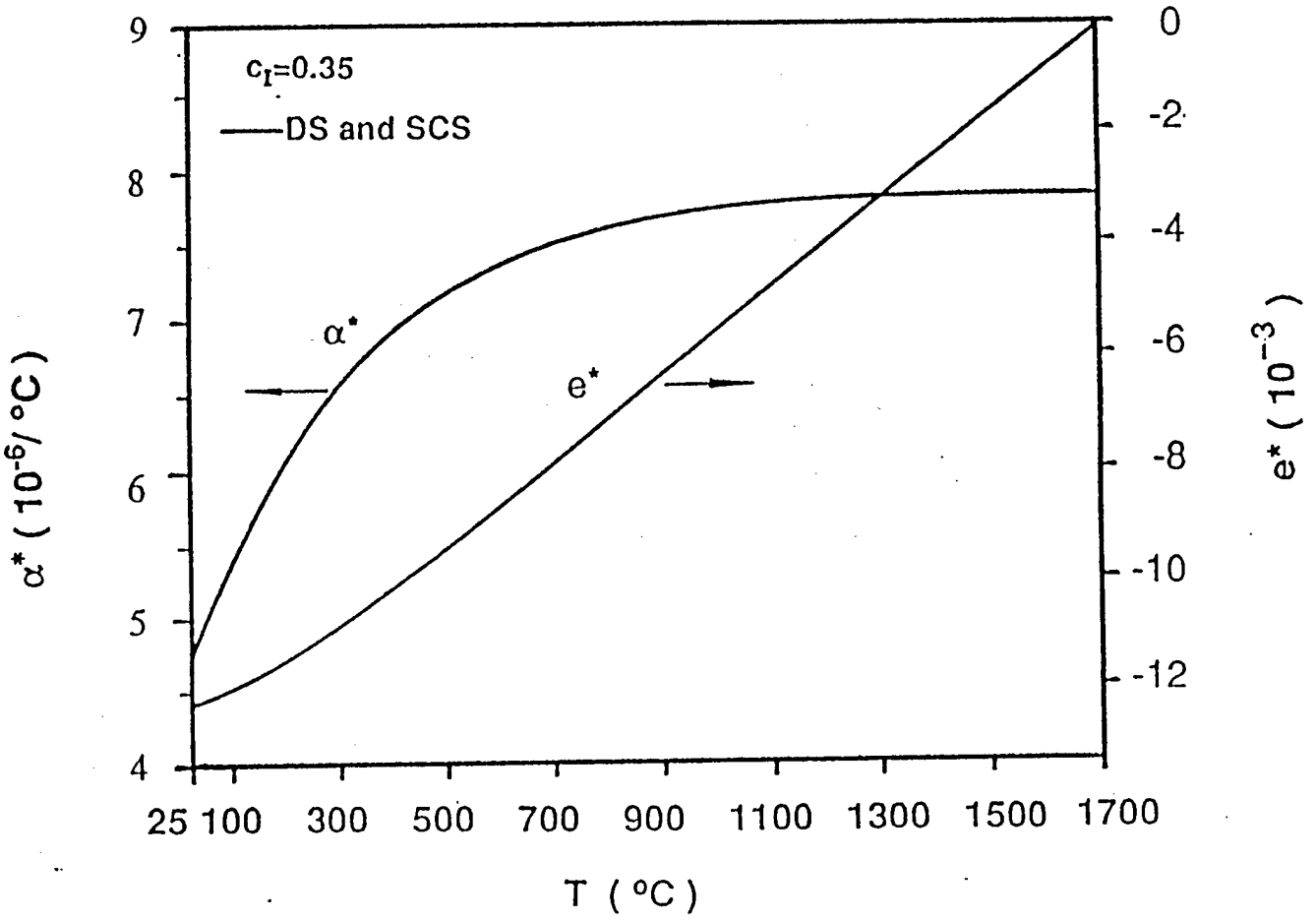

Fig. 5 Temperature dependence of e* and α* for composite with c_I = 0.35.

Contract Technical Report

EFFECTS OF AGING ON HIGH-TEMPERATURE FRACTURE OF POLYIMIDE POLYMERS

by

S.A. Swan* and S. S. Wang**
Department of Mechanical Engineering
University of Houston
Houston, TX 77204-0900

(Prepared for Aerospace Science Directorate, U.S. Air Force Office of Scientific Research, Bolling AFB, Washington, D.C., Contract No.: F49620-95-1-0204)

---

* Graduate Research Assistant, Mechanical Engineering Department
** Professor of Mechanical Engineering, and Director of CEAC

ABSTRACT

The effect of high temperature aging on the crack initiation toughness of a polyimide neat resin system is investigated. To get a basic understanding of the material behavior, strength and creep properties are studied first. For the temperature, aging condition, and time frame of interest, the material is found to be approximately linear visco-elastic. However, the fracture testing was done using linear elastic fracture mechanics because the time dependent strains were found to be insignificant over the time frame from load application until crack initiation. The K_{IC} values increase initially with aging but show a dramatic decline with further aging. Increasing temperature reduces the K_{IC} values regardless of aging condition. Aging studies are also performed to characterize the change in glass transition temperature and to determine the aging strains accumulated. A correlation between the aging behavior and the fracture toughness is found.

CHAPTER 1: INTRODUCTION

Polymers, generally in the form of composites, are finding their way into increasingly more demanding environments owing to their many advantages over conventional materials such as aluminum and steel. Most attractive among these advantages is the higher specific strength and stiffness of the polymer composites. However, as the temperature of the targeted environment increases the polymer composite may be subject to continual property changes. These changes are mainly caused by the continual processes of aging (in some cases both physical and chemical) and oxidation. Changes also occur due to time and temperature dependent deformations under load (creep or relaxation). Therefore, it is of paramount importance that the effects of aging, oxidation, and creep on material properties be thoroughly understood if these effects are to be separated so that systems can be optimized and not over designed. Since the polymer composite's performance normal to the fiber direction is largely controlled by the polymer matrix, the understanding of how aging, oxidation, and creep effect the polymer should be studied first and then expanded to include the composite.

The focus of this study is to examine the fracture initiation toughness of a polyimide neat resin and determine how it is affected by high temperature and aging. In order to characterize the fracture toughness of this polyimide, this study first determines which fracture model fits this particular material system. This will be done with a study of the tensile, creep, aging, and finally the fracture behavior. The tensile tests will give basic stiffness and strength data. Tests will also be done that determine the strain recovery of the material after a load slightly less the ultimate load has been applied. This will help determine what material model to use (i.e., elastic-plastic, visco-elastic,

etc.). The creep tests will then be used to determine if the time dependent deformations need to be included in the fracture model and to also check the compliance data for linearity with respect to stress and time. Aging studies will be conducted that characterize the change in the glass transition temperature (T_g) and also determine the aging strains accumulated as the specimens are aged at elevated temperatures. With this aging information, the effects of chemical aging (T_g change) and physical aging (collapse of free volume) on the initiation fracture toughness can be separated.

In the next section, will be a brief literature review of related topics. This will be followed in Chapter 3 with a detailed description of the experimental studies. Included are: a description of the material system studied, the specimen configurations used for the testing, the experimental setup is discussed, and the experimental procedures are given. Results are given in Chapter 4 with the highlight being fracture toughness values as a function of aging time and test temperature. In addition, scanning electron microscope (SEM) images of the fracture surface are given to help explain the behavior of the fracture data. And, finally in Chapter 5, several summarizing conclusions are drawn from the study.

CHAPTER 2: REVIEW OF RELATED TOPICS

In this chapter, the subjects related to this research are reviewed. This includes reviews on: high temperature polymers, aging effects on physical properties, and creep fracture.

2.1 High Temperature Polymers

There has been a growing demand for polymers capable of withstanding temperatures in excess of 150 °C. Although there are some polymers capable of reaching this temperature regime, they often are not viable candidates due to their extremely difficult processing. High temperature polymers can be divided into four groups: 1) polyimides, 2) phenolics, 3) polybenzimidazoles, and 4) epoxy [18].

Polyimides, phenolics, and polybenzimidazoles have been used successfully in high temperature applications but, suffer from some form of processing difficulty due to the evolution of volatiles. Epoxy on the other hand has been the polymer of choice for most composite and adhesive systems due to its relatively good temperature capability and the ease of processing. Epoxies can be processed without solvents and do not evolve volatiles during the curing process.

Numerous research effort have made strides at providing high temperature resistance polymers that also possess improved processing characteristics. Some of the most important advances have been made in the area of polyimides. The traditional processing problem with condensation polyimides has been the removal of solvents and the byproducts requiring the use of clever venting schemes and high pressure processing to eliminate void formation. One of the attempts to eliminate this problem focused on forming low molecular weight polymers where the imidization occurs prior to processing and an addition process is used to crosslink reactive endcaps [12,13]. Among this type of

polyimide is PMR-15 (the subject of this study) developed at NASA Lewis Research Center.

2.2 Aging Effects on Physical Properties of Polymers

Aging can have a dramatic effect on mechanical properties such as creep and stress relaxation, and on rate dependent failure properties (e.g., tensile strength, toughness, creep fracture, etc.) [2].

Aging in polymers can be separated into two categories, physical and chemical aging. Chemical aging is caused by irreversible chemical reactions (e.g. chain scission, crosslinking, and polymerization reactions.). Chemical aging can occur if the polymer is exposed to high temperatures. Physical aging is a reversible collapse of free volume occuring in amorphous polymers below the glass transition temperature (T_g). When the temperature is raised above T_g, the molecules are free to move and maintain the equilibrium volume associated with that temperature. However, as the polymer is cooled below T_g the molecules no longer have the freedom to move easily to the equilibrium position. Thus, the polymer is in a nonequilibrium state and as a result, will continue to shrink in an attempt to achieve equilibrium. A method to measure free volume has been developed in recent years. It consists of measuring the lifetime of positrons (Positron Annihilation Lifetime - PAL) injected into a polymer sample. This method of measuring free volume was used by Chang et al [22] to correlate free volume and relaxation times of three miscible blends: polystyrenem/poly (2,6-dimethyl, 1,4-phenylene oxide), polystyrene/poly (vinylmethylether), and poly (methylmethacrylate)/poly (ethyleneoxide)

at temperatures below T_g. It was found that as the free volume of the specimen increased the molecules ability to move in an effort to dissipate stress also increased.

2.2.1 Aging Effects on Creep

Most polymers exhibit time-temperature dependent deformations under load (creep or relaxation). Polymers exhibit this rate sensitivity to a much higher degree than do metals. The long molecules of the polymer move in response to loading. The amount the molecules can move is governed by many factors. Among these are: whether or not the polymer is crosslinked, aging condition (both physical and chemical), temperature, and the time allowed for the molecular motion to take place.

Physical and chemical aging can have a large effect on time dependent creep properties. Struik [1] outlines that physical aging is similar in a number of materials in that it is a fundamental reduction in molecular mobility due to the collapse of free volume. He also points out that chemical aging may exhibit similar effects on properties as it also can result in decreasing molecular mobility (e.g., due to additional crosslinking). The effect of chemical aging on creep properties and on T_g has been studied previously [19,20,21]. It was shown that chemical aging, in the form of additional crosslinks, leads to an increase in T_g. Also, it was shown that chemical aging (additional crosslinks) shifts creep curves horizontally to longer times but, by a much larger amount, than physical aging. This shifting of relaxation curves is directly related to the coupling of relaxing molecules. The degree of coupling can be measured with a β parameter which indicates the width of the relaxation spectrum [22]. Specifically, increasing β indicates a decrease in the width of the relaxation spectrum and a weaker coupling of relaxing elements. It

was shown that as the temperature is raised closer to T_g , β increases and the coupling of molecular elements is reduced leading to shorter relaxation times. It was also shown that as the free volume was reduced during aging that β decreased and the coupling of molecular elements increased leading to longer relaxation times.

2.2.2 Aging Effects on Modulus

Aging can effect the modulus of a polymer different ways. Chemical and physical aging have been shown to lead to an increase in the high temperature modulus of polymers [3]. Low temperature (i.e. well below T_g) modulus however has been shown to be effected very little by chemical or physical aging [21, 23, 24]. The increase in the high temperature modulus is due to the increase in T_g (more crosslinks) caused by chemical aging and physical aging causes the molecules to be more tightly packed thus limiting their mobility [20]. The fact that low temperature modulus in relatively unaffected by chemical and physical aging is a manifestation of the fact that the molecules are already frozen in place due to the low temperature and any increase in this constraint due to aging is minimal.

2.2.3 Aging Effects on Strength

Aging affects both yield strength and the ultimate tensile strength. It has been shown by numerous researchers that the yield strength increases with physical and chemical aging due to the increased molecular packing and additional crosslinking respectively. The ultimate tensile strength has been shown to be affected by chemical and physical aging. In a study conducted by Truong [24] it was shown that for a chemically stable epoxy (i.e. no chemical aging) that the yield strength increased when physically

aged at temperatures below T_g. It was also shown that the increase in yield strength was not sustainable and that an asymptotic maximum was reached.

Chemical aging in the form of crosslinking has a similar effect on tensile strength. A failure curve originally developed by T.L. Smith was presented as a convenient way to condense stress-strain data into a single diagram [21]. In this diagram, the logarithm of tensile strength is plotted against the logarithm of elongation at break. It is interesting to note that the shape of this curve in nearly unchanged with testing speed or temperature. Changes in testing speed or temperature merely shift the experimental data around the curve. However, increasing the cross-linking density shifts the curve up and to the left (i.e. increasing tensile strength and a reduction in elongation to break). It is also pointed out that while most polymers exhibit an initial increase in strength with additional cross-linking, after the polymer has become highly cross-linked a sometimes severe reduction in strength is realized. In theory the strength should increase with additional cross-links because the weak Van der Waal's bonds are replaced by strong covalent bonds. It is speculated by Nielsen [21] that the reduction in strength is a result of submicroscopic flaws that are inherent in the polymer. The size of these flaws is probably dependent on aging condition (chemical and physical). It is the flaws that then lead to failure of the material upon application of stress. This failure process can be discussed in the same realm as fracture mechanics. Therefore, failure is dependent, among other things, on flaw size c and surface energy γ. The surface energy is the amount of energy required to produce new surface area. In general it is not known how aging effects surface energy.

Separating the effects of flaw size and surface energy effects is needed if a detailed understanding of the failure process is to be understood.

2.2.4 Aging Effects on Toughness

The study of long term aging effects on time independent fracture toughness of polymers has not been investigated extensively by past researchers. A study conducted by Poole and Lin [20] investigated the effect of high temperature aging and test temperature on the mode I and mode II fracture toughness of a graphite/polyimide (IM7/K3B) system. This polyimide is reported to be a thermoplastic so no crosslinking effect should play a role in the changes in fracture toughness. The glass transition temperature of the IM7/K3B system was around 216 ^{0}C. In this study, double cantilever beam specimens were aged at various temperatures up to 204 ^{0}C for nine months. The specimens were then tested at the same temperature they were aged at. It was shown that for all aging temperatures, the fracture toughness shows an initial increase with aging up to one month (720 hours), then declines with further aging up to three months, and then shows a slight recovery with further aging. No explanation was given for the increase in toughness with initial aging up to one month. The reason for the drop in toughness with aging beyond one month was speculated to be chemical degradation but no data was given to substantiate the claim. It was also shown that regardless of aging condition the fracture toughness as a function of test temperature dropped when the test temperature was increased above 150 ^{0}C.

In a second study conducted by Troung [24], it was shown that for a chemically stable (i.e. no chemical aging) epoxy the fracture toughness showed a dramatic decline

after aging (physical aging only) in nitrogen for 35 days. This was shown to be related to an associated increase in the yield strength of the epoxy caused by physical aging.

2.3 Visco-elastic Fracture

Most polymers exhibit time and temperature dependent deformations under load (creep or relaxation). Polymers exhibit this rate sensitivity to a much higher degree than do metals. The long molecules of the polymer move in response to loading. The amount the molecules can move is governed by many factors. Among these are: whether or not the polymer is cross-linked, aging condition (both physical and chemical), temperature, and the time allowed for the molecular motion to take place.

In general, cross-linked polymers will undergo fracture primarily by rupture of the molecular network whereas uncross-linked polymers may flow rather than fracture [17] of course the exact character of the fracture is dependent on many aspects such as aging condition, temperature, time, etc.. When temperature is raised molecules have more freedom to move in response to loading. This tends to make the forces exerted on individual molecular chains more uniform [4]. As the temperature is decreased molecular motion becomes much more difficult and the imposed load is distributed over a much smaller number of molecular chains leading to earlier chain rupture. The process zone at the tip of a crack in which the material fails is also affected by these same concerns. In a highly cross-linked polymer, the size of this process zone is very small (on the order of a few hundred angstroms) especially when rapid crack growth is concerned but, in the case of a lightly cross-linked polymer the size of the cohesive zone may be on the order of millimeters when slow crack growth is concerned [17]. The modeling of this cohesive

zone has been the subject of many research studies. Most notably is the work by Schapery [6, 7, 8]. In Schapery's initial formulation, no restrictions were placed on the material in the failure zone and the material outside the zone was assumed to be linear visco-elastic. Later, an energy failure criteria is used to describe the failure in the process zone at the crack tip. Other notable studies done by Knauss [15,16] were also done for a linear visco-elastic material. The main difference in these studies was the modeling of the failing material at the crack tip. Knauss pointed out that the exact distribution of the stresses in the cohesive zone are only of secondary importance when predicting crack growth as most of the details of the disribution are lost in integration processes.

A study by Williams [19] showed that Linear Elastic Fracture Mechanics (LEFM) could be applied to polymers exhibiting brittle fracture. The assumption was made that these polymers were nearly linearly visco-elastic. The time dependent strains were represented by,

$$e(t) = C(t)\,\sigma,$$

where e(t) is the time dependent strain,

C(t) is the time dependent compliance,

and σ is the applied stress level.

CHAPTER 3: EXPERIMENTAL STUDIES

3.1 Material System

The material used in this study PMR-15, Polymerization of Monomeric Reactants, was provided by NASA Lewis Research Center. It is a highly cross-linked polyimide. The PMR-15 neat resin panels (132 mm x 132 mm x 2.5 mm thick) were processed as shown in table 3-1 (information provided by NASA Lewis Research Center). The neat resin panels (post stage 2) are then cured an additional 16 hours at 316 °C to further complete the cross-linking reactions. These panels were ultransonically C-scanned upon receipt and found to be free of any large voids.

Table 3-1: PMR-15 Neat Resin Processing

Stage	Description
	Start with mix of Methanol and monomers
1	Ramp from room temperature to 93 °C in oven and hold
	for 2 hours. Results in uncross-linked molding powder.
2	Place molding powder in press and increase pressure
	and temperature gradually to 9.0 Mpa and 316 °C and
	hold for 2 hours. Results in well consolidated, partially
	cross-linked panel.

3.2 Specimen Geometry

Three specimen configurations were used in this research. The first was a dogbone specimen configuration, shown in Figure 3-1. It was used in tensile tests to determine the basic stress-strain response of the PMR-15 resin. The second configuration was a standard compact tension specimen (per ASTM D 5045-91a) used for fracture

testing (shown in Figure 3-2). The third was a creep specimen which were straight-sided specimens with dimensions 9.7 mm x 75.0 mm x 2.5 mm.

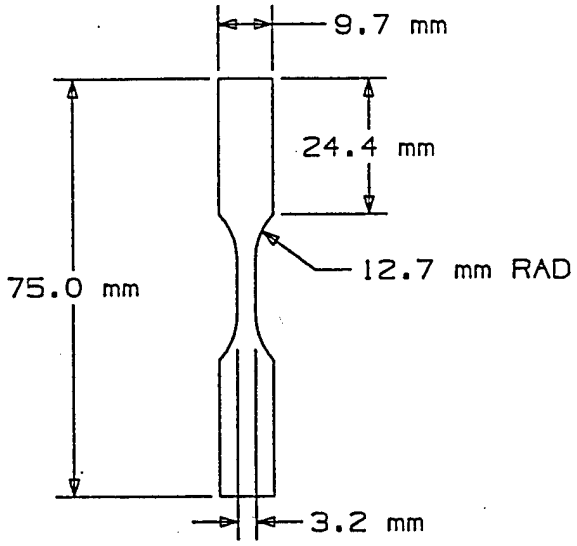

Fig 3-1: Dogbone specimen (thickness 2.5 mm)

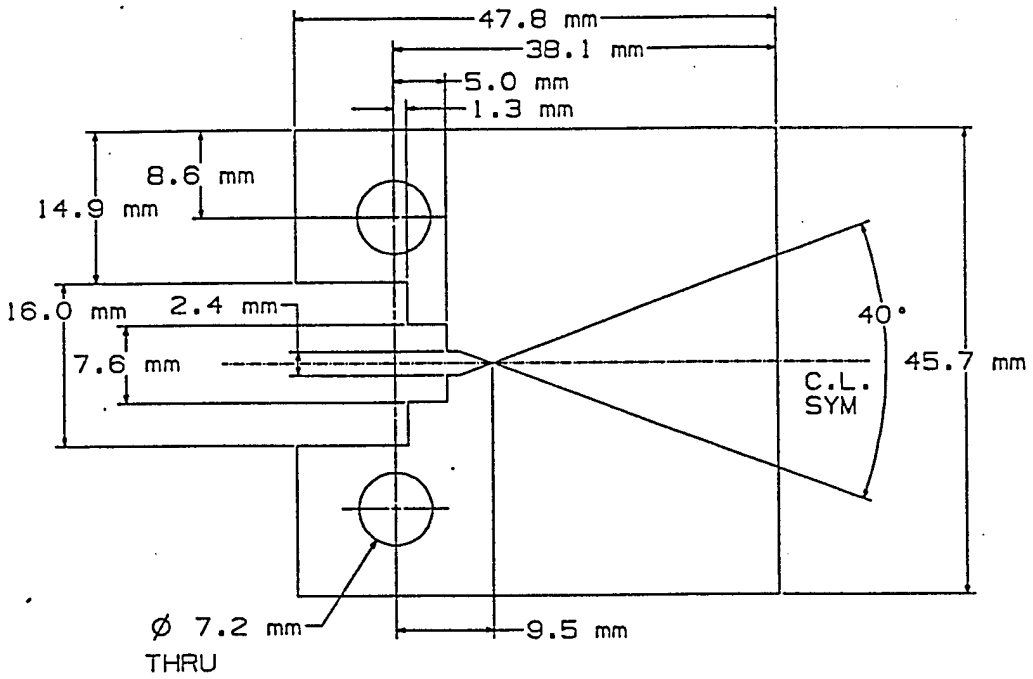

Fig 3-2: Compact tension specimen (thickness 2.5 mm)

3.3 Experimental Setup

The following section will discuss the equipment used in each type of testing conducted. This will include testing in the areas of; fracture, creep, and aging.

3.3.1 Fracture Test

The fracture tests were conducted using a screw driven Instron machine model 4505 with an Applied Test System (ATS) oven shown in Figure 3-3. Loads were measured using an Instron load cell with a full scale reading of 224 lbs. Load-line displacement measurements were taken with a capacitance based gage that was clipped to two knife edges that were attached to the compact tension specimen (reference Figure 3-4). The time, load, and load-line displacement were stored on a data acquisition system for later analysis.

Fig. 3-3: Instron machine with oven used in fracture testing

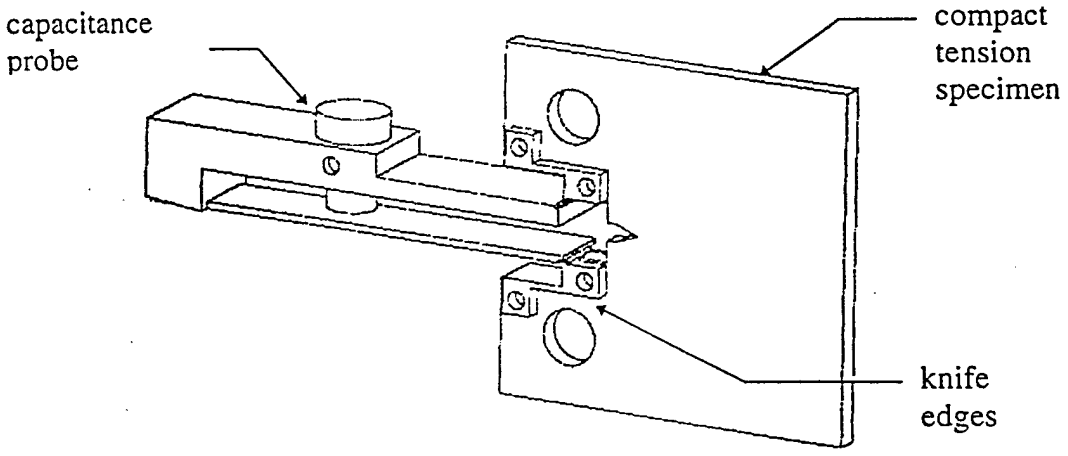

Fig. 3-4: Load-line displacement gage with knife edges used in fracture testing of the compact tension specimen

3.3.2 Tensile/Creep Test

The equipment used in the creep testing was a uniaxial servo hydraulic test machine manufactured by Instron fitted with a ATS oven. Displacements were measured with the aid of a capacitance based gage (similar to that used in the fracture testing). The gage was equipped with knife edges that were secured to the surface of the specimen with springs. Load measurements were taken with a MTS Systems Corporation load cell with a full scale reading of 1000 lbs. The time, load, and displacement data was recorded on a data acquisition system for later processing.

3.3.3 Aging Test

Aging tests were conducted by two different methods, one method for short term aging studies and one for long term studies. The short term (0-100 hours) method was to use the oven and capacitance probe used for the creep and tensile testing. The tests were conducted in an air environment and the time and strain data were recorded on a data acquistion system. Long term aging studies needed to be conducted in an inert enviroment and for that reason and other logistical reasons these tests were conducted by using a small tube furnace that was continually purged with helium. Strain measurements were taken by hand using a dial caliper with resolution down to 0.025 mm (0.001 in)

3.4 Experimental Procedure

Section 3.4 will present a discussion of the details of any further processing that took place on the test samples and will also describe methods used. It should also be noted at this time that all specimens were dried for 24 hours at 125 °C before testing. This was to prevent any influence that moisture content may have had on the test results.

3.4.1 Monotonic Tensile Loading and Unloading

There were two different types tests conducted in this section. The first test was done to get the basic stress-strain response to failure. This test was conducted at several different temperatures. The dogbone samples mentioned in Section 3.2 were used for this testing. These tests were repeated at least twice at each test condition and an initial strain rate of 4.5 [%/min] was used in all cases. The results of these tests are shown in Section 4.1.

The second loading scheme was also performed on the dogbone sample but in this case the load was applied again to achieve a strain rate of 1.5 [%/min] but, this time only 72% of the ultimate load at the given temperature was applied. The load was then immediately removed and the strain recovery was observed. A further discussion of this test and the results can be found in Section 4.1

3.4.2 Creep

All creep testing was done on the straight sided specimens. This testing was done to ascertain the time dependent deformations at a given temperature and to determine if the creep compliance was linear with respect to stress and time. Before the creep testing was conducted the specimens were first aged for various times in order to determine the effect that aging had on the creep strains and on the linearity. When the aging was completed, a servohydraulic uniaxial test machine manufactured by Instron was used for the testing. Constant stress levels were applied (0.2 σ_{UTS}, 0.3 σ_{UTS}, 0.4 σ_{UTS}, 0.5σ_{UTS}) at 316 °C (600 °F) and 343 °C (650 °F) and the strain buildup with time and the load were

recorded on the data acquisition system. Even though the specimens were aged before the creep tests began it should be pointed out that there was also continual aging (both physical and chemical) during the creep tests since these tests were conducted at relatively high temperatures. This continual aging process slowed the creep strains produced (see Figure 4-9). Results from this testing can be found in section 4.1.

3.4.3High Temperature Aging

The purpose of the aging tests were two-fold. First the aging strains needed to be acquired to determine if any relationship existed between aging strain accumulation and fracture toughness. The second purpose was to separate the effects of chemical and physical aging and to determine over which time and temperature ranges each operated and to what extent.

Three types of aging studies were conducted. In the first test the aging strains (due both to chemical and physical aging) were determined by placing small specimens (50 mm x 9.7 mm x 2.5 mm) in a high temperature oven and continually measuring the contraction of the specimen with no load applied. These tests were conducted in air. The test time was limited to approximately 100 hours because other testing was planned with this oven. The purpose of the second aging test was the same as the first (i.e., to determine aging strains) but, it was conducted for much longer times (2000 hours) and was conducted in a helium environment to prevent oxidation (i.e. oxidation would remove material from the surface being measured and effect the strain measurement). The aging strains were determined by simply removing the specimens at specified time intervals and measuring them with a micrometer. The dimensions measured on these

samples were kept large (approximately 75 mm) so that the aging strain could be accurately measured with a micrometer. The third type of aging study performed consisted of measuring the change in glass transition temperature (T_g) as the samples were aged to varying degrees. This was done using a Differential Scanning Calorometer (DSC). As mentioned earlier changes in the T_g reflect chemical aging and are irreversible. See Section 4.3 for results of the aging tests.

3.4.4 Fracture

After fabrication of the compact tension specimens, they were aged in helium at 316 °C (600 °F) for various times, up to 2000 hours. The next step proved to be the most difficult. It was the production of a sharp crack tip. This was done by cutting a small chevron notch at the apex of the prefabricated notch and growing the crack to the desired length using the Precrack Device shown in Figure 3-5. This device allowed for a very controlled application of mode I loading which was essential to grow stable cracks that could be stopped at a desired location. The crack tip location was monitored with the aid of a telemicroscope. The specimens were then fitted with knife edges and a capacitance based load-line deflection gage (shown in Figure 3-4) and placed in the oven for testing. Once the oven was at the desired temperature the crosshead was driven at 0.0025 mm/sec.

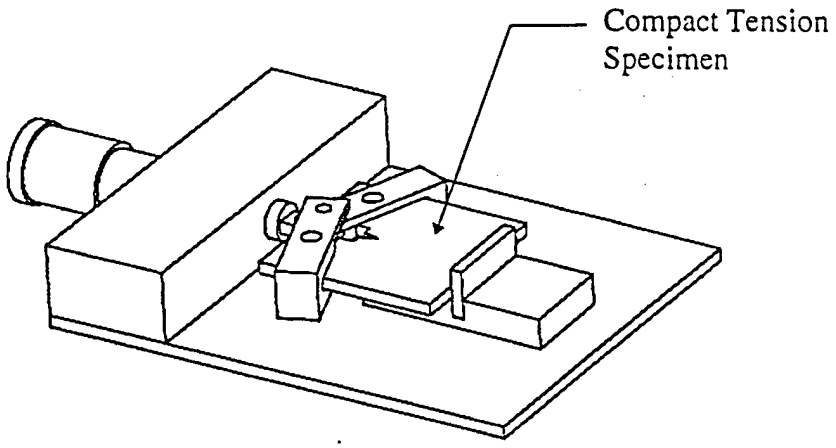

Fig 3-5: Precrack device

CHAPTER 4: RESULTS AND DISCUSSION

4.1. Material Model Determination

4.1.1 Monotonic Tensile and Unloading Tests

As mentioned earlier, one of the first tasks was to determine the stress-strain response of PMR-15 neat resin for the conditions (time, temperature, and aging condition) of interest. This was done with a series of monotonic tensile tests in which the specimens were taken to failure and then a set of tests in which only 72% of the breaking load was applied and then removed in order to characterize the unloading characteristics. The results of the monotonic tensile tests are shown in Figure 4-1. These tests were conducted at three different temperatures. As can be seen from Figure 4-1 the modulus of the material decreases with temperature Also, it should be noted that the ultimate strength (S_{ult}) decreases from about 80 MPa (11.6 Ksi) at room temperature to around 30 MPa (4.3 Ksi) at 343 °F (650 ^{0}F). The strain to failure shows a dramatic increase from roughly 2.3% at room temperature to over 8.0% at at 343 °F (650 ^{0}F). Since aging (chemical and physical) can dramatically shift these curves it should be noted that these tests were conducted on specimens that had only been aged for 16 hours at 316 °C (600 ^{0}F). Further aging would have tended to increase the stiffness of the specimens and make them behave as if they were being tested at a lower temperature. The increased stiffness with aging can be seen by observing the creep compliance curves shown in Figure 4-9.

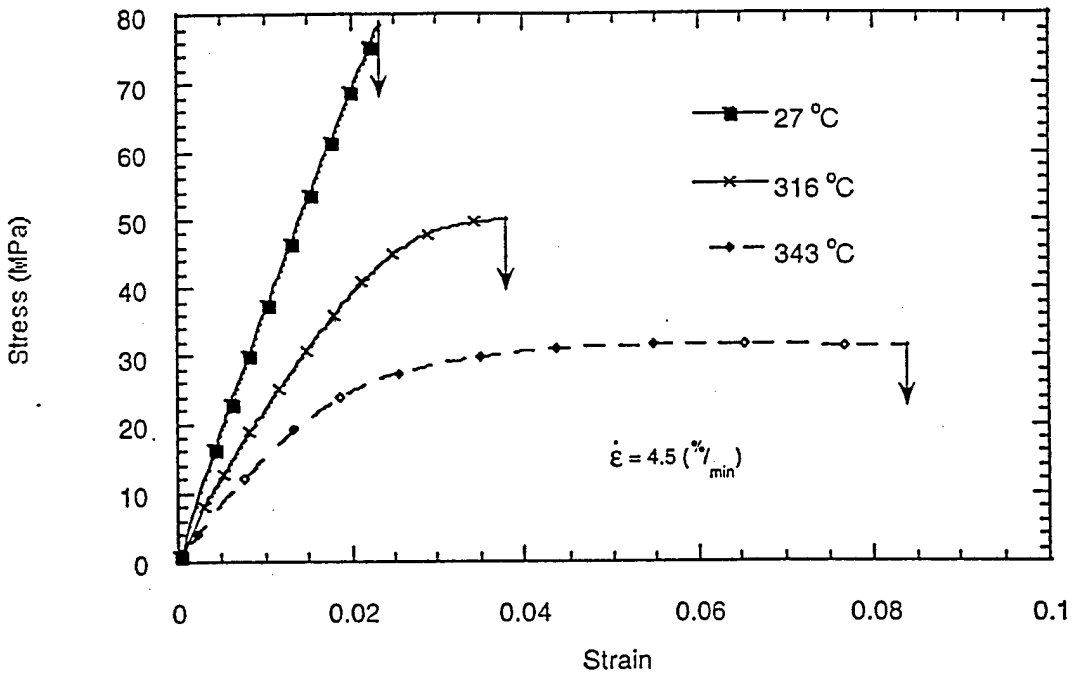

Fig 4-1: Stress-strain relationship for PMR-15 neat resin at various temperatures (note: all specimens conditioned for 16 hours at 316 °C (600 °F) before testing)

The other type of tensile test conducted was to apply the load up to 72% of the breaking load and then remove the load and observe the strain recovery. This was done to determine the material model whether it be linear elastic, elasto-plastic, visco-elastic, etc. The loading and unloading curves are shown in Figure 4-2. These tests were all conducted at 316 °C (600 °F) as this was the highest temperature used in the fracture testing and at this temperature the largest time dependent strains would be observed. As can be seen from the figure, all the strain was recovered. Most of the recovery strain was elastic (approximately 1.25%) and only a small portion was visco-elastic (about 0.10%).

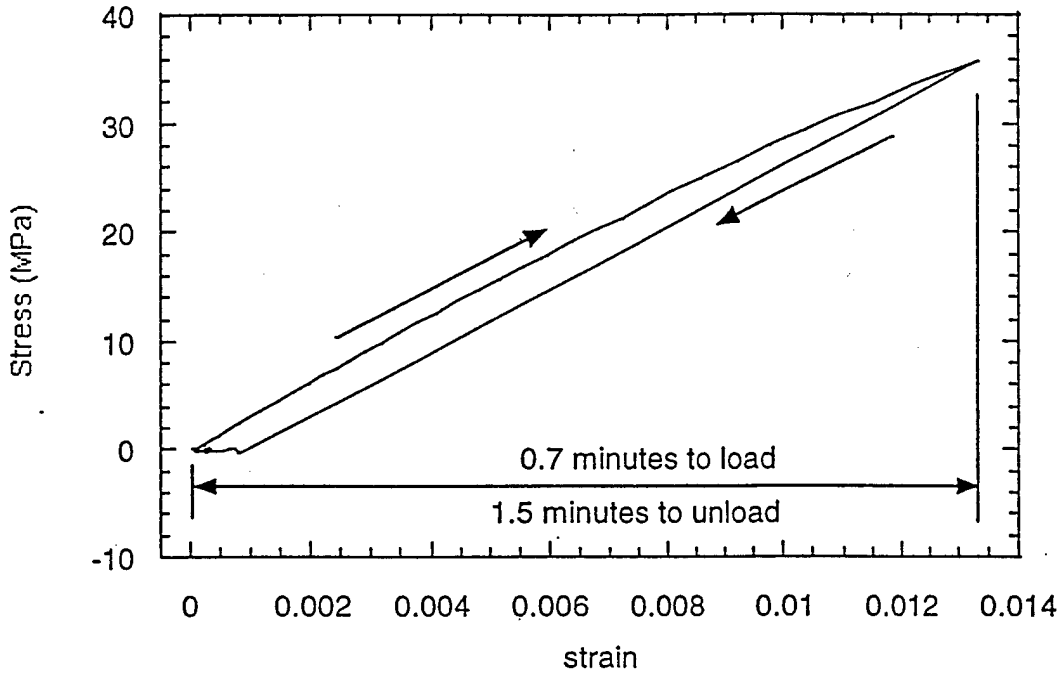

Fig 4-2: Loading and unloading for PMR-15 neat resin tested at 316 °C (600 °F) (note: conditioned for 16 hours at 316 °C (600 °F) before testing, strain rate 1.5 %/min)

4.1.2 Creep Tests

Creep testing revealed the magnitude of the time dependent strains and were also used to verify the linearity of the creep compliance with respect to stress level and loading time. The specimens were loaded at various stress levels up to 50% of the ultimate strength and the creep strains were recorded. Creep strains for 316 °C and 343 °C are shown in Figures 4-3 and 4-6 respectively. Also, shown on these figures is a no load strain which is the shrinkage due to the high temperature aging. In figures 4-4 and 4-7, creep compliance curves for 316 °C and 343 °C are shown. To more easily see the stress and time linearity of the creep compliance the data contained in Figures 4-4 and 4-7 is sliced at certain time intervals and plotted in Figures 4-5 and 4-8 for 316 °C and 343 °C

respectively. From these figures it is easily seen that the creep compliance is more linear with respect to stress and time at 316 °C than it is at 343 °C. The compliance becomes more nonlinear with time at both temperatures however, it is much more pronounced at 343 °C.

Included for reference are short term creep compliance curves in Figure 4-9. These curves show how the PMR-15 creep strains decrease with aging time (t_a). Also shown is the increase in stiffness with increased aging time. This is indicated by the downward shift of the compliance curves.

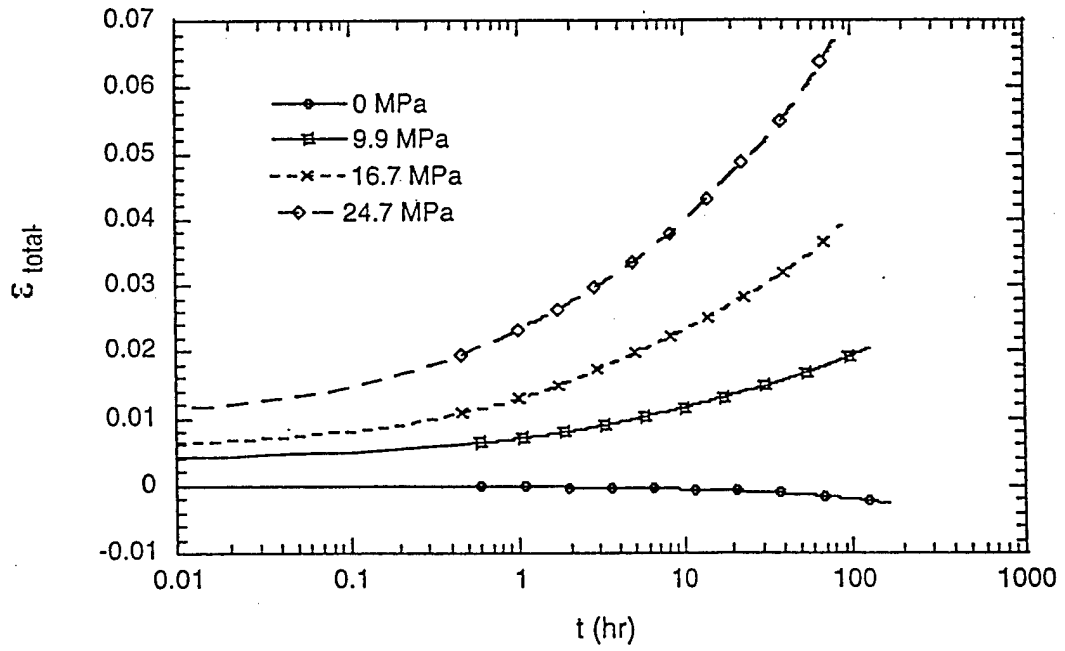

Fig. 4-3: Total creep strains for PMR-15 neat resin tested at 316°C under various applied loads
(note: all specimens conditioned for16 hours at 316°C before testing)

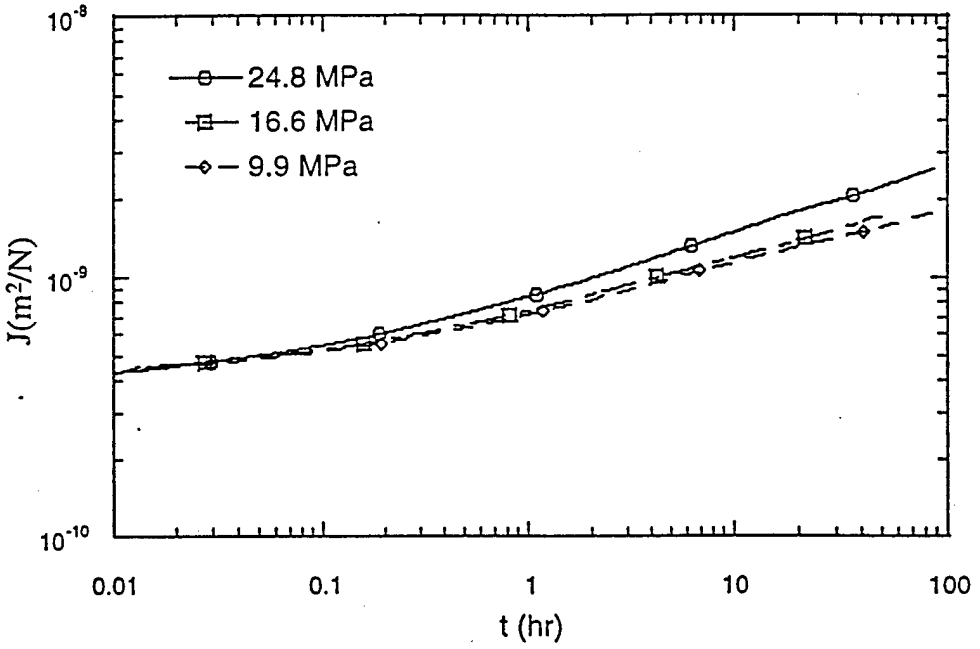

Fig. 4-4: Total creep compliance at various stress levels for PMR-15 neat resin tested at 316 °C (600 °F) (note: all specimens conditioned for16 hours at 316 °C before testing)

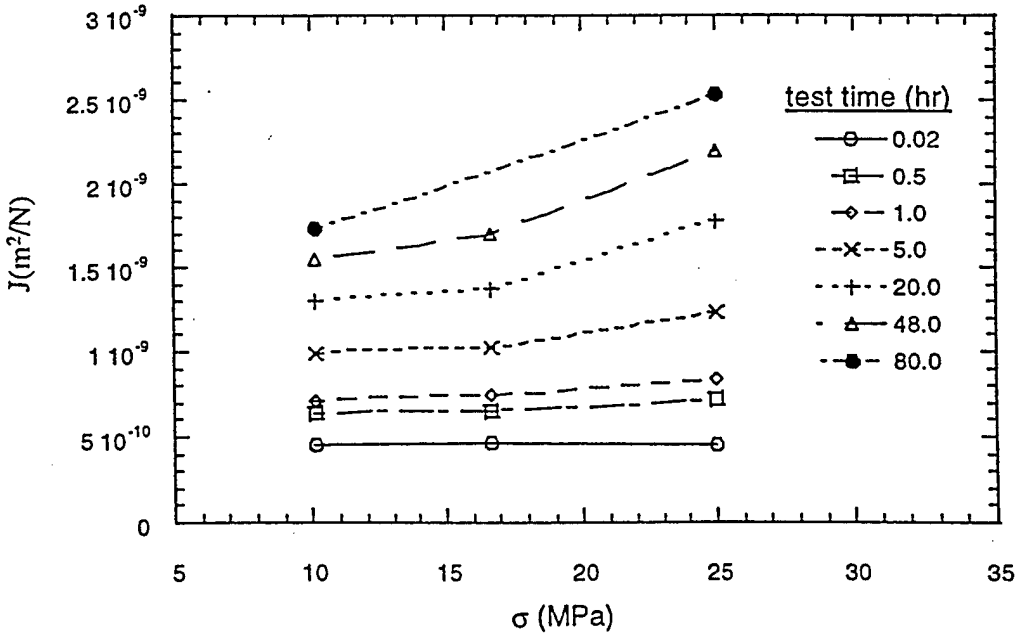

Fig. 4-5: Total creep compliance as a function of stress level for PMR-15 neat resin tested at 316 °C (600 °F) (note: all specimens aged 16 hours at 316 °C before testing)

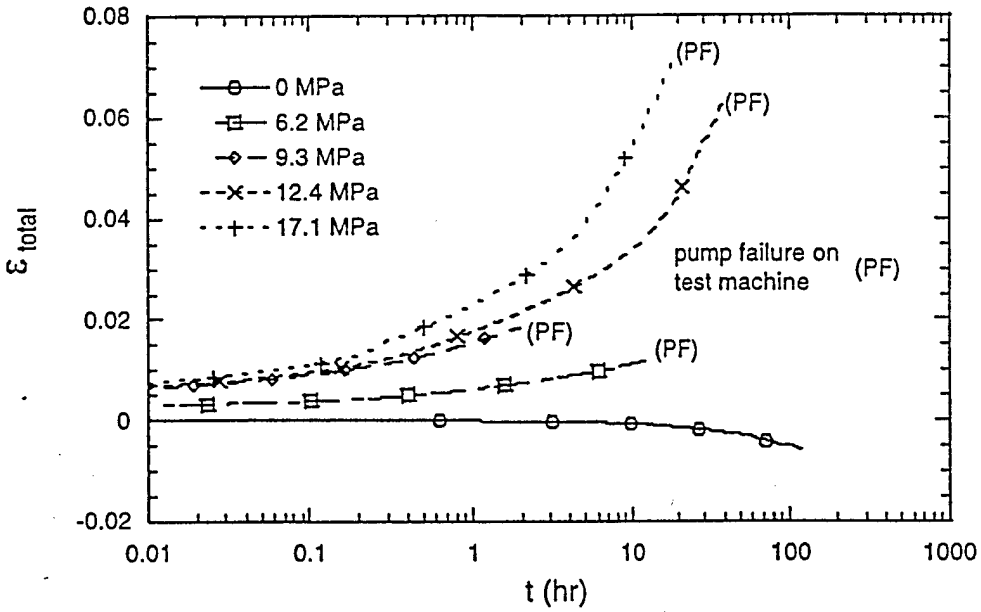

Fig. 4-6: Total creep strains for PMR-15 neat resin tested at 343°C (note: all specimens conditioned 16 hours at 316°C before testing)

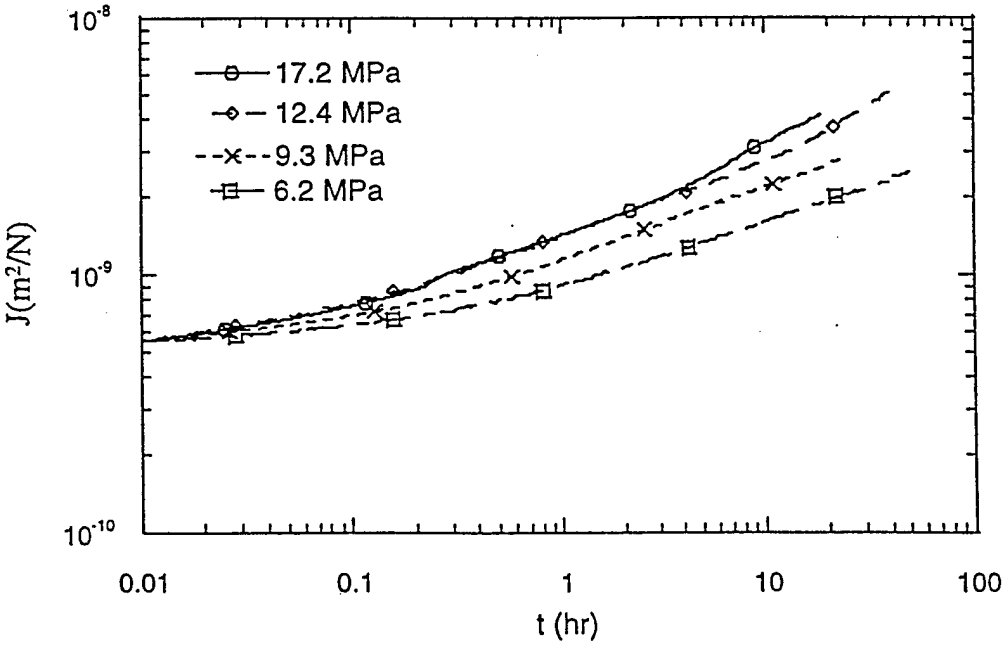

Fig. 4-7: Total creep compliance curves at various stress levels for PMR-15 neat resin tested at 343°C (650°F) (note: all specimens aged 16 hours at 316°C before testing)

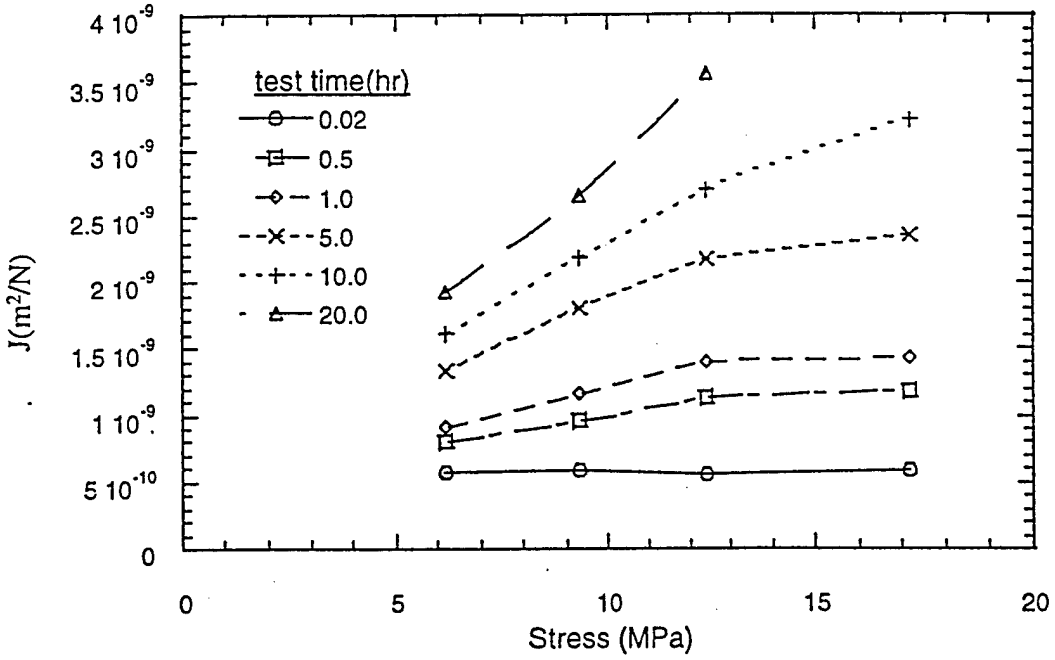

Fig. 4-8: Total creep compliance curves as a function of stress level for PMR-15 neat resin tested at 343 °C (650 °F) (note: all specimens conditioned 16 hours at 316 °C before testing)

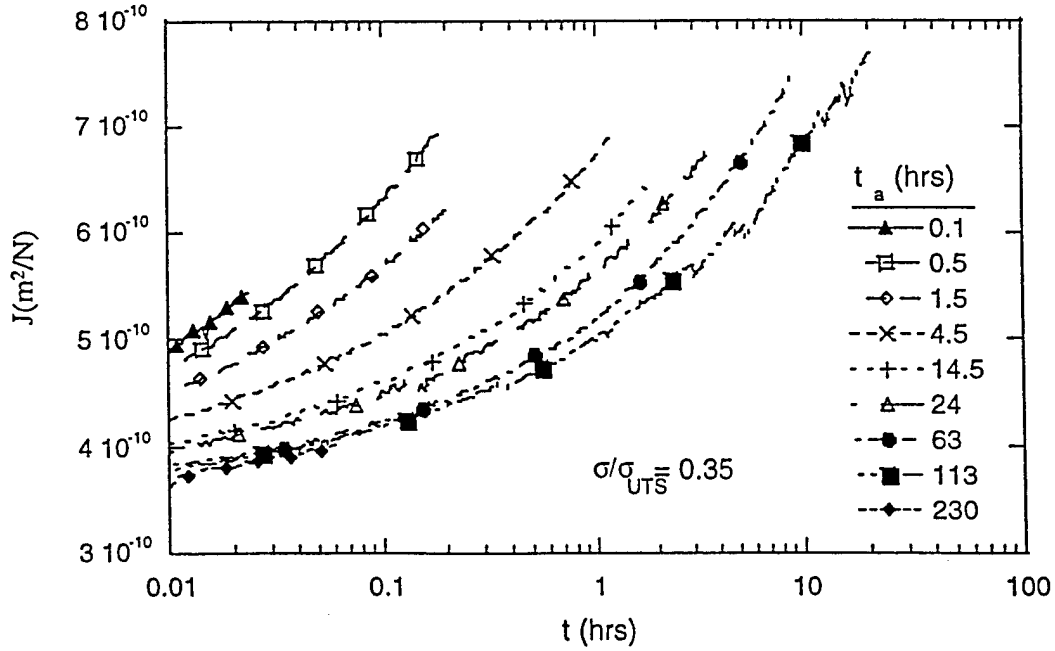

Fig 4-9: Series of short term creep tests for PMR-15 neat resin at 316 °C *(note t_a is the aging time and t is the time the load was applied)*

4.2 Fracture Model Selection

In this section: the time from initial loading of the fracture specimen until crack growth initiates will be established, the maximum size of the process zone attending the crack tip will be estimated, and the use of Linear Elastic Fracture Mechanics (LEFM) will be justified.

The time from initial load application until fracture initiation will be called the initiation time (t_i) throughout the remainder of this paper. This use of t_i should not be confused with the conventional use of the term which is the time from application of a constant stress ($\sigma < \sigma_c$) until the crack tip moves. As shown in Figure 4-10, the longest timeframe (t_i) from the initial loading of the fracture samples until crack initiation, was on the order of 1.6 minutes which occurred at the highest test temperature 316 °C (600 °F). All fracture tests conducted at 316 °C were approximately of this time scale. Tests conducted at lower temperatures showed lower crack initiation times as can be seen in Figure 4-10 for a room temperature test. Therefore, the worst time dependent strains occur in the 316 °C fracture tests and can accumulate for up to 1.6 minutes.

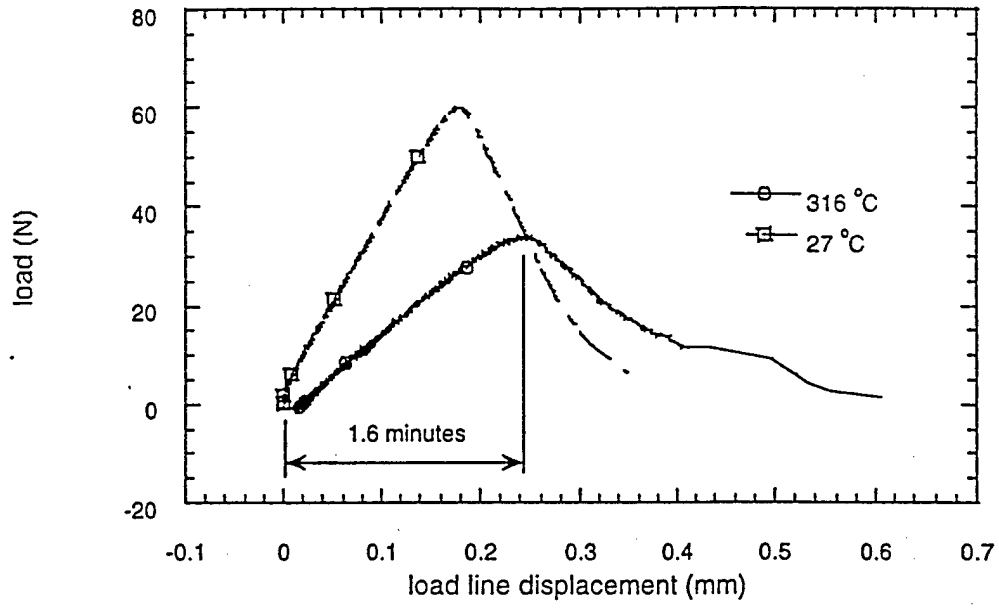

Fig. 4-10: Load versus load-line displacement for PMR-15 neat resin fracture (note: specimens conditioned for 16 hours at 316 °C before testing)

The process zone at the crack tip will be defined as the zone in which something other than linear elastic behavior is present. In this zone the material behavior is unknown. However, it is most likely a combination of non-linearly visco-elastic and viscoplastic behavior. For the estimation of the maximum size of this zone, the stress distribution assumed in Figure 4-11 will be assumed with the maximum stress level (σ^*) being that which has been shown in Figure 4-2 (36 Mpa). As was mentioned, at this stress level and a loading time comparable to the fracture initiation time, the strain accumulation was approximately 90% elastic and 10% visco-elastic.

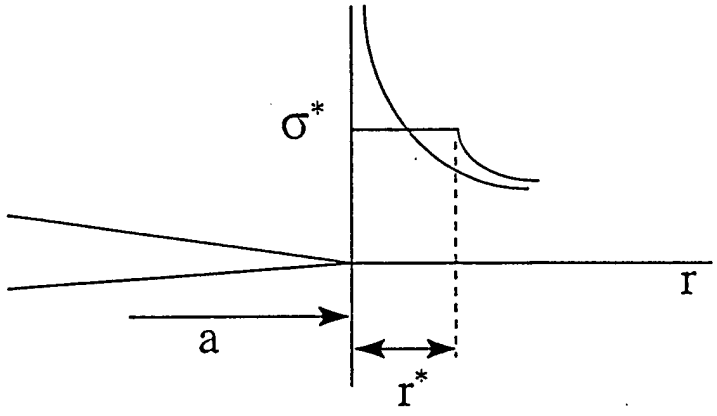

Fig 4-11: Crack tip model used to determine size of process zone attending the crack tip

For plane stress, $r^* = (1/\pi)(K_I/\sigma^*)^2$,

where r^* is the size of the process zone,

K_I is the mode I fracture initiation toughness,

and σ^* is the maximum stress level where linear-elastic behavior is observed.

For this material the maximum size of the process zone is found to occur at the maximum temperature tested (316 °C) and when K_I is maximum. This occurs at a aging time of 650 hours at 316 °C. At this point the K_{IC} value is 0.84 Mpa-$m^{1/2}$. The maximum size of the process zone is found to be 0.17 mm (at the conditions of 650 hours aging and 316 °C).

The use of LEFM is verified by checking several limiting conditions as defined in ASTM D 5045-91a (Plane-Strain Fracture Toughness and Strain Energy Release Rate of Plastic Materials). These conditions have primarily to do with verifying that the size of

the process zone is small with respect to other characteristic dimensions of the test specimen. This data is presented in Table 4-2. The dimensions of the specimen are to be less than the largest quantity (where σ_y is defined as the ultimate stress determined at approximately the same temperature and time scale that the fracture test was conducted)

$$2.5(K_{IC}/\sigma_y)^2 \text{ (mm)},$$

listed in Table 4-2. The dimension of the specimen that are to compared to this quantity are, the crack length, a = 11-20 mm,

the thickness B = 2.5 mm,

and the minimum ligament length (W-a) = 25 mm.

Table 4-1: Specimen size criteria for PMR-15 neat resin fracture testing

T (°C)	t_a (hrs)	σ_y (MPa)	K_{Ic} (MPa-$m^{1/2}$)	$(K_{Ic}/\sigma_y)^2$ (mm)	$2.5(K_{Ic}/\sigma_y)^2$ (mm)
27	16	78	1.25	0.26	0.64
316	16	50	0.70	0.20	0.49
316	650	50	0.82	0.27	0.67

Also, time dependence of the modulus is checked by verifying the linearity of the initial loading portion of the load versus load-line deflection curve. The linearity criteria basically states that the maximum load sustained by the specimen must fall within a certain range of a zone formed by offsetting the initial compliance curve by 5%. All fracture data was successfully verified against this criteria. As can be seen in Figure 4-10 even at the highest temperature tested (316 °C) during the fracture tests, the initial loading portion of the curve is linear.

4.3 Aging Test Results

As mentioned earlier, aging in polymers can take two forms. The first is physical aging which is a reversible collapse of free volume. The second is chemical aging which can take the form of crosslinking, chain scission, and polymerization. The first set of tests were used to gather information about aging strains that accumulate as the specimens are exposed to high temperature environments (316 °C and 343 °C). It should be pointed out that this is a load free test and the strains are produced only from aging. Figure 4-12 shows the aging strains as a function of aging time. Only the 316 °C test data was continued beyond 100 hours as this was the temperature at which the fracture samples were aged. The aging strain data below 100 hours was gathered in an air environment using a capacitance gage similar to the system shown in Figure 4-2. Tests data beyond 100 hours was done in a helium environment, to limit oxidation damage, and the measurements were made at discrete time interval (approximately every 100-150 hours) using a micrometer.

As can be seen in Figure 4-12, the aging strains accumulate much faster at 343 °C than they do at 316 °C. As a comparison, the aging strains at 100 hours are around 0.18% at 316 °C and almost 0.45% at 343 °C. It can also be seen that after approximately 800 hours the accumulation of aging strains appear to stop. This indicates that an equilibrium condition has been reached and that no further free volume collapse will be experienced at this aging temperature. This will be an important point later when the aging effect on fracture toughness is discussed.

It should be noted that during the above mentioned aging tests, the PMR-15 was also undergoing both chemical and physical aging. In an attempt to determine over what time-frame each is active, tests were conducted to verify the T_g change (chemical aging) with aging time. This data is shown in Figure 4-13. It should be noted that T_g° referenced on this figure is the glass transition temperature after the stage 2 cure mentioned earlier in Table 3-1. As can be seen by the figure, the chemical aging is essentially complete after approximately 50 hours. Therefore, from this T_g information it can be seen that for the 316 °C case, the aging strains produced prior to 50 hours were a combination of chemical and physical aging and after 50 hours were predominantly caused by physical aging.

To separate the aging strains produced by chemical and physical aging, the method outlined by Kung et al [16] was used. In this study, a method to determine chemical aging induced volumetric change $\Delta v_a^{(c)}$ from knowledge of the coefficient of free volume expansion α_f and the T_g change with aging is presented.

$\frac{\Delta v_a^{(c)}}{v} = -\alpha_f \Delta T_g$ where,

v is the total macroscopic volume and, ΔT_g is the change in the glass transition temperature caused by chemical aging. Here, it has been assumed that the fractional free volume is constant up to T_g and then increases linearly with temperature [25]. The aging induced volumetric change for an isotropic material may be expressed as

$$\frac{\Delta v_a^{(c)}}{v} \approx \varepsilon_{11}^c + \varepsilon_{22}^c + \varepsilon_{33}^c = 3\,\varepsilon_{xx}^c \text{ where}$$

ε_{ii}^c is the chemical aging induced strains in the *ii* direction. Therefore,

$$\varepsilon_{xx}^{(c)} = -\frac{1}{3}\alpha_f \;\; \Delta T_g$$

is the portion of the total strain production that is caused by chemical aging. The coefficient of free volume expansion was determined experimentally for PMR-15 neat resin and found to be 1.5 E-4 K^{-1}. With this information and a knowledge of the T_g change with aging time, the chemical aging induced strains can be calculated. The physical aging strain can then be determined by subtracting the chemical aging strain from the total aging strain. This is shown in figure 4-14. In this figure it can be seen that chemical and physical aging are present for about the first 50 hours but then chemical aging ceases and the strain production is strictly from physical aging.

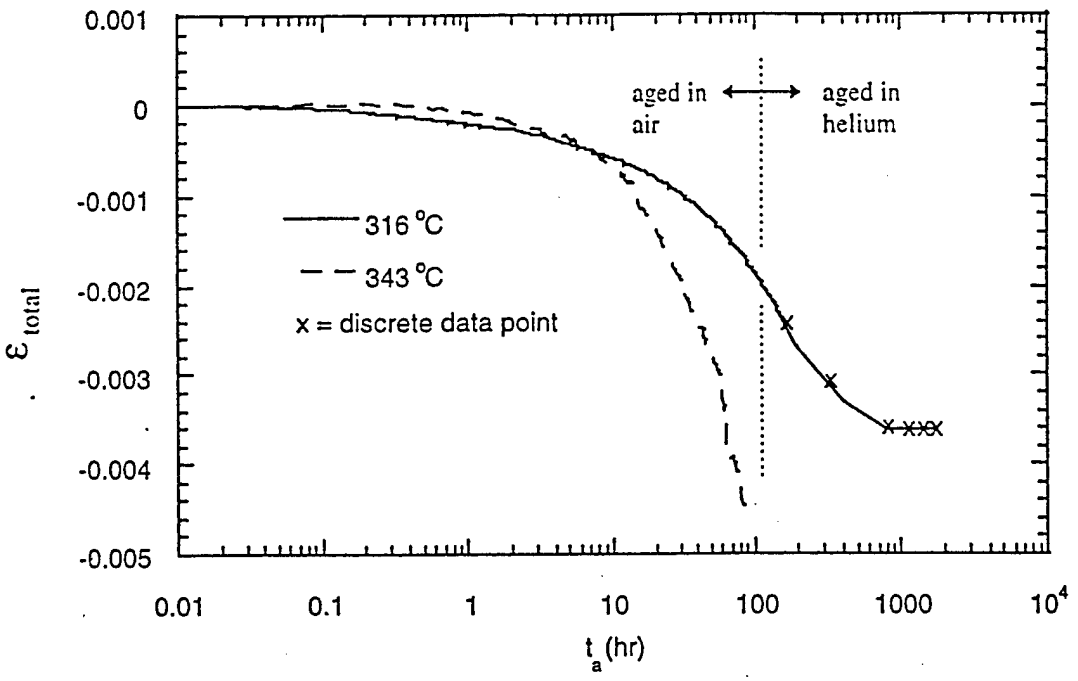

Fig 4-12: Aging strains in PMR-15 neat resin as a function of aging time for 316 °C and 343 °C.
(note: specimens conditioned 16 hours at 316 °C before testing)

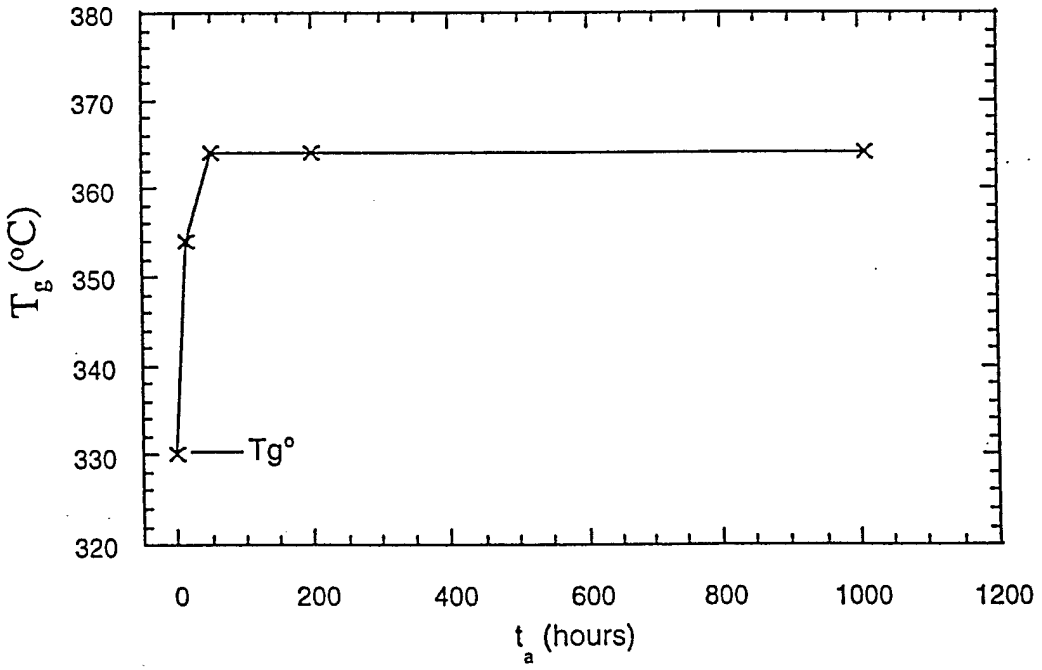

Fig 4-13: Glass transition temperature T_g as a function of aging time at 316 °C
(note: aging done in helium environment, T_g measured by DSC)

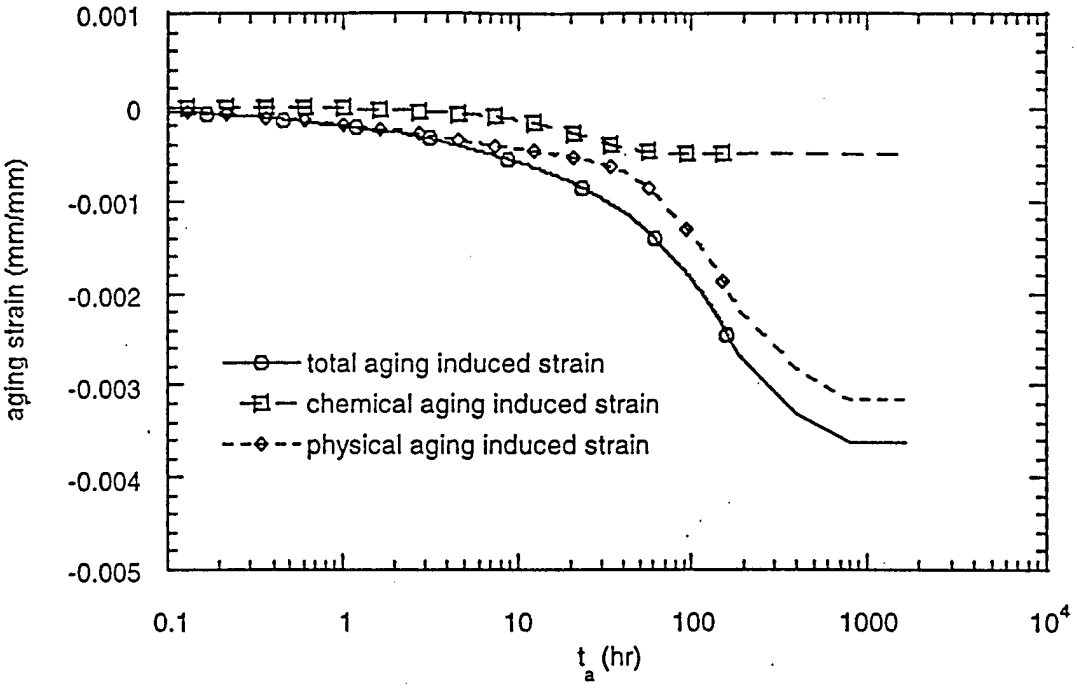

Fig 4-14: Physical and chemical aging induced strains in PMR-15 neat resin aged isothermally at 316 °C in helium.
(note: specimens conditioned 16 hours at 316 °C before testing)

4.4 Fracture Test Results

Fracture testing was conducted to characterize the effect of temperature and aging condition on K_{IC}. From section 4.2, it was determined that LEFM could be used for PMR-15 for the conditions stated. The basic governing equation for mode I fracture is

$$K_I = \sigma\sqrt{2\pi r}\, f(\sin\theta \ \cos\theta),$$

where r is the distance from the crack tip,

σ is the applied stress level,

and K_I is the mode I initiation fracture toughness.

From ASTM D 5045-91a the corresponding equation for the compact tension specimen used in the fracture testing is

$$K_Q = \left[\frac{P_Q}{B\sqrt{W}}\right] f(a/W),$$

where P_Q is applied load,

B is the thickness of specimen,

W is the width of specimen,

a is the crack length, and the geometry factor,

$$f(a/W) = \frac{\left\{[2+a/W]\left[0.886+4.64(a/W)-13.32(a/W)^2+14.72(a/W)^3-5.6(a/W)^4\right]\right\}}{(1-a/W)^{1.5}}.$$

The fracture tests were conducted at three different temperatures 93 °C (200 °F), 250 °C (480 °F), and 316 °C (600 °F). The specimens were aged for various times up to 2200 hours prior to testing. The fracture data shown in Figure 4-15 is plotted against aging time and the data is plotted again in Figure 4-16 to more clearly show the temperature effect. From Figure 4-16 it is clear that increasing temperature decreases the fracture initiation toughness regardless of the aging condition. A similar temperature effect was found by Wang and Desoutter for a thermoplastic polymer [5].

Aging also had a dramatic effect on K_{IC}. As can be seen in Figure 4-15 aging actually improved high temperature (i.e. above 93 °C) fracture toughness when aged approximately 650 hours aging at 316 °C in helium. Beyond 650 hours the fracture toughness declines until about 1000 hours aging where it levels off. The reason for the initial (up to 650 hours aging) improvement of K_{IC} with aging is thought to be primarily attributed to decreased molecular mobility brought on by aging. As mentioned earlier, the polyimide resin system (PMR-15), when aged at 316 °C, ages both chemically and physically. Chemical aging is only active for approximately the first 50 hours but, it does leads to an increase in the glass transition temperature (T_g) which can be seen in Figure 4-13. This increase in T_g results in an increase between T_g and the test temperature. Therefore, it appears as though the specimen is being tested at a lower temperature and, as mentioned earlier K_{IC} increases with decreasing temperature. Physical aging may also play a role in that it will cause a reduction in free volume and as a result lead to decreased molecular mobility. It can be observed from Figure 4-15 that the fracture toughness for the 93 °C test does not improve during the first 650 hours of aging as it does with the

higher temperature tests. The molecules at 93 °C are essentially frozen in place and therefore the aging induced decreased molecular mobility did not improve K_{IC} in this case. However, at more elevated temperatures where more molecular motion is permitted, the reduction in mobility due to the aging led to an increase in K_{IC}.

The cause for the dramatic drop in toughness beyond 650 hours is unknown. It may be due to chemical degradation. Some evidence of degradation was seen in the form of microscopic voids that formed after aging. An example of the voids detected is shown in Figure 4-18. This micrograph sample was fabricated by polishing off the fracture surface. This was done for samples with various aging conditions but insufficient micrograph samples were fabricated to determine the correlation between aging condition and void formation. A similar drop in the fracture toughness was reported by Poole et al for a graphite/polyimide composite. Their speculation was that degradation also caused the drop for the graphite/polyimide system.

As was shown in Figure 4-12, aging strains continue to build until approximately 800 hours where they level off. This corresponds to the same time in Figure 4-15 when fracture toughness levels. The point at which K_{IC} first reaches its minimum is shown to be around 1000 hours in Figure 4-15. This minimum probably occurs at a slightly earlier time (around 800 hours) as indicated by the aging curves. As mentioned earlier the diminishing of the aging strain would indicate an equilibrium condition had been reached and no further collapse of free volume from physical aging or possibly degradation was occurring. However, no fracture data exists between 650 and 1000 hours aging.

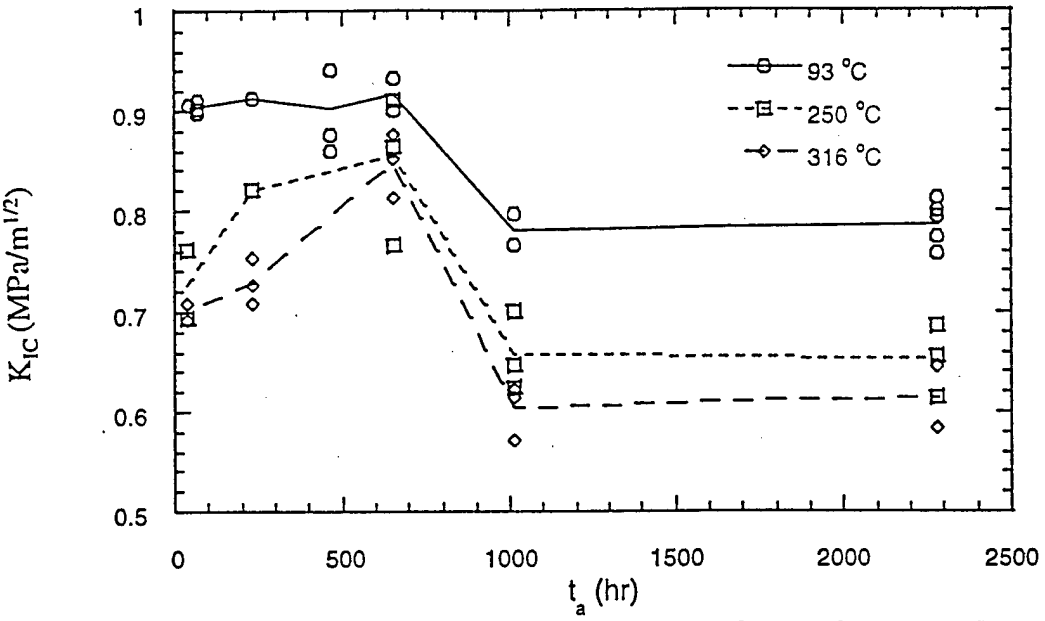

Fig 4-15: Fracture initiation toughness K_{IC} as a function of aging for PMR-15 neat resin.

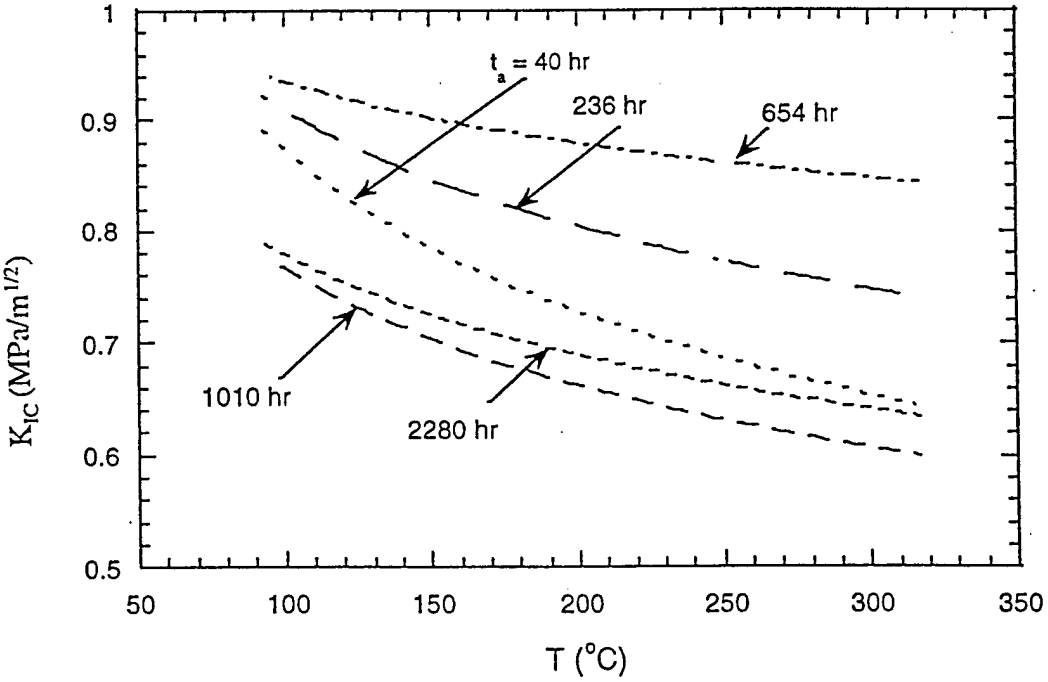

Fig 4-16: Fracture initiation toughness (K_{IC}) as a function of temperature for PMR-15 neat resin.

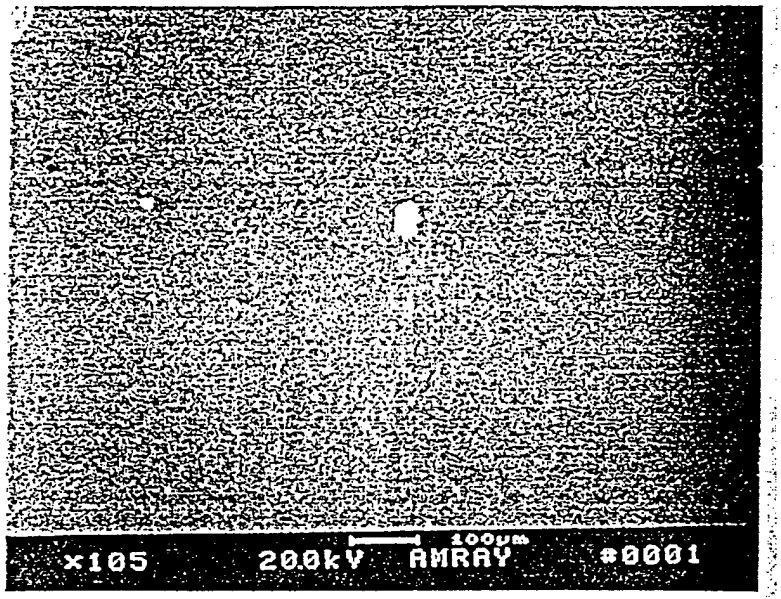

Fig 4-17: Micrograph of void free PMR-15 neat resin after conditioning 40 hours at 316 °C in helium
(note: this was an interior surface that was not exposed directly to helium environment)

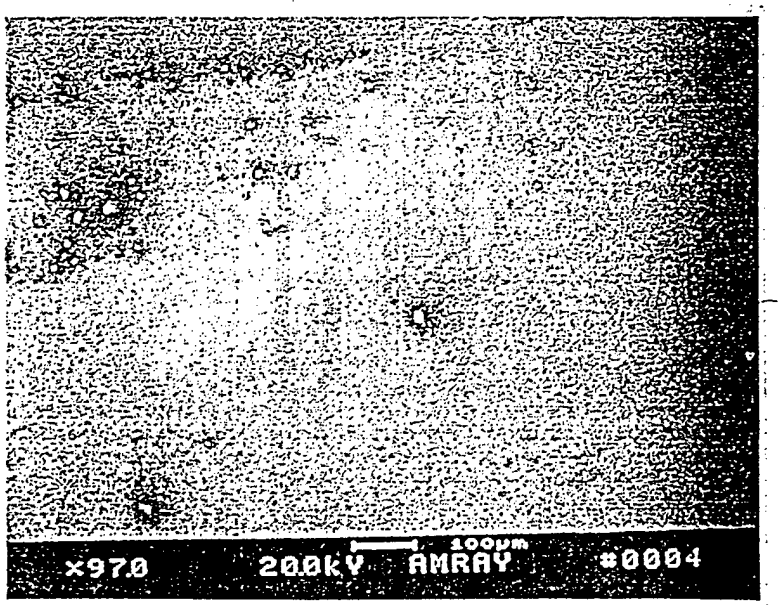

Fig 4-18: Micrograph of voids in PMR-15 neat resin after conditioning 1000 hours at 316 °C in helium
(note: this was an interior surface that was not exposed directly to helium environment)

4.5 Microscopy of Fracture Surfaces

Shown in Figure 4-19 is the fracture surface looking normal to the crack plane. This figure shows the transition line between room temperature fracture and 316 °C fracture. The room temperature fracture is shown in the upper portion of the figure and the 316 °C fracture is shown at the bottom. As can be seen, the morphology of the lower temperature fracture is much flatter than that at elevated temperature. A higher magnification of the 316 °C fracture zone is shown in Figure 4-20. The surface appears to be a platelike structure with larger and fewer plates as the temperature increases. Due to the large difference in fracture toughness with aging condition it is also believed that the fracture surfaces are also quite different for specimens with different aging conditions that were tested at the same temperature. However, this difference was not as easy to detect as the temperature variation shown in Figures 4-19 and 4-20. Because the aging variation was not contained on the same specimen, several different specimens had to be compared to determine the effect aging had on fracture surface morphology. Due to the specimen to specimen variation in fracture surface morphology, it was extremely difficult to determine differences between the specimens.

The only conclusion that could be made from these micrographs is that at higher temperatures the molecular mobility is greater thus leading to more drawn material on the fracture surface. The increased temperature (more drawn material) must therefore lead to the reduction in the surface energy of this material thus leading to lower fracture toughness. Since no meaningful micrographs could be obtained for the changes in the fracture surface with aging time, no conclusions can be drawn from the fracture surface

morphology as to why aging increased fracture toughness up to 650 hours aging and then decreased toughness beyond this point.

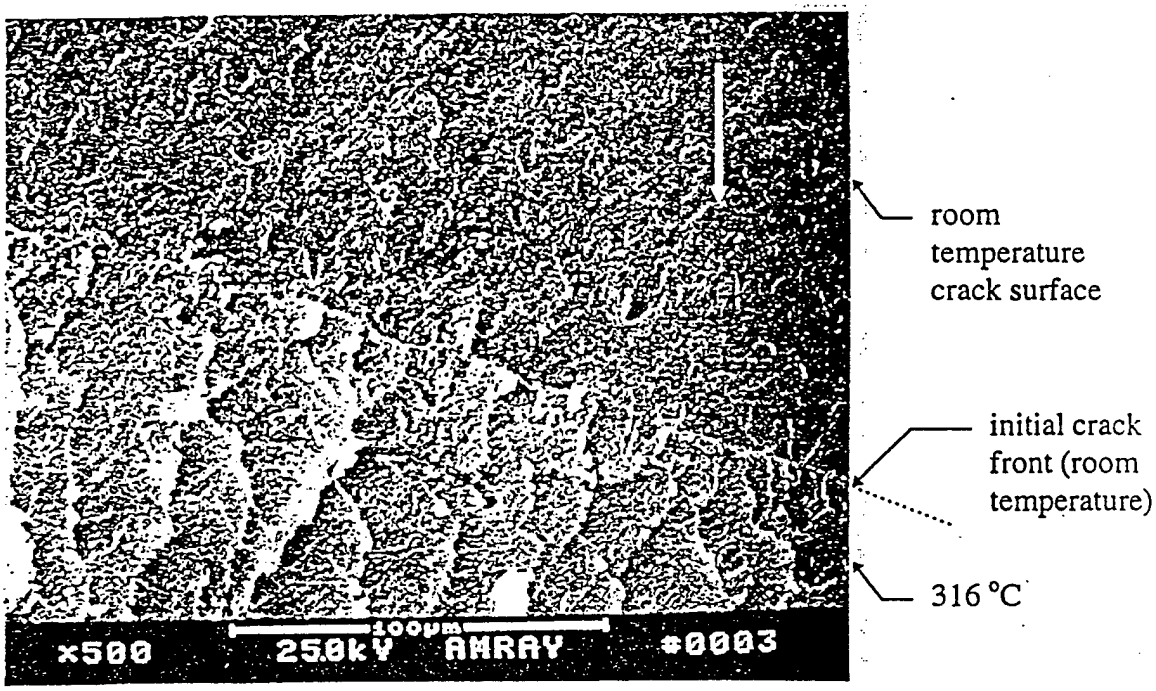

Fig 4-19: Fracture surface for PMR-15 neat resin at 316 °C

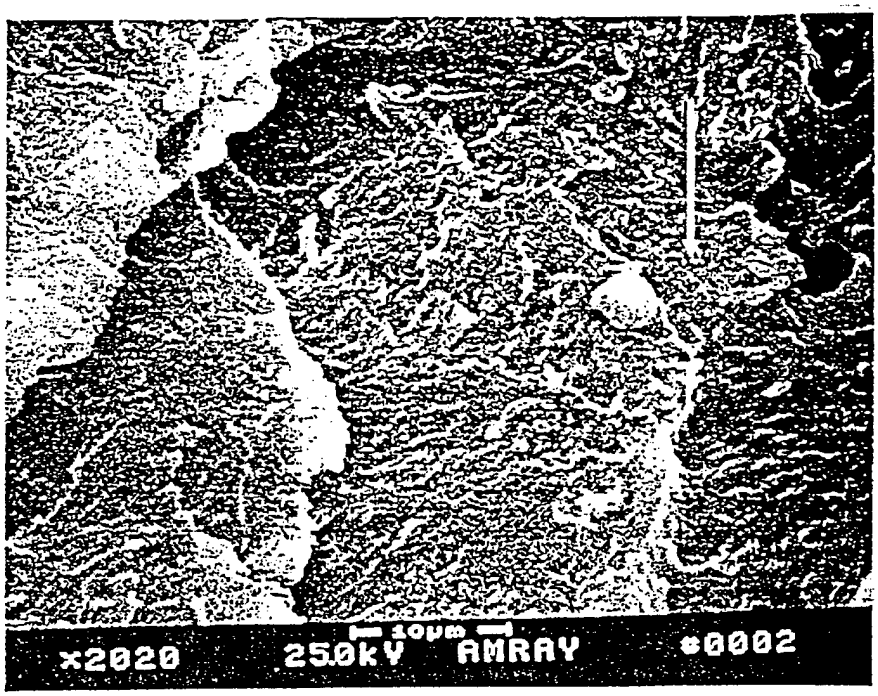

Fig 4-20: Fracture surface morphology of PMR-15 neat resin tested at 316 °C. (Note: same 316 °C fracture zone as shown in figure 4-18 above)

CHAPTER 5: SUMMARY AND CONCLUSIONS

Based on the reference material cited and the experimental work conducted in this study the following conclusions can be drawn:

1) PMR-15 exhibits nearly linear elastic behavior from room temperature up to 316 °C for the time duration of the fracture testing (approximately 1.6 minutes). The use of LEFM was verified with criteria set forth in ASTM D 5045-91a.

2) Aging strains (at 316 °C) in PMR-15 accumulate for up to 800 hours and then level off. An equilibrium is reached and no further free volume collapse is realized upon further exposure at 316 °C.

3) The glass transition temperature (T_g) for PMR-15 increases with aging time up to about 50 hours and then levels off. However, the aging strains continue to build up to 800 hours. Therefore, the aging strains prior to 50 hours aging at 316 °C must be caused by a combination of chemical and physical aging whereas after 50 hours the strains are predominantly produced by physical aging.

4) The fracture toughness (K_{IC}) of PMR-15 drops, regardless of aging condition, when the temperature increases. For a given temperature, the K_{IC} values show an increase with aging (up to 650 hours aging at 316 °C) and then drop off dramatically until 1000 hours aging where they level off. The initial increase in toughness is caused by a combination of chemical and physical aging effects. The cause for the drop in toughness beyond 650 hours is not known but, it is speculated to be caused by chemical degradation that was exhibited in the form of microscopic voids. The leveling off of the K_{IC} values at 1000 hours happens at approximately the same time the aging strains levels off.

5) The fracture surface morphology indicates that the surface becomes more drawn as the temperature is increased. No conclusions could be drawn as to the effect of aging on fracture surface morphology due to the specimen to specimen variations.

REFERENCES

[1] Struik, L.C.E., 1978, Physical Aging in Amorphous Polymers and Other Materials, Elsevier Scientific Publishing Co., Amsterdam.

[2] Kamvouris, John E., Gary D. Roberts, J. Michael Pereira, and Christopher Rabzak, 1997, Physical and Chemical Aging Effects in PMR-15 Neat Resin, ASTM STP 1302, vol. 2

[3] Skontorp, Arne, 1995, Isothermal High-Temperature Oxidation, Aging and Creep of Carbon-Fiber/Polyimide Composites, Ph.D. Dissertation, University of Houston.

[4] Knauss, W.G., 1973, Mechanics of Polymer Fracture, Applied Mechanics Review, vol. 26, pp. 1-17.

[5] Wang, S.S., Desoutter, P., 1989, Elevated Temperature Crack Growth and Fracture in Thermoplastic Polymers, ONR-URI Composites Program, Technical Report No. 19, University of Illinois.

[6] Schapery, R.A., 1975, A Theory of Crack Initiation and Growth in Visco-elastic Media (Theoretical Development), International Journal of Fracture Mechanics, vol 11, pp. 141-159.

[7] Schapery, R.A., 1975, A Theory of Crack Initiation and Growth in Viscoelastic Media (Approximate Methods of Analysis), International Journal of Fracture Mechanics, vol 11, pp. 369-388.

[8] Schapery, R.A., 1975, A Theory of Crack Initiation and Growth in Viscoelastic Media (Analysis of Continuous Growth), International Journal of Fracture Mechanics, vol 11, pp. 549-562

[9] Knauss, W.G., 1974, On the Steady State Propagation of a Crack In a Visco-elastic Sheet: Experiment and Analysis, Deformation and Fracture of High Polymers, pp.. 501-541.

[10] Knauss, W.G., Mueller, H.K., 1971, Crack Propagation in a Linearly Visco-elastic Strip, Journal of Applied Mechanics, vol. , pp 483-488.

[11] Knauss, W.G., 1970, Delayed Failure-The Griffith Problem for Linear Visco-elastic Materials, Int. Journal of Fracture Mechanics, vol. 6, pp. 7-20.

[12] Meador, M.A., Cavano, P.J., Malarik, D.C., 1990, High Temperature Polymer Matrix Composites for Extreme Environments, Proceedings of the Sixth Annual ASM/ESD Advanced Composites Conference, Detroit, Michigan, October 1990.

[13] Wilson, Douglas, 1988, PMR-15 Processing, Properties and Problems - A Review, British Polymer Journal, vol. 20, pp. 405-416.

[14] Wang, S.S., Skontorp, A., 1994, High-Temperature Aging, and Associated Micro-structural and Proerty Changes in Carbon-Fiber Reinforced Polyimide Composites, Technical Report No. UH-LCMS-94005, University of Houston.

[15] Wang, S.S., Skontorp, A., 1995, High-Temperature Creep With Physical and Chemical Aging, and Associated Viscoelastic Constitutive Equations of Polyimide-Matrix Composties, Technical Report No. UH-LCMS-95004, University of Houston.

[16] Kung, H.,Wang, S.S., Skontorp, A., 1995, High-Temperature Physical and Chemical Aging in Carbon-Fiber Reinforced Polyimide Composites: Experiment and Theory, Technical Report No. UH-LCMS-95002, University of Houston.

[17] Knauss, G. W., 1976, Fracture of Solids Possessing Deformation Rate Sensitive Material Properties, The Mechanics of Fracture, AMD-vol. 19, pp. 69-103.

[18] Shaw, S.J., 1987, High-Temperature Polymers for Adhesive and Composite Applications, Material Science and Technology, vol. 3, pp. 589-599

[19] Williams, J.G., 1978, Application of Linear Fracture Mechanics, Advances in Polymer Science, vol. 27, pp. 67-120.

[20] Poole, E.L., Lin, K.Y., Effects of Isothermal Aging on the Toughness of Polymeric Composite Materials, The Tenth International Conference on Composite Materials, Whistler, British Columbia, Canada, August 15-18, 1995, pp. 205-212.

[21] Nielsen, L.E., 1969 Cross-linking Effect on Physical Properties of Polymers, Journal of Macromolecular Science Part C, vol. 3, pp. 60-103.

[22] Chang, G., Jamieson, A.M., Yu, Z., McGervey, J.D., 1996, Physical Aging in the Mechanical Properties of Miscible Polymer Blends, Journal of Applied Polymer Science, vol. 63, pp. 483-496.

[23] Twardy, H., Aging of Polymer Matrix Composites At Elevated Temperatures, Proceedings from International Conference 'Spacecraft Structures and Mechanical Testing', Noordwijk, The Netherlands, April 24-26, 1991.

[24] Truong, V.T., Ennis, B.C., 1991, Effect of Physical Aging on the Fracture Behavior of Crosslinked Epoxies, Polymer Engineering and Science, vol. 31, pp. 548-557.

[25] Ward, I.M., 1983, Mechanical Properties of Solid Polymers, Wiley, NY.